Chloride (Cl^-) transport and its regulation by nitric oxide (NO) in porcine ciliary body / epithelium (CBE)

Kong Chi Wing, Marco

Doctor of Philosophy

School of Optometry

The Hong Kong Polytechnic University

2005

CERTIFICATE OF ORIGINALITY

I hereby declare that this thesis is my own work and that, to the best of my knowledge and belief, it reproduces no material previously published or written, nor material that has been accepted for the award of any other degree or diploma, except where due acknowledgement has been made in the text.

Kong Chi Wing, Marco (Candidate)

Professor Chi-ho To (Supervisor)

TABLE OF CONTENTS

ACKNOWLEDGEMENTS

I thank the Lord for His graces and everlasting guidance. I treasure every experience in my life and believe both bitter and sweet trials are meant to prepare me for the responsibilities the furture brings.

I appreciate my mom and dad for bringing me to the world to live and enjoy life.

I am grateful to Prof. Chi-ho To, my supervisor, for his direction and inspiration throughout the period of study. His patience and continuous support are essential to the completion of this project. I would also give my sincere thanks to him for granting me luxurious opportunities to work on my own ideas in many occasions.

I would like to express my gratitude to Dr. Chi-Wai Do for his help in particular during the early stage of my project and his esteemed comments on my thesis. I thank Dr. Mohammad Shahidullah for introducing me to an interesting area: nitric oxide signalling and Mr. Andy Kong for his technical assistance whenever I need. I am also thankful for all my colleagues in the Laboratory of Experimental Optometry. Without them, those days I spent in the laboratory would have been much less enjoyable.

Last but not least, I must give my heartful thanks to Grace for her care in every way. The encouragement, patience and understanding from her and her family are cherished impetus to me.

I wish to dedicate this work to my grandma who would have been so proud to see the completion of my research thesis.

Kong Chi Wing, Marco

“If I have been able to see further, it was only because I stood on the shoulders of giants.”

Sir Isaac Newton

“It is the duty of a scientist to remain obscure.”

Dr. Albert Einstein

Abstract of thesis entitled

"Chloride (Cl^-) transport and its regulation by nitric oxide (NO) in porcine ciliary body / epithelium (CBE)"

submitted by **Kong Chi Wing, Marco**

for the degree of **Doctor of Philosophy**

at The Hong Kong Polytechnic University in April 2005

ABSTRACT

Glaucoma is a potentially sight-threatening disease that is frequently associated with the aqueous humor (AH) dynamics of the eye. Elevated intraocular pressure (IOP) which causes damages to the optic nerve fibres in glaucoma patients, is resulted from an altered AH dynamics via an increase of aqueous humor formation (AHF) or a decrease of AH outflow or a combination of both. Clinically, reducing IOP appears to be the only way that can effectively slow down the progression of glaucomatous defect. At present, topical pharmacological agents are used as the mainstay of glaucoma treatment and these agents lower the IOP by reducing AHF. However, the mechanism of AHF is still poorly understood. In order to devise better glaucoma drugs that are potent and specific, a clear understanding of the AHF mechanism and regulation is of paramount importance.

It is generally agreed that the fluid secretion in AHF is secondary to active transport of ions and solutes across the ciliary epithelium (CE) in the stromal-to-aqueous direction. Data in ox and rabbit have shown that active chloride (Cl^-) transport across the CE may be the major driving force for AHF. However, the machineries that

constitute and regulate the transepithelial Cl^- transport are yet to be fully characterized. Therefore, we investigated the AHF mechanism and regulation by studying the ion transport and electrophysiology of porcine CBE.

In the first part of the present work, the electrical properties and Cl^- transport across the isolated porcine ciliary body / epithelium (CBE) were studied with the Ussing chamber technique. Viable porcine CBE preparations were maintained *in vitro*. A spontaneous transepithelial potential difference (*TEP*) of approximately 1 mV was found across the porcine CBE (aqueous side negative). The magnitudes of the *TEP* and short-circuit current (I_{sc}) were dependent on both the bathing Cl^- and bicarbonate (HCO_3^-) concentrations. Under short-circuited condition, a significant net Cl^- transport (1.01 $\mu Eqhr^{-1}cm^{-2}$, n = 109, $p < 0.001$) in the stromal-to-aqueous direction ($J_{net}Cl$) was detected which may be a driving force for the AHF in pig eye. The magnitude of the Cl^- current (I_{Cl}) carrying by the $J_{net}Cl$ was about 2.2 times of the measured I_{sc}, suggesting either there was cation (e.g. Na^+) transport along with Cl^- or anion transport (e.g. HCO_3^-) in the opposite direction or both. To characterize the machineries driving the Cl^- transport across the porcine CBE, the effects of transport inhibitors on the transepithelial electrical parameters and Cl^- transport were investigated. For the uptake of Cl^- into the pigmented epithelium (PE), our results indicated that the bumetanide-sensitive $Na^+/K^+/2Cl^-$ cotransporter (NKCC) played a significant role (bilateral bumetanide reduced the $J_{net}Cl$ by 57%) while the DIDS-sensitive Cl^-/HCO_3^- anion exchanger (AE) did not. The intercellular gap junctions between the nonpigmented epithelium (NPE) and PE were also important for the transepithelial Cl^- transport. Blockage of the gap junction by its inhibitor, heptanol, abolished the I_{sc} and dramatically reduced the $J_{net}Cl$ (-82%). The efflux of Cl^- from the NPE into AH is

believed to be via Cl^- channels. The present results indicated that the Cl^- channel on the NPE of the porcine CE was a niflumic acid (NFA)-sensitive but NPPB-insensitive type.

In the second part of the present work, the modulatory roles of nitric oxide (NO) signalling on the transepithelial electrical parameters and Cl^- transport across the porcine CBE were investigated. cGMP analog (8-pCPT-cGMP) triggered a sustained hyperpolarization of the I_{sc} (102%). NO donors (SNAP and SNP) induced a transient hyperpolarization of the I_{sc} that returned to baseline if SNAP was used but produced a sustained depolarization (-46%) if SNP was used. Furthermore, 8-pCPT-cGMP produced a sustained significant increase of the steady-state $J_{net}Cl$ (31%) while SNP reduced the steady-state $J_{net}Cl$ (-44%) and SNAP produced no significant change in the steady-state $J_{net}Cl$. The reduction of the steady-state $J_{net}Cl$ by SNP (-63%) and SNAP (-25%) were further aggravated after the porcine CBE was pre-treated with ODQ, a soluble guanylate cyclase (sGC) inhibitor. These results indicated that NO might exert two opposite effects on the steady-state $J_{net}Cl$. It might have enhanced the steady-state $J_{net}Cl$ via a cGMP-dependent pathway but inhibited it via a cGMP-independent pathway. In general, it was noted that the NO related steady-state I_{sc} changes correlated well with the changes in the steady-state $J_{net}Cl$. Therefore, the steady-state I_{sc} changes were studied in details so as to elucidate the mechanism of the unknown cGMP-independent pathway. Being a heme-containing protein, cytochrome P450 enzyme (Cyt P450) is a likely target of NO in additional to sGC and is involved in lipid signalling via its functions in metabolizing arachidonic acid (AA). Inhibition of Cyt P450 by its inhibitor, ABT, alleviated the depolarization produced by the NO donors on the steady-state I_{sc}. This result indicated that the activation of a Cyt P450-pathway by NO might be, at least in part, responsible for the reduction of NO on the steady-state $J_{net}Cl$.

NO may modulate the transepithelial Cl^- secretion via two opposing pathways: the cGMP-dependent and cGMP-independent pathways. The cGMP-independent pathway was apparently the dominant pathway since the NO-cGMP-dependent hyperpolarization of the I_{sc} was only transient and the steady-state $J_{net}Cl$ after treatment of NO donors was never increased, contrasting to a sustained increase of the I_{sc} and steady-state $J_{net}Cl$ by cGMP analog. The downstream cascades and the final molecular targets of the cGMP-independent pathway including the Cyt P450-dependent pathway are yet to be determined.

ABBREVIATIONS

AA	Arachidonic acid
ABT	1-aminobenzotriazole
AC	Adenylate cyclase
AE	Cl^-/HCO_3^- anion exchanger
AH	Aqueous humor
AHF	Aqueous humor formation
AQ	Aqueous side
ATP	Adenosine triphosphate
BMT	Bumetanide
BS	Bilateral / Both sides
$[Cl^-]_i$	Intracellular Cl^- concentration
CA	Carbonic anhydrase
CBE	Ciliary body / epithelium
CE	Ciliary epithelium
CFTR	Cystic fibrosis transmembrane conductance regulator
CNG	Cyclic GMP-gated ion channel
cGK	Cyclic GMP-dependent protein kinase
cGMP	Cyclic guanosine 3',5'-monophosphate
CP	Continuous perfusion type chamber
Cyt P450	Cytochrome P450 enzyme
DDH_2O	Double distilled water
DIDS	4,4'-diisothiocyanatostilbene-2,2'-disulfonic acid disodium salt
DMSO	Dimethyl sulfoxide
EET	Epoxyeicosatrienoic acid
EPMA	Electron probe X-ray microanalysis
ETOH	Ethanol
FSM	Furosemide
GTP	Guanosine triphosphate
ICB	Iris-ciliary body preparation
I_{Cl}	Cl^- current

I_{sc}	Short-circuit current
IOP	Intraocular pressure
NFA	Niflumic acid
NHE	Na^+/H^+ exchanger
NKCC	$Na^+/K^+/2Cl^-$ cotransporter
NO	Nitric oxide
NOS	Nitric oxide synthase
NPE	Nonpigmented epithelium
NPPB	5-nitro-2-(3-phenylpropylamino)-benzoic acid
NRR	Normal Ringer solution
ODQ	1H-[1,2,4]Oxadiazolo[4,3-a]quinoxalin-1-one
ORC	Opened re-circulating type chamber
PCR	Polymerase Chain Reaction
PDE	Phosphodiesterase
PE	Pigmented epithelium
P-gp	P-glycoprotein, a multidrug resistance gene product
pH_i	Intracellular pH
PKC	Protein kinase C
R	Electrical resistance
R_b	Blank resistance of bathing medium used in Ussing chamber
R_t	Tissue resistance
RPE	Retinal pigmented epithelium
RVD	Regulatory volume decrease
RVI	Regulatory volume increase
sGC	Soluble guanylate cyclase
SNAP	S-nitroso-N-acetylpenicillamine
SNP	Sodium nitroprusside
ST	Stromal side
TEP	Transepithelial electrical potential difference
8-pCPT-cGMP	8-(4-chlorophenylthio)guanosine 3':5'-cyclic monophosphate sodium

LIST OF FIGURES

LIST OF TABLES

CHAPTER 1

INTRODUCTION

1.1 Aqueous humor (AH)

Aqueous humor (AH) is a transparent fluid that is formed by the ciliary processes of the ciliary body. After production, AH flows from the posterior chamber to the anterior chamber via the pupil. In the anterior chamber, the temperature difference between the warmer iris and the cooler cornea results in a convectional circulation of the aqueous fluid. Finally, AH exits the eye via one of the two principal outflow pathways, the pressure-dependent trabecular pathway and the pressure-independent uveoscleral pathway (Krupin and Civan, 1995; Freddo, 1999).

The rate of aqueous humor formation (AHF) demonstrates a circadian rhythm with the highest production rate in the morning right after awakening and the lowest during sleeping (Brubaker, 1991). On average, the rate of AHF ranges from 2.5 to 3.0 μl/min. Since the total volume of the aqueous chamber is about 300 μl, the entire volume of AH is recycled in every 100 minutes (Freddo, 1999).

1.1.1 Functions of AH

AH serves four principle functions in the eye (Krupin and Civan, 1995):

(1) To maintain adequate intraocular pressure (IOP) for structural integrity and normal optical functioning of the eye;
(2) To supply nutrients for avascular structures of the anterior segment;
(3) To maintain a high concentration of ascorbate in most species, including human. Ascorbate may serve a number of functions including an antioxidative role to combat oxidative damages; and
(4) To participate in cellular and humoral immune responses under adverse conditions, such as inflammation and infection.

1.1.2 Composition of AH

AH has a carefully controlled composition by virtue of the selective secretion mechanisms discussed later in Section 1.3. However, as AH flows through the anterior segment, its composition is altered due to the metabolic interchanges with various tissues such as vitreous, crystalline lens, iris and cornea.

1.1.2.1 Proteins in AH

AH contains only a small amount of protein ranging from 0.05 to 0.15 mg/l as compared to the protein in blood plasma (60 to 70 mg/l) (Davson, 1990). The low concentration of protein in AH is important for the optical clarity of the anterior eye

(Cole, 1984; Abdel-Latif, 1997). The major protein components in AH are identical in ox, monkey, dog, rabbit and human as revealed by capillary isotachophoresis (ITP) analysis (Bours, 1990). The proteins in AH are mainly those of low molecular weight (e.g., albumin and β-globulins) although trace amounts of high-molecular-weight proteins (e.g., β-lipoproteins and heavy immunoglobulins) are also present. This protein pattern indicates the blood-aqueous barrier is functionally semiporous possessing pore size of approximately 105 Å (Krupin and Civan, 1995). In addition to the traditional route of plasma protein entry through the blood-aqueous barrier, evidences also suggested there is an alternative anterior diffusional protein pathway in the normal eye (Freddo et al., 1990; Barsotti et al., 1992). Through this pathway, plasma derived proteins move directly from its storage in the ciliary stroma into the anterior chamber, bypassing the posterior chamber.

1.1.2.2 Ascorbate in AH

Ascorbate exists in a substantially high concentration in the AH of many species (Reiss et al., 1986; Rose and Bode, 1991). It is maintained by active transport process via the ciliary epithelium (CE) as demonstrated in rabbit (Chu and Candia, 1988; Mead et al., 1996) and ox (To et al., 1998b). The concentration of ascorbate in the anterior chamber is lower than that in the posterior chamber, probably due to its diffusional exchange with the iris (Kinsey, 1953).

Ascorbate has numerous functional roles in the anterior segment. It may be (1) acting as an antioxidant thus reducing oxidative damages, (2) modulating the sol-gel balance of glycosaminoglycans in the trabecular meshwork, (3) absorbing ultraviolet

radiation that may aggravate cataract formation, and (4) affecting catecholamine storage in the iris (Krupin and Civan, 1995).

1.1.2.3 Oxygen tension and pH of AH

In rabbit, oxygen in AH is supplied by both transcorneally diffusion from the atmosphere (McLaren et al., 1998) and uveal vascular system (Kawahara et al., 1990). Oxygen tension in the anterior chamber of rabbit ranged between 13 and 35 mm Hg (Kleinstein et al., 1981; Stefansson et al., 1987; Kawahara et al., 1990; McLaren et al., 1998). Experimental error rather than physiological variation was suggested as the cause of such variation (Krupin and Civan, 1995).

The pH of AH depends largely on the bicarbonate (HCO_3^-) concentration (Krupin and Civan, 1995). Different species possess different ionic composition in their AH. For instance, the AH of horse and human have a higher concentration of Cl^- and a lower concentration of HCO_3^- as compared to the blood plasma while the opposite is true in rabbit and guinea pig (Davson, 1990). The pH of the AH with relatively lower HCO_3^- concentration is acidic while that with higher HCO_3^- is alkaline with respect to the blood plasma.

1.1.2.4 Lipids in AH

As most plasma lipids are bound to high-molecular-weight lipoproteins, they can hardly traverse an intact blood-aqueous barrier and therefore the lipid concentration in AH is low (Krupin and Civan, 1995). From the AH of ten patients undergoing cataract surgery, the mean total lipid concentration was 16.4 mg/dl (Jahn et al., 1983).

1.1.2.5 Amino acids in AH

In the AH of rabbit, monkey, and human, big variations in the aqueous / plasma ratios of various amino acids are seen. Such variations may be due to the different rates of diffusion, secretion and metabolic interchange of the amino acids with the anterior segment tissues in different species (Riley, 1983).

1.2 The Ciliary Body: The site of AHF

The ciliary body is the exclusive site of AHF. It is the intermediate portion of the uvea extending from the root of the iris posteriorly to the ora serrata. When viewing from posterior, the whole ring of ciliary body is composed of about 70 radially projecting major ciliary processes, with minor processes intervening between them. All processes are villiform-ridged in shape and project into the posterior chamber.

The ciliary processes are further subdivided into two regions: the pars plicata and the pars plana. The pars plicata is the anterior-most region of the ciliary processes, which begins at the root of the iris. The region is so named because it is composed of numerous fin-like processes. The pars plana is the flatter portion located posterior to the pars plicata and ends at the ora serrata. Functionally, the pars plicata is considered to be the dominant region for AHF as ion transporters were more abundant in this region (Muther and Friedland, 1980; Ghosh et al., 1991; Dunn et al., 2001).

Histologically, the ciliary body is composed of an epithelial bilayer, a stroma and an inner capillary core.

The epithelial bilayer covers the surface of the ciliary body and faces the posterior chamber. This anatomically and functionally unique bilayer functions as a single unit, or so-called, syncytium (Section 1.4).

The ciliary body stroma is a loose, areolar connective tissue adjoining the iris stroma anteriorly and the choroid posteriorly. The stroma is thin at the pars plana region but is thickened towards the pars plicata direction. Finally in the pars plicata region, the stromal tissues extend into the core of each of the ciliary process, together with a microvascular system that nourishes the local environment.

The microvascular pattern of the ciliary body is very delicate. Morrison and Van Buskirk (1984) reported a dual vascular supply to each of the ciliary processes. The two supplies, anterior and posterior arterioles, are both originated from the major circle of the iris with an anterior-to-posterior direction of flow. The anterior arteriole is relatively larger in diameter, fenestrated and supplies the tip of the ciliary processes while the narrower posterior arteriole is non-fenestrated and responsible for nourishment of the ciliary muscle. The blood flow further leads to a network of choroidal veins and leaves the ciliary body.

1.3 Mechanisms of AHF

Macroscopically, AHF across the ciliary body involves four steps (Bill, 1975):

(1) Bloodstream flows through the microvasculature within the ciliary stroma.
(2) An ultrafiltrate is derived from the blood plasma into the interstitial space within the ciliary stroma via the fenestrated anterior arteriole.
(3) Solutes in the ultrafiltrate are selectively transported across the CE from the stroma into the posterior chamber.
(4) An osmotic gradient is thus created across the CE and bulk flow of fluid is followed.

The solutes transport across the CE is a crucial step of AHF. Theoretically, this can be achieved by three interdependent physiologic processes:

(1) diffusion - the passive movement of solutes (especially those with high lipid solubility) across the cell membrane down a concentration gradient;
(2) ultrafiltration - the passive bulk flow of water and water-soluble substances across the cell membrane by the interplay of the hydrostatic pressure within the stromal microvasculature, the osmotic pressure and oncotic pressure in the ciliary stroma and the IOP; and
(3) active secretion - the energy-dependent movement of solutes across the cell membrane.

The proposition that diffusional process being the major driving force of AHF was inconsistent with the fact that the concentrations of a number of elements (e.g. Cl^- and ascorbate) were higher than expected from a Gibbs-Donnan equilibrium with the blood plasma.

Ultrafiltration was thought to be important and it was suggested that ultrafiltration could account for 80 % of AHF due to the high hydraulic conductivity of the ciliary processes *in vitro* (Green and Pederson, 1972). A small short-circuit current (I_{sc}) which was thought to indicate weak ion transport activities, in early electrophysiological study on isolated iris-ciliary body preparation (ICB) (Cole, 1961b) has also indirectly supported the ultrafiltration hypothesis. However, a lot of experimental findings would oppose ultrafiltration or other passive process as the major mechanism of AHF. Firstly, AHF can be suppressed by a variety of metabolic inhibitors (Cole, 1960; Becker, 1963; Kodama et al., 1985; Shahidullah et al., 2003). Secondly, anoxia can reduce the indicators of active transport across the isolated ciliary body preparations such as the short-circuit current (I_{sc}) (Watanabe and Saito, 1978; Krupin et al., 1984). Thirdly, there is a net ascorbate transport from the stroma to aqueous (Chu and Candia, 1988; Mead et al., 1996; To et al., 1998b). Furthermore, the hydrostatic pressure in the ciliary stroma was found to be smaller than the sum of the intraocular pressure (IOP) and the oncotic pressure and thus reabsorption rather than ultrafiltration would have been favored (Bill, 1973). Moreover, in *in vitro* perfused bovine eye, the measured IOP was not affected by even a large increase in the perfusion flow rate and perfusion pressure (Wilson et al., 1993). Therefore, AHF should be largely driven by active process, rather than by passive process. It has been estimated that ultrafiltration may only be responsible to about 20-30% of AHF (Bill, 1975; Cole, 1977).

1.4 Ciliary epithelium (CE)

The CE covers the entire surface of the ciliary body. It is formed by two epithelia with their apical surfaces abutting each other. This arrangement can be attributed to the invagination of the neuroectoderm of the optic vesicle to form the optic cup during embryologic development. This bilayer arrangement is unique in the body.

1.4.1 Pigmented epithelium (PE)

The outer layer, with its convoluted basal surface resting on the basal lamina of the ciliary body stroma, is a layer of cuboidal melanin-containing cells, called pigmented epithelium (PE). The PE layer adjoins the anterior myoepithelium of the iris anteriorly and the retinal pigmented epithelium (RPE) at the ora serrata. The extensively folded basal membrane greatly facilitates solute uptake from the filtrate of blood in the ciliary stroma (Edelman et al., 1994).

1.4.2 Non-pigmented epithelium (NPE)

The inner layer next to the posterior chamber is the non-pigmented epithelium (NPE). It is a layer of columnar cells containing no melanin pigment granules. The basal surface is markedly folded and lies on a thin basal lamina, which is an extension of the internal limiting membrane of the retina. This NPE continues anteriorly with the pigment epithelium of the iris and posteriorly with the neurosensory retina at the ora serrata. The numerous infoldings at the basal membrane of NPE serve to maximize the surface area for optimal fluid transport as in other typical secretory epithelia.

1.4.3 Tight junctions (zonula occludens)

In the CE, tight junctions were only found between the apical portions of adjacent NPE cells (Raviola and Raviola, 1978). Morphological study demonstrated that the tight junction in the NPE was formed by variable numbers of superimposed strands of fibrils (mean 3 to 4) that produced variable “tightness” even within the same cell perimeter (Noske et al., 1994). Nonetheless, this framework of tight junction constitutes the major component of the blood-aqueous barrier (Cunha-Vaz, 1979). The fact that the concentration of proteins in the anterior chamber is much lower than that in the blood plasma (Krause and Raunio, 1969; Davson, 1990) reflects the normal functioning of this blood-aqueous barrier. Functionally, an intact blood-aqueous barrier limits paracellular diffusion of blood borne macromolecules but allows finite passage of low-molecular weight solutes and ions. Therefore, the electrical and osmotic gradients originating from transcellular active transport can be maintained and AH is produced by the CE as described according to the modified model for standing gradient osmotic flow (Diamond and Bossert, 1967). Recent investigations have extended our understanding of the tight junction complexes on the molecular level. The tight junctions are now regarded as multi-components and multifunctional complexes possessing a wide variety of physiological functions in addition to being a permeability barrier (Schneeberger and Lynch, 2004). In the blood-aqueous barrier of rabbit eye, multi-components such as occludin and zona occludens (ZO)-1 have been found (Wu et al., 2000).

1.4.4 Gap junctions

Gap junctions were first noticed in the intercellular spaces of heart and liver (Revel and Karnovsky, 1967). They are present virtually in all animal tissues and act as an intercellular bridge for communication between adjacent cells (Larsen and Veenstra, 2001).

A complete extracellular gap junction channel permits diffusion of molecules smaller than 1 kDa and is formed when two connexons, one from each of the neighboring cells, merge with each other (reviewed in Goodenough (1996); Kumar (1996)). Each connexon is composed of six transmembrane core proteins called connexin, which possesses four membrane-spanning regions, two extracellular loops containing highly conserved cysteine residues, and an internal loop and amino and carboxyl termini extending into the cytoplasm (Beyer et al., 1990). In human, 20 different subtypes of connexin have been identified (Willecke et al., 2002). Each connexin is named according to their molecular weights. For example, a 43-kDa connexin in human tissue is called human connexin 43 (human Cx43). Typically, gap junctions within any given tissue are composed of only one or a few subtypes of connexin. Therefore, it is believed that different connexins may be responsible for the differential functions of different gap junctions (Larsen and Veenstra, 2001).

In the CE, gap junctions are ubiquitous and connect both between adjacent cells and also between the bilayer (Raviola and Raviola, 1978). The presence of numerous gap junctions between the PE and NPE cells implied an intimate relationship between them. The observations of dye coupling (Green et al., 1985; Oh et al., 1994), similar membrane potential (Wiederholt and Zadunaisky, 1986; Carre et al., 1992) and intracellular ion contents (Bowler et al., 1996) in the two layers further illustrated this

intimacy. Coca-Prados et al. (1992) were the first to identify that Cx43 was an important component of the gap junctions in the CE. In a recent study in rat, Cx26 and Cx31 were found in gap junctions between NPE cells with different locations while Cx40 and Cx43 were both localized to the PE-NPE interface where they formed discrete homomeric / homotypic gap junction plaques (Coffey et al., 2002).

1.5 Overview of ionic transport across the CE

At first, the NPE was thought to be the key player contributing to the active ionic transport for AHF based on the following observations:

(1) The tight junctions forming the blood-aqueous barrier against paracellular diffusion were located only at the apical portion between the NPE cells (Raviola and Raviola, 1978).
(2) Stronger activity of Na^+,K^+-ATPase (Riley and Kishida, 1986; Flugel and Lutjen-Drecoll, 1988), higher metabolic activities (Shimizu et al., 1967) and more adenylate cyclase (AC) (Tsukahara and Maezawa, 1978; Elena et al., 1984) were found in the NPE than in the PE.
(3) AHF can still be maintained even when the PE was destroyed selectively while the NPE remained intact (Okisaka and Kuwabara, 1974).

However, the PE has also been suggested to play an important role in AHF. The notion is supported by the presence of carbonic anhydrase (CA) and Na^+,K^+-ATPase in the PE (Eichhorn et al., 1991) and the existence of a large number of gap junctions at the interface between the PE and NPE (Raviola and Raviola, 1978). These gap junctions allow free passage of ions and thus signify electrical coupling between the PE and NPE.

In view of the different physiological properties of the PE and NPE cells, Wiederholt et al. (1991) proposed a functional syncytium model for the CE bilayer. The model suggests that the tight communication and asymmetric characteristics of the PE

and NPE cells corroborate in the transepithelial vectorial transport in three steps (Figure 1-1):

(1) transmembrane uptake of ions and solutes from the stromal side to the cytoplasm of the PE cells;

(2) transfer of ions and solutes across the gap junctions, and

(3) diffusion and/or pumping out of ions and solutes from the NPE cells to the aqueous side.

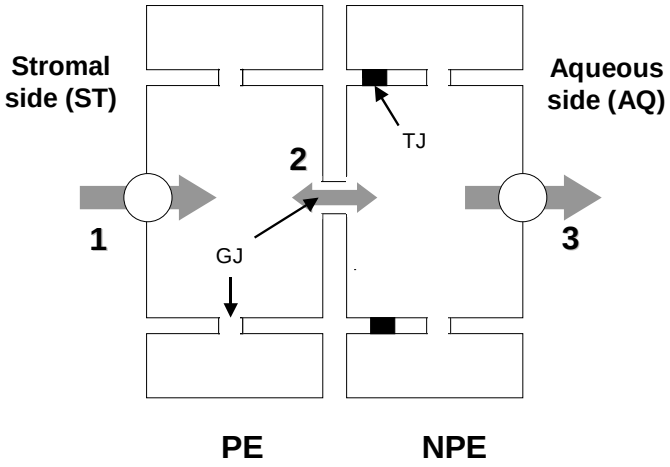

Figure 1-1 The major steps of ions transport across the CE. (1) transmembrane uptake of ions and solutes from the stromal side to the cytoplasm of the PE cells, (2) transfer of ions and solutes across the gap junctions, and (3) diffusion and/or pumping out of ions and solutes from the NPE cells to the aqueous side. GJ and TJ stands for gap junction and tight junction, respectively.

This hypothesis of a single functional unit, syncytium, is consistent with a number of the observations, such as the electrical coupling of the bilayer revealed by

intracellular potential measurement (Green et al., 1985); the free dye diffusion between paired PE and NPE cells after microinjection of Lucifer yellow (Edelman et al., 1994); the same intracellular potential in the PE and NPE by microelectrodes study (Wiederholt and Zadunaisky, 1986; Carre et al., 1992), and the similar ion contents in the PE and NPE (Bowler et al., 1996).

The final outcome is a transepithelial ion transport across the CE into the eye that drives osmotic water flow into the posterior chamber. Extensive efforts by various investigators have been devoted to identify the various molecular entities including ion transporters, channels, and pumps in the CE, which may participate in the vectorial transport mechanism across the functional syncytium (Helbig et al., 1987; Helbig et al., 1988a; Helbig et al., 1988b; Helbig et al., 1989b; Helbig et al., 1989d; Coca-Prados et al., 1995).

Several ions are thought to be important in AHF since active secretion of these ions have been demonstrated (Holland and Gipson, 1970; Chu and Candia, 1987). The most important ions are Na^+, HCO_3^- and Cl^- and they are the major ions in both the blood plasma and AH. Variations in the concentrations of these ions would likely lead to more drastic osmotic effect than that of the other constituents (Davson, 1956). The transport of these 3 important ion species across the CE is reviewed.

1.5.1 Na^+ transport

The sodium pump is ubiquitous in eukaryotic cells and is an imperative entity controlling the flow of Na^+ and K^+ through the plasma membrane. The Na^+,K^+-ATPase is better known as the sodium pump, which pumps 3 Na^+ ions out of the cells and 2 K^+ ions into the cells at the expense of an ATP (Glynn, 1993). As reflected by its

stoichiometry, the sodium pump maintains a chemical and an electrical ionic gradient across the cell membrane that are vital for many cellular functions including the regulation of osmotic balance, cell volume and intracellular pH and the generation of transmembrane electrical potential. It also contributes to cellular excitability and provides driving forces for various secondary active transport (Balshaw et al., 2001). The sodium pump activity is specifically inhibited by cardiac glycosides, a plant-derived steroids including ouabain.

The normal functioning of the sodium pump is essential for AHF as ouabain was effective in reducing the AHF in cat (Garg and Oppelt, 1970), *in vitro* perfused rabbit eye (Kodama et al., 1985) and *in vitro* perfused bovine eye (Shahidullah et al., 2003). In the CE, the Na^+,K^+-ATPase was found along the basolateral infoldings and interdigitations of both the PE and NPE cells (Usukura et al., 1988; Mori et al., 1991). Previous works have suggested that the Na^+,K^+-ATPases of the PE and NPE cells differ in terms of their relative activities (Riley and Kishida, 1986; Usukura et al., 1988), the quantities of the α-subunit (Dunn et al., 2001) and the isoforms expressed (Ghosh et al., 1991). These results implied that the Na^+,K^+-ATPase on the PE and NPE cells might have different functions. For instance, it has been suggested that the Na^+,K^+-ATPase of the PE cells functioned to maintain the intracellular ionic balance only but did not involve in transepithelial Na^+ transport (Watanabe and Saito, 1978; Kishida et al., 1982; Wiederholt et al., 1991). In addition, regional differences in the distribution of different isoforms of the Na^+,K^+-ATPase have also been reported (Ghosh et al., 1990; Ghosh et al., 1991). Ghosh et al. (1991) found that in the NPE cells, both α- and β-isoforms of the enzyme were more abundant in the par plicata than in the pars plana region. The findings were consistent with the proposition that the pars plicata is the primary site of AHF (Lutjen-Drecoll, 1982).

The evidence of net Na^+ transport across the CE came from the pioneering works by Cole (Cole, 1961a; Cole, 1962). In his study of *in vitro* bovine and rabbit ciliary body mounted in Ussing chamber, Na^+ dependent aqueous-positive *TEP* was detected. Cole (1961b) also observed a positive PD *in vivo* by inserting an electrode into the posterior chamber of rabbit eye. Based on these findings, he proposed that active Na^+ transport played a role in AHF. Several later studies that observed the accession rate of Na^+ from blood into the posterior chamber also lend support to a central role of active Na^+ transport. For instance, the Na^+ accession rate was approximately equal to the fluid formation rate in a study of dog (Maren, 1976) and the Na^+ accession rate in dog (Maren, 1976) and monkey (Maren, 1977) were reduced by 30-50% after intravenous administration of ouabain.

However, the role of active Na^+ transport in AHF was questioned by subsequent aqueous-negative *TEP* observed in electrophysiological studies in various species (Holland and Gipson, 1970; Watanabe and Saito, 1978; Kishida et al., 1981; Iizuka et al., 1984; Krupin et al., 1984; Chu et al., 1987). The negative *TEP* pointed to an active anion (HCO_3^- and/or Cl^-), rather than a Na^+ transport system. Two possible explanations for the discrepancy have been proposed:

(1) Kishida et al. (1981) suggested that the positive *TEP* observed by Cole may be due to the lack of HCO_3^- in the bathing solution.

(2) Iizuka et al. (1984) suggested that the positive PD found by Cole (1961b) by inserting an electrode into the posterior part of the eye might actually have come from the retinal pigment epithelium which was positive at the retinal side (Steinberg et al., 1978; To and Hodson, 1998).

Failure in detecting net Na^+ transport across the ciliary body of rabbit (Kishida et al., 1982; Pesin and Candia, 1982), cat (Holland and Gipson, 1970), toad (Saito and Watanabe, 1979) and recently in ox (To et al., 1998a) apparently dismissed the role of active Na^+ transport in AHF. However, in two studies with rabbit (Pesin and Candia, 1982) and toad (Saito and Watanabe, 1979), although ouabain produced marked inhibitory effects on the electrical parameters, it slightly stimulated the unidirectional fluxes of both directions. Candia et al. (1991) suggested that the large diffusional and/or bi-directional Na^+ fluxes had prevented a small net Na^+ flux from being detected. They then measured the unidirectional Na^+ fluxes in a low bathing Na^+ (30mM) condition so as to minimize the effects of diffusional fluxes. A statistically significant net Na^+ transport from stroma to aqueous was then found. Nevertheless, the net Na^+ flux obtained was too small to account for the rate of AHF *in vivo*.

1.5.2 HCO_3^- transport

Active HCO_3^- transport and carbonic anhydrase (CA) have long been proposed to play an important role in AHF. One of the major impetus is the fact that carbonic anhydrase inhibitor (CAI) reduces AHF and IOP in a number of experimental animals (Stein et al., 1983; Bar-Ilan et al., 1984; Kishida et al., 1986; Wang et al., 1991) and in human (Dailey et al., 1982; Rosenberg et al., 1998), without significant effect on outflow facility. Clinically, CAIs including dorzolamide and brinzolamide have been using for glaucoma treatment due to its hypotensive effect (Balfour and Wilde, 1997; Sugrue, 2000).

The contribution of active HCO_3^- transport and CA to AHF is not fully understood. CA is an enzyme present in almost all secretory epithelia which catalyses the reversible hydration of carbon dioxide (CO_2):

$$CO_2 + H_2O \xleftrightarrow{CA} H_2CO_3 \longleftrightarrow H^+ + HCO_3^-$$

So far, seven isozymes of CA (CA I to CA VII) have been cloned and sequenced in mammal. Different isozymes have different kinetic properties, susceptibility to inhibitors, intracellular location and tissue distribution (Sly and Hu, 1995; Lindskog, 1997). The physiological functions of CA include regulation of pH, CO_2 and HCO_3^- transport, and water and electrolyte balance (Sly and Hu, 1995).

Friedenwald (1949) was the first to propose a role of CA in AHF. He suggested that CA facilitates the secretion of HCO_3^- into AH. Na^+ also enters the eye from the blood plasma to maintain electroneutrality (Maren, 1977). The hypothesis was supported by the fact that there was a rapid accession rate of HCO_3^- into the posterior chamber and acetazolamide reduced the concentration and accumulation of HCO_3^- in AH (Becker, 1955; Becker, 1959; Kinsey and Reddy, 1959). Moreover, relative higher steady-state HCO_3^- concentration in the AH than plasma of rabbit and guinea pig (Kinsey, 1953; Davson, 1956) was found which also provided indirect evidence to support Friedenwald's hypothesis. In these studies, the excess of HCO_3^- was usually accompanied with a relative deficit of Cl^- in AH.

However, the role of HCO_3^- and CA in the physiology of AHF appears to be much more complicated as species like monkey and human (Davson, 1956; Becker, 1959), and recently ox, pig and sheep (Gerometta et al., 2005) showed an opposite

profile of the ion composition in their AH. In these species, an excess of Cl^- and a deficit of HCO_3^- as compared to the plasma were found and their AH showed an acidic pH. Becker (1959) observed that systemic acetazolamide produced opposite effects in rabbit and human. In rabbit, the drug reduced the aqueous-to-plasma ratio of HCO_3^- but increased the ratio of Cl^-. But in human, it reduced the aqueous-to-plasma ratio of Cl^- but increased the ratio of HCO_3^-. The author suggested that, first of all, CA catalysed the hydration of CO_2 to HCO_3^- and H^+ in both species. In rabbit, the HCO_3^- was secreted into AH with the residual H^+ returned to the ciliary stroma by Na^+/H^+ exchanger. In human, the same process occurred in a reverse direction. The HCO_3^- exchanged with Cl^- in the blood plasma and the Cl^- entered into AH. The residual H^+ may also enter AH directly or be exchanged with Na^+ to return to the blood plasma. The proposed mechanism highlighted the importance of CA in the AHF in both species while also addressed the differences in the ion composition profiles and pH of their AH.

The importance of HCO_3^- was also demonstrated in electrophysiological studies with rabbit iris-ciliary body preparation (ICB). The aqueous-negative *TEP* across the ICB depended on the presence of bathing HCO_3^- (Kishida et al., 1981; Krupin et al., 1984). The HCO_3^- dependence of the *TEP* was also observed later in ox to a lesser extent (Do and To, 2000). Moreover, transmembrane transporters for HCO_3^- have been identified in the CE in a number of studies. These included Cl^--dependent, DIDS-sensitive Na^+/HCO_3^- cotransporter in cultured bovine PE cells (Helbig et al., 1989b; Helbig et al., 1989c), Na^+- and Cl^--dependent HCO_3^- uptake in rabbit PE cells (Butler et al., 1994), and Cl^-/ HCO_3^- anion exchanger (AE) at the basolateral membrane of the NPE cells (Wolosin et al., 1991; Wolosin et al., 1993).

However, the most direct evidence that an active ion flux of HCO_3^- across the CE is still intangible. It may be due to the fact that ion flux study with radiolabeled HCO_3^- is extremely difficult to do due to the dynamic conversion of HCO_3^- ions to CO_2 (To et al., 2002). A recent study of HCO_3^- flux in ox (To et al., 2001) also failed to demonstrate any net transport of the ion even with a tailor-made closed circulating chamber (Candia, 1996) which could control the conversion of HCO_3^- ions to CO_2. Therefore, the authors suggested that CA and HCO_3^- ions were likely to exert their effects on AHF indirectly by modulating Cl^- secretion via pH regulation and transmembrane transport.

1.5.3 Cl^- transport

The importance of Cl^- in cell physiology has not been fully recognized until recent years. It was earlier believed that Cl^- was distributed in thermodynamic equilibrium across most cells (Alvarez-Leefmans, 2001) and it did not contribute to active transport. The existence of net Cl^- secretion across the CE towards AH has been a controversial issue. Holland and Gipson (1970) were the first to detect a net Cl^- secretion from the stroma to aqueous in cat ciliary body preparation. Subsequent studies reproduced the net Cl^- secretion in toad (Saito and Watanabe, 1979) and rabbit (Kishida et al., 1982). These findings suggested the importance of active Cl^- secretion in AHF and were supported by a clear dependence of the short-circuit current (I_{sc}) on bathing Cl^- in the ciliary bodies of cat (Holland and Gipson, 1970), toad (Watanabe and Saito, 1978) and rabbit (Kishida et al., 1981). However, the existence of active Cl^- secretion has been challenged by Pesin and Candia (1982) as they did not found any net

Cl^- transport in their study. They also noticed that the electrical conductance calculated from unidirectional fluxes was larger than that obtained from the measured conductance. Therefore they proposed cation transport might be coupled to the Cl^- transport rendering any anionic transport electrically silent. This hypothesis may also explain the general fact that the net Cl^- transport detected in the CE was many times higher than that expected from the I_{sc} (Holland and Gipson, 1970; Saito and Watanabe, 1979; Kishida et al., 1982). In ox, statistical significant net Cl^- secretion from the stroma to aqueous was found recently (To et al., 1998a; To et al., 1998b; Do and To, 2000). The finding rekindled the importance of active Cl^- secretion as a driving force for AHF.

Influx of ions into the PE across its basolateral membrane facing the ciliary stroma is the first step of ion transport across the CE. Based on the observations in cultured bovine PE (Helbig et al., 1988a; Helbig et al., 1988b; Helbig et al., 1988c; Helbig et al., 1989a), Wiederholt et al. (1991) proposed that there are two major influx pathways for loading the PE cells with NaCl (Figure 1-2): (1) the bumetanide-sensitive $Na^+/K^+/2Cl^-$ cotransporter (NKCC), and (2) the Cl^-/HCO_3^- (AE) and Na^+/H^+ (NHE) double exchangers. Both pathways make use of the standing Na^+ gradient created by the Na^+,K^+-ATPases at the basolateral membrane of the PE to transport ions in an electroneutral manner. The two mechanisms are not mutually exclusive and their relative dominance may vary among species (To et al., 2002).

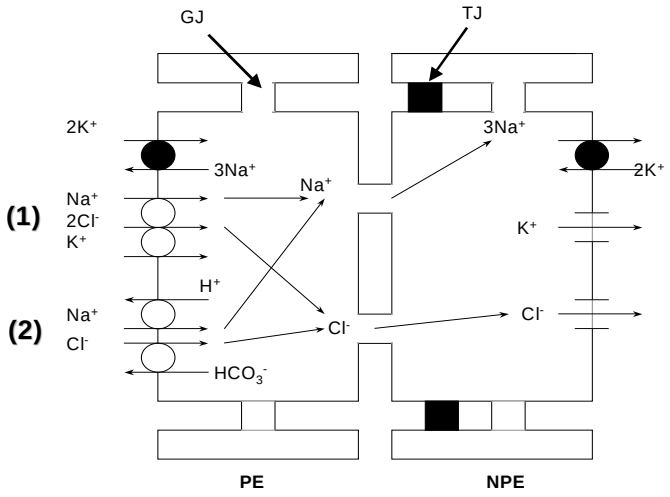

Figure 1-2 Schematic diagram showing the possible pathways for the uptake of NaCl into the CE: (1) the $Na^+/K^+/2Cl^-$ cotransporter (NKCC), and (2) the Cl^-/HCO_3^- (AE) and Na^+/H^+ (NHE) double exchangers. GJ and TJ stands for gap junction and tight junction, respectively.

1.5.3.1 $Na^+/K^+/2Cl^-$ cotransporter (NKCC)

$Na^+/K^+/2Cl^-$ cotransporter (NKCC) is a class of membrane proteins which transports Na^+, K^+ and Cl^- ions in a coupled and electroneutral manner with the usual stoichiometry of 1 Na^+ : 1 K^+ : 2 Cl^- (Haas and Forbush, 2000; Russell, 2000). The direction of net cotransport may be into or out of the cells depending on the chemical potential gradient of the transported ions. However, the cotransporter usually serves to actively accumulate intracellular Cl^- concentration ($[Cl^-]_i$) above the predicted electrochemical equilibrium physiologically. Among the numerous physiological functions serve by NKCC, its role in salt-transporting epithelia is well characterized. For instance in secretory epithelia including intestine (Dharmsathaphorn et al., 1985), airway (Boucher and Larsen, 1988) and salivary gland (Nauntofte, 1992), Cl^- enters the cells with Na^+ and K^+ via the basolateral NKCC and then diffuses into the lumen via

the apical Cl^- channels, creating a lumen-negative electrical potential. The negative potential acts to drive passive flow of Na^+ from the serosa into the lumen and finally bulk flow of water is driven osmotically by the NaCl gradient.

The 5-sulfamoylbenzoic acid loop diuretics including furosemide (FSM), bumetanide (BMT), and benzmetanide are inhibitors of the NKCC transport (O'Grady et al., 1987). In the CE, numerous evidences support a key role of NKCC for solute uptakes into the PE cells. Firstly, FSM decreased the intracellular Cl^- activity of intact shark CE (Wiederholt and Zadunaisky, 1986). Secondly, uptake of $^{22}Na^+$ and $^{36}Cl^-$ in the cultured bovine PE cells could be blunted by BMT (Helbig et al., 1989a). Thirdly, a Na^+, K^+, and Cl^--dependent, BMT-inhibitable uptake which can be activated by iso-osmotical shrinkage has been demonstrated in the freshly dissociated bovine PE but not NPE cells (Edelman et al., 1994). Moreover, NKCC has been localized intensely to the basolateral membrane of bovine PE cells and faintly in the cytoplasm of NPE cells by immunofluorescence staining (Dunn et al., 2001). In Ussing chamber studies, BMT inhibited Cl^- secretion in rabbit CE bilayer (Crook et al., 2000) and bovine CBE preparations (Do and To, 2000) with larger inhibition at the stromal (ST) side. All the above findings are consistent with the proposed solute uptake role of NKCC at the PE cells. However, evidences against a key role of NKCC in solutes uptake in the PE cells have also been reported. It was found that BMT has no inhibitory effect on the intracellular Cl^- accumulation in isolated rabbit PE cells (McLaughlin et al., 1998). In addition to its PE localization, NKCC has also been detected in the NPE cells (Crook et al., 1992; Dong et al., 1994) that may argue against its role in vectorial transport of Cl^-.

1.5.3.2 Cl^-/HCO_3^- (AE) and Na^+/H^+ (NHE) double exchangers

AE and NHE exist virtually in all cells. They are responsible for a number of crucial physiological functions including the regulation of intracellular pH (pH_i), cell volume and transepithelial transport (Lowe and Lambert, 1982; Wakabayashi et al., 1997). In the CE, AE and NHE have been functionally demonstrated in both the PE (Helbig et al., 1988a; Helbig et al., 1988b; Helbig et al., 1988c; Helbig et al., 1989c) and NPE cells (Wolosin et al., 1991; Matsui et al., 1996; Wu et al., 1998). Although AE and NHE are primarily physically independent entities, Wiederholt et al. (1991) proposed that the two separate entities could be a NaCl uptake mechanism at the PE cells by functionally coupling to carbonic anhydrase (CA). In their model they proposed that two different CAs (CA II and CA IV) are involved. The membrane-bound CA IV dehydrates the carbonic acid in the ciliary stroma to produce CO_2. The CO_2 then diffuses into the PE cells through the basolateral membrane. The exogenous CO_2 together with intracellular CO_2 from cellular metabolism serve as substrates for the cytoplasmic CA II which converts the CO_2 to HCO_3^- and H^+. These two ions are then exchanged with Na^+ and Cl^- (via AE and NHE) from the ciliary stroma. This model assigned a central role to HCO_3^- in mediating NaCl uptake without an active HCO_3^- transport across the CE. The presence of this NaCl uptake mechanism was further indicated in an electron probe X-ray microanalysis (EPMA) (McLaughlin et al., 1998; Macknight et al., 2000) which showed that both PE and NPE cells contained more Cl^- when incubated in HCO_3^--rich solution and the Cl^- content could be decreased by acetazolamide.

However, in bovine CBE preparation, Do and To (2000) found that DIDS, an inhibitor of AE did not reduce the net Cl^- secretion into AH while bumetanide, an

inhibitor of NKCC greatly reduced the net Cl^- secretion by almost 90%. They therefore suggested NKCC is the major Cl^- uptake pathway at the PE cells. AE may only play a minor role in the transepithelial Cl^- transport, in addition to its housekeeping functions such as regulation of pH_i.

1.5.3.3 Cl^- Channel

After the PE cells taking up Na^+ and Cl^-, the ions have to diffuse to the NPE cells. At the basolateral membrane of the NPE cells, Na^+ may be excreted into the posterior chamber by the sodium pump, which pumps Na^+ out in exchange for K^+ in AH. The K^+ ion may be recycled back to AH through K^+ channels (To et al., 2001). Cl^- in the NPE may passively diffuse through Cl^- channels into AH.

Theoretically, the rate-limiting step of the ion transport across the CE could be resigned in one of the three steps as shown in Figure 1.1: (1) basolateral membrane of the PE cells, (2) gap junction, and (3) basolateral membrane of the NPE cells. Civan et al. (1997) suggested the most likely rate-limiting step of AHF is the Cl^- channel located at the basolateral membrane of the NPE. Their reasons were:

(1) The intracellular Cl^- activity was much higher than that predicted from electrochemical equilibrium (Wiederholt and Zadunaisky, 1986), indicating that uptake of Cl^- by the PE cells is not likely rate-limiting.
(2) The membrane potential (Wiederholt and Zadunaisky, 1986) and intracellular ion contents (Bowler et al., 1996) were similar in the PE and NPE cells, indicating that ions could move freely within the syncytium.

(3) The baseline activity of Na^+,K^+-ATPase and the standing permeability of the K^+ at the basolateral membrane of the NPE cells were high, suggesting that they are not rate-limiting (Jacob and Civan, 1996; Civan et al., 1997).

The finding of aqueous addition of a Cl^- channel inhibitor, NPPB, inhibited the net Cl^- secretion into AH by 92% in ox (Do and To, 2000) also indicated the Cl^- channel is of paramount importance in AHF.

The mechanisms underlining regulatory volume decrease (RVD) were suggested to play a part in AHF (Farahbakhsh and Fain, 1987; Yantorno et al., 1992). By applying the whole-cell patch-clamp technique in the cell line (ODM C1-2/SV40) derived from human NPE, Yantorno et al. (1992) were the first to detect a hypotonic-activated Cl^- current that was responsible for the RVD. Various approaches were then applied to try to unravel the nature of this Cl^- current. In fresh bovine NPE, Wu et al. (1996) tested the Cl^- current with different inhibitors and concluded the Cl^- channel was associated with the multidrug resistance gene product, P-glycoprotein (P-gp). On the other hand, Coca-Prados and colleagues (1995) found that the protein kinase C (PKC) inhibitor, staurosporine stimulated a Cl^- current with its kinetics similar to the hypotonic-activated Cl^- current in the same cell line (ODM C1-2/SV40), suggesting that the cystic fibrosis transmembrane conductance regulator (CFTR) or Cl^- channel regulator pI_{Cln} could be the possible Cl^- channel at the NPE. However, Northern blotting analysis failed to find the mRNA of the CFTR in both the cultured NPE cells and ciliary body tissue whilst a high level of the pI_{Cln} transcripts was revealed. Therefore, the authors concluded the Cl^- channel observed was not the CFTR but of the type regulated by the pI_{Cln}. In addition, it was also found that patients with cystic fibrosis, in which the CFTR is defective, displayed a normal circadian pattern of AHF

and they were responsive to timolol treatment (McCannel et al., 1992). These findings apparently argued against a role of the CFTR in regulating the Cl^- secretion in AHF. Using Polymerase Chain Reaction (PCR) method, Coca-Prados et al. (1996) later revealed the expression of Cl^- channel transcripts of the ClC-3 in human NPE cells. As ClC-3 has not been shown to be volume activated, the authors suggested that the ClC-3 may be regulated by the pI_{Cln} and thus provides the same conduit for both volume-activated and isotonically staurosporine-activated Cl^- channels in human NPE cells. In a later study with native bovine NPE cells, the pI_{Cln} protein was also detected and it was suggested that the intrinsic pI_{Cln} is important in the activation pathway of volume-activated Cl^- current and cell volume regulation (Chen et al., 1999).

The roles of the pI_{Cln} and ClC-3 in regulating Cl^- secretion in AHF are still controversial since conflicting findings have been reported. For the $pI_{Cln,}$ Sanchez-Torres et al (1999) found that hypotonically-treated NPE cells showed neither a translocation of the pI_{Cln} from the cytoplasm into the plasma membrane nor changes in the pI_{Cln} expression at the protein level. Instead, a 30% decrease in the pI_{Cln} mRNA expression was noted. As a result, they suggested that the pI_{Cln} might not exist in the plasma membrane of the NPE cells and its effect on the ClC-3, if any, was small. For the ClC-3, although the ClC-3 protein was detected in bovine NPE, the predominance localization was within the nucleus (Wang et al., 2000). Moreover, the authors could not detect any basal activity of the Cl^- current. They therefore argued against the ClC-3 being the only, or even the main, volume-activated Cl^- channel in the NPE cells. The identity of the Cl^- channel in the CE is still unknown and further investigation is needed to clarify the situation.

1.6 Regulation of AHF by nitric oxide (NO)

NO is a simple diatomic molecule which has multifaceted biological functions. It plays significant roles in 3 aspects: protective, regulatory and deleterious (Wink and Mitchell, 1998). In biological system, NO is produced by the conversion of L-arginine into L-citrulline by nitric oxide synthase (NOS) (Moncada et al., 1991). There are three NOS isoforms (Masters, 2000):

(1) NOS I or previously called neuronal NOS (nNOS). It is a low output NOS regulated by Ca^{2+} and calmodulin.
(2) NOS II or previously called inducible NOS (iNOS). It is a high output NOS and is Ca^{2+}/calmodulin-independent
(3) NOS III or previously called endothelial NOS (eNOS). It is also a low output NOS regulated by Ca^{2+} and calmodulin.

NO plays important regulatory roles in various physiological functions ranging from altering the cardiovascular system to modulating neuronal function (Ignarro, 1989; Moncada et al., 1991; Culotta and Koshland, 1992). The direct effects of NO function by binding to the “heme complexes” in molecules such as guanylate cyclase (GC), cytochrome P-450 (Cyt P450), nitric oxide synthase (NOS), and haemoglobin (Miranda et al., 2000). The most notable heme protein that forms an iron-nitric oxide adduct *in vivo* is the soluble GC (sGC) (Murad, 1994). When NO binds to sGC, it changes the protein configuration and activates the sGC. Activated sGC then facilitates the conversion of guanosine triphosphate (GTP) to cyclic guanosine 3’,5’-monophosphate (cGMP) (Miranda et al., 2000). The NO-sGC-cGMP signal transduction pathway is a

major NO signalling pathway (Ignarro et al., 1982). The cGMP produced by the activation of sGC is an important second messenger that acts on three main classes of effector proteins (Ignarro, 2000): cGMP-dependent protein kinase (cGK), cGMP-gated ion channel (CNG), and cGMP-regulated phosphodiesterase (PDE). The biological effects of cGMP are terminated when it is broken down by the PDE.

In the eye, NO has been shown to regulate vascular tone (Haefliger et al., 1994), aqueous humor dynamics (Nathanson and McKee, 1995), retinal phototransduction (Perez et al., 1995), and ocular immune responses (Becquet et al., 1997). NO has also been extensively studied in terms of its effects on the intraocular pressure (IOP) and potential pharmacological values in glaucoma treatment. However, interpretation of the results in those NO studies was difficult because of the multiple physiological actions of NO on ocular tissues including the ciliary muscle, trabecular meshwork, and endothelial and vascular smooth muscle cells in the aqueous drainage system (Becquet et al., 1997). NO donors have been shown to reduce IOP in normal and glaucomatous animals (Nathanson, 1992; Schuman et al., 1994; Wang and Podos, 1995) and human (Chuman et al., 2000) and the hypotensive effect was largely attributed to its role in vasodilatation and/or relaxation of smooth muscle such as the modulation of ocular blood flow (Schmetterer and Polak, 2001), trabecular meshwork and ciliary muscle relaxation (Wiederholt et al., 1994) and AH outflow (Schuman et al., 1994). However, conflicting data have also been reported that NO may not contribute to ocular hypotension in human (Kiss et al., 1999).

Recent demonstration of NOS activities in porcine (Haufschild et al., 1996) and bovine (Geyer et al., 1997) ciliary processes, and the localization of NOS in porcine CE (Meyer et al., 1999) all suggested the direct involvement of NO in AHF physiology. In an *in vitro* perfused bovine eye study, a nitrovasodilator, sodium azide lowered the IOP

by acting on the CE but not by relaxing the vascular smooth muscles (Millar et al., 2001). Later in an electrophysiological study, activation of the classical NO-sGC-cGMP pathway stimulated a transmembrane anionic current in porcine CE, which can be inhibited by Cl^- channel inhibitors (Fleischhauer et al., 2000). This finding provided the first evidence that NO plays a direct modulatory role on the ionic transport across the CE. In a more recent study, activation of the sGC-cGMP-PKG pathway was shown to produce a transient hyperpolarization of the I_{sc} across the porcine CBE (Wu et al., 2004). Based on the transient changes of the I_{sc}, the authors concluded that NO could stimulate anion secretion and increase AHF via the sGC-cGMP-PKG pathway. However, such transient changes in the I_{sc} may not necessarily reflect a sustained increase in the transepithelial ion transport. Therefore, the exact mechanism of NO regulation on AHF is still incomplete at present.

1.7 The purposes of investigation

The ionic transport mechanism leading to AHF has been studied for several decades and many working models have been proposed. To date, a major consensus is that active secretion of Cl^- is the major driving force for AHF. However, the detailed machineries that regulate the transmembrane transport of Cl^- across the individual cell layer of the CE remain controversial. In particular, the mechanism of NaCl uptake at the PE is not fully understood. Both NKCC and AE / NHE double exchanger have been proposed as the major uptake pathway for NaCl from the ciliary stroma into the PE. In addition, the identity of the exit pathway at the NPE is also an unknown entity for a number of years. The NO effects on the AH dynamics has been the focus of research studies in recent years. A direct role of NO on the ion transport across the CE has been suggested but yet to be fully characterized. Therefore, the aims of the present project are to:

(1) study the electrical parameters across the isolated porcine ciliary body / epithelium (CBE).

(2) identify the presence of net Cl^- transport across the porcine CBE.

(3) investigate the effects of transport inhibitors on the transepithelial electrical parameters and Cl^- transport which may provide further information on the ionic transport mechanism driving AHF.

(4) study the modulatory role of NO and its related reagents on the Cl^- transport across the porcine CBE.

The findings from the present study could enhance our understanding of the ionic transport mechanism in AHF and of NO as a potential pharmacological agent regulating AHF.

CHAPTER 2

USSING-ZERAHN-TYPE CHAMBER

2.1 Background

"Ussing-Zerahn-type chamber" or "Ussing chamber" was invented by Ussing and Zerahn (1951) in their study of sodium (Na^+) transport across the frog skin. In addition to its original function for studying vectorial transepithelial ion transport, modified Ussing chambers have been applied to studies ranging from the cellular integrity to invasiveness of cancer cells.

Basically, an Ussing chamber has two functional components as illustrated in Figure 2-1. The chamber itself mimics a physiological environment in which an isolated epithelial preparation is kept alive by bathing solution (nutrient supply). Another component is the electrical circuitry, which consists of two pairs of electrodes: V_1&V_2 and I_1&I_2. They are connected to an external voltage and current clamp device as shown so that the transepithelial electrical parameters can be continuously monitored. V_1&V_2 are responsible for measuring the spontaneous transepithelial potential difference (*TEP*) (Section 2.2) while I_1&I_2 serve to pass external electrical current through the chamber for assessing the tissue resistance (R_t) and the blank resistance without the tissue (R_b) (Section 2.2) or achieving short-circuited condition in isotopic fluxes experiments (Section 2.3).

The Ussing chamber technique can directly investigate the transport properties of preparation free from systemic influences. In addition, the effects of changing bathing solution and pharmacological agents on each side of the preparation can be studied separately.

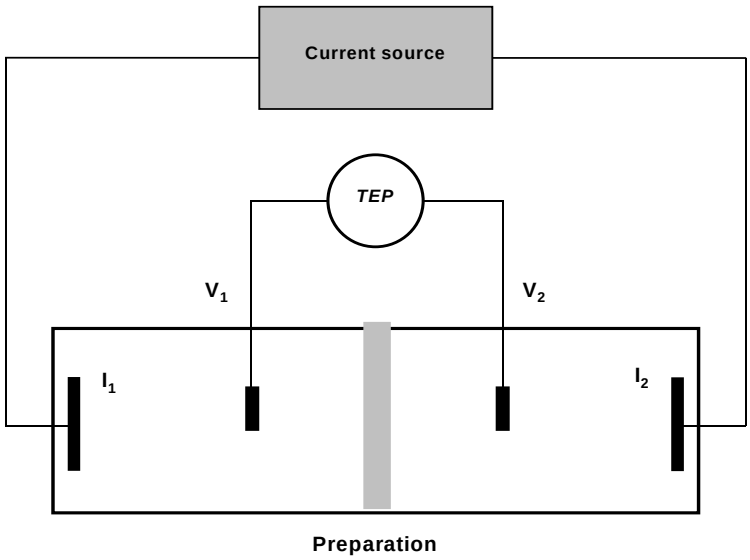

Figure 2-1 A diagram illustrates the basic concept of an Ussing-Zerahn-type chamber.

2.2 Transepithelial electrical parameters

Spontaneous transepithelial electrical potential difference (*TEP*), short-circuited current (I_{sc}) and tissues resistance (R_t) are the three major parameters that can be monitored with the Ussing chamber technique. The three parameters reflect the polarity and tightness of the preparation and they are important features that distinguish epithelia from other cell types.

The *TEP* of a preparation is a resultant of all transepithelial ions transport and has been termed “active transport potential” (Koefoed-Johnsen and Ussing, 1958; Fromter, 1979). The I_{sc} is defined as the external current required to abolish the spontaneous *TEP*. The two parameters are conceptually interrelated that they reflect the overall transport activities, metabolic processes and electrochemical gradient along the transcellular pathway. Thus provide an insight of the charges and direction of active ions flow across a preparation. In simple epithelial transport systems such as frog skin and toad urinary bladder, the I_{sc} can be solely attributed to the net Na^+ transport (Civan et al., 1989).

The R_t is an indicator of the “tightness” of a preparation. Practically, the electrical resistance across a preparation mounted in chamber (R) can be obtained either by measuring the potential change (ΔPD) with a known external current (ΔI) (“current clamp”) or by applying a potential (ΔPD) and measuring the resulting change in current (ΔI) (“voltage clamping”). By knowing the values of ΔPD and ΔI, the R can be calculated by Ohm’s law:

$$R = (\Delta PD / \Delta I) \times A$$

where A is the surface area of the exposed aperture of the chamber used. The unit of R is Ωcm^2.

It should be noted that the value of the above R is actually a serial summation of the tissue resistance (R_t) and the blank resistance of the bathing medium (R_b) between the preparation and the potential sensing electrodes (V_1&V_2) (Figure 2-2). Therefore, the R_b has to be determined in the absence of the preparation so that the R_t can be obtained with the following equation:

$$R_t = R - R_b$$

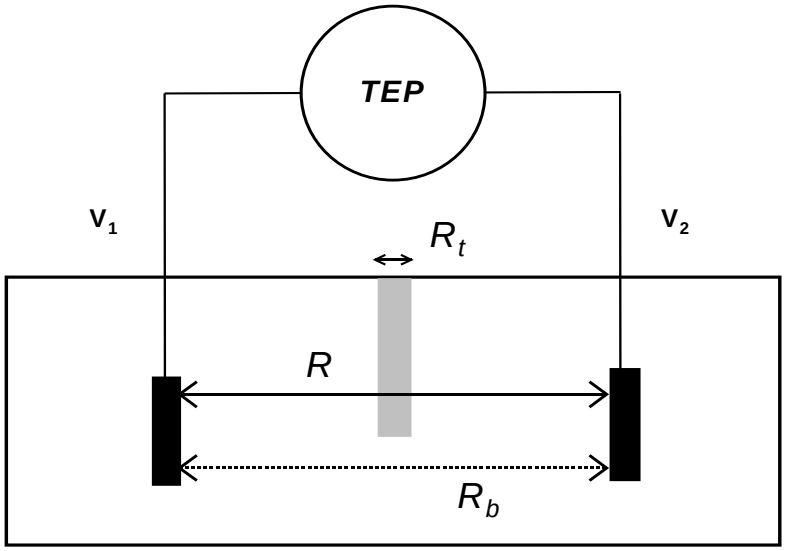

Figure 2-2 A diagram illustrates the tissue resistance (R_t), the total electrical resistance (R) with a preparation and the blank resistance of bathing medium (R_b) without a preparation in an Ussing chamber.

2.3 Short-circuiting technique and isotopic fluxes measurement

The spontaneous *TEP* of a preparation creates an electrical gradient and induces passive transepithelial movement of charged ions and solutes that may masquerade active transport movement. Experimentally, this can be prevented by short-circuiting the preparation. When the spontaneous *TEP* generated by a preparation is abolished by applying an external current, the preparation is considered to be under a short-circuited condition.

When a preparation is short-circuited, the electrical gradient between the two half-chambers is nullified. The transepithelial transport of a specific ion can therefore be accurately quantified by measuring the unidirectional fluxes of its radiolabeled ions. In these experiments, the two unidirectional fluxes in opposite directions (e.g. the stromal-to-aqueous and aqueous-to-stromal in the case of ciliary epithelium) are measured. The difference between them is the net flux in virtue of active transepithelial transport (Ussing and Zerahn, 1951). The isotopic flux approach can provide definitive evidence on the existence of active ion transport across a preparation. However, it should be cautious that the resolution of this approach depends on the leakiness of the preparation. In case of a very “leaky” epithelium, the resolution would be low since large ions leak in the paracellular pathway could easily mask the small difference between the two unidirectional fluxes created by active transcellular transport.

CHAPTER 3

METHODS

3.1 Tissue selection and preparation

Ussing chamber technique for the study of transport properties across the ciliary epithelium (CE) have been applied in various species including ox (Cole, 1961a; To et al., 1998a), rabbit (Cole, 1962; Kishida et al., 1982; Krupin et al., 1984; Chu and Candia, 1987; Carre and Civan, 1995; Matsui et al., 1996; Crook et al., 2000), cat (Holland and Gipson, 1970; Carre and Civan, 1995), dog (Iizuka et al., 1984), monkey (Chu et al., 1987)**,** toad (Watanabe and Saito, 1978), shark (Wiederholt and Zadunaisky, 1987), and recently in porcine and human (Wu et al., 2003). In the present study, freshly isolated porcine ciliary body / epithelium (CBE) was used. There are several advantages for the choice of porcine eye. First of all, they are readily available in the required numbers. Secondly, instead of sacrificing animals purely for research purpose, porcine eyes were collected after they were killed in a slaughterhouse. Thirdly and the most importantly, pig appears to be a better model for human than many other animals because there are considerable similarities between pig and human in terms of size, dietary habits, digestive physiology, kidney structure and function, pulmonary physiology, coronary artery distribution and haemodynamics and propensity to obesity (Cooper, 1992; Niekrasz et al., 1992). Besides, the rich tissue source of enzymes, which are protein in nature and determining the activity of biological tissue, in human and pig are strikingly unlike those in rat, mouse, guinea pig, rabbit, dog, cat, pigeon, horse, and

ox (Douglas, 1972). All these factors have raised the interests of using pig organs for xenotransplantation (Cooper, 1992).

In the present experiments, fresh porcine eyes were obtained from a local slaughterhouse immediately after the death of the animals. The eyes were kept on ice (4 to 8 °C) and transported to laboratory immediately (travelling time was approximately 70 minutes). The eye was used for experiment if: (1) it was intact with no leakage of aqueous or vitreous humor, and (2) the anterior segment and the crystalline lens appeared healthy.

3.2 Method of dissection

The method of dissection is shown as Figure 3-1. First of all, connective, muscular and fatty tissues around the surface of eyeball were removed with a razor blade, leaving behind the sclera. Care was taken to avoid piercing through the sclera and thus damaging the underlying tissues. Cuts were made through the sclera from the equatorial region, two on the nasal and temporal sides respectively. The cuts were then extended into the cornea by about 1.5 mm. The central cornea was then removed leaving behind its periphery. Iris, anterior chamber and anterior crystalline lens capsule were exposed and irrigated with cool Ringer solution. To detach the sclera from the underlying choroid, incision was made by a pair of curved scissors and the tissues were separated all the way to the equator. After the superior CBE was detached from the sclera, the whole procedure was then repeated for the inferior sector.

As both the superior and inferior CBE were isolated from the sclera, the original cuts at the limbal region were extended so that the two sectors of CBE were separated from the whole ring. An extra fine forceps was then used to hold the anterior lens capsule of either sector, which is firmly attached to the ciliary body and can act as a "handle" for holding the CBE. Therefore, the CBE was not directly contacted and damaged in the process. Residual vitreous attached to the CBE was carefully trimmed away. Finally, a cut was made to isolate the CBE sector from the eyeball. The isolated CBE were bathed in a Petri dish containing cool Ringer solution before mounting in a chamber.

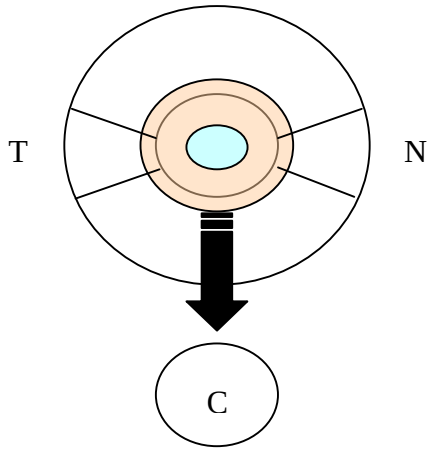

Step 1: Intact fresh eyeball. Cuts were made on both the temporal (T) and nasal (N) sides. Cornea (C) was removed and the anterior chamber was exposed.

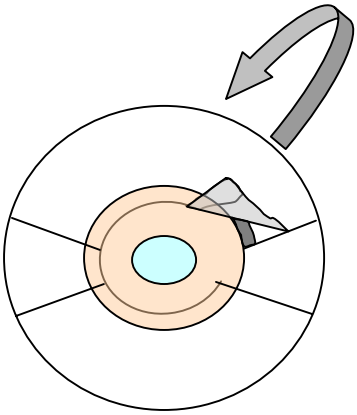

Step 2: The limbal cornea was held by a forceps. An incision was made tangentially to the choroidal surface at the anterior angle. The sclera was flipped away so as to expose the stromal side of CBE.

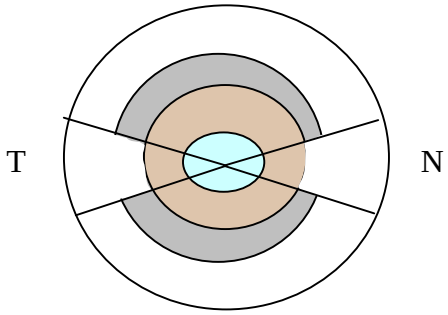

Step 3: The stromal side of both the superior and inferior CBE were exposed. The cuts original rested on the limbal region of iris were extended until the center of the lens.

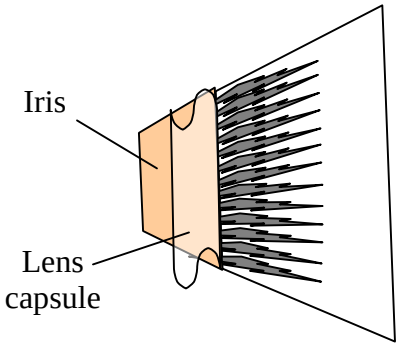

Step 4: Two sectors of whole CBE were isolated. An isolated CBE viewed from the aqueous side is shown on the right.

Figure 3-1 The dissection method of porcine CBE.

3.3 The modified Ussing-Zerahn-type chambers

Two types of custom-made modified Ussing-Zerahn-type chamber have been used throughout experiments. The continuous perfusion type (CP) was mainly used for the preliminary study of spontaneous electrical parameters including transepithelial potential difference (*TEP*), short-circuit current (I_{sc}), tissue resistance (R_t) and basal transepithelial chloride (Cl^-) transport under short-circuited condition. However, the inter-preparation variations of the unidirectional Cl^- transport were too high which made it difficult to compare the Cl^- transport with and without drugs in two different groups of preparations. Therefore, an opened re-circulating type chamber (ORC) was made. With the ORC chamber, studies of the steady-state basal Cl^- transport and the steady-state Cl^- transport after drugs added could be readily performed in the same preparation sequentially. As a result, measurements of the transepithelial Cl^- transport and effects of drugs on it were mainly performed in the ORC.

3.3.1 Continuous perfusion type chamber (CP)

3.3.1.1 Configuration of the CP chamber

Figure 3-2 shows the detailed configuration of a CP chamber. The chamber was made of Perspex, consisting of two half-chambers standing on sliding tables. The sliding tables minimise sideway movement of the half-chambers during assembly and improve viability of tissues. The stages for tissue mounting were located on the top central position of the two supporting blocks, one on each block. A cavity (aperture area 0.1 cm^2, depth 0.4 cm) in each half-chamber formed the exposed area for the CBE.

Each half-chamber has an exact dimensions and a position complementary to the opposite half-chamber. To minimise the damage to tissue and leakage from chamber during assembly, silicon plates (1 mm thick) were glued around the cavity of each half-chamber to enhance clamping. The silicone plate and the cavity on a tissue-mounting stage therefore formed a half-chamber of 0.05 cm^3 in volume. Wing nuts and flat-end screws were used to assemble the two half-chambers. To ensure an evenly distributed pressure around the aperture on which the tissue mounted, the flat-end screws were held on the same horizontal level as the cavity and the chamber cavity was located right in the middle of the two flat-end screws.

Fine bore polyethylene tubing (PE90; CLAY ADAMS®, Becton Dickinson, USA) was fitted in place with epoxy resin for continuous perfusion to each half-chamber. These tubings (perfusion inlets) were connected to 60 ml plastic syringes (Plastipak®; Becton Dickinson, UK) that were driven by a digital syringe infusion pump (Cole-Parmer Instrument Co., USA).

The transepithelial electrical parameters were monitored by a system consisting of two components. A blunt syringe needle (18-guage, Becton Dickinson, Singapore), one on each half-chamber, was used for monitoring of the *TEP* via the potential-sensing bridge (details in Section 3.4). Silver-silver chloride (Ag / AgCl) electrodes (2 mm in diameter; E201; Harvard Apparatus Ltd., UK) fitting at the back of each half-chamber formed a circuit for passing external current for resistance measurement and short-circuiting.

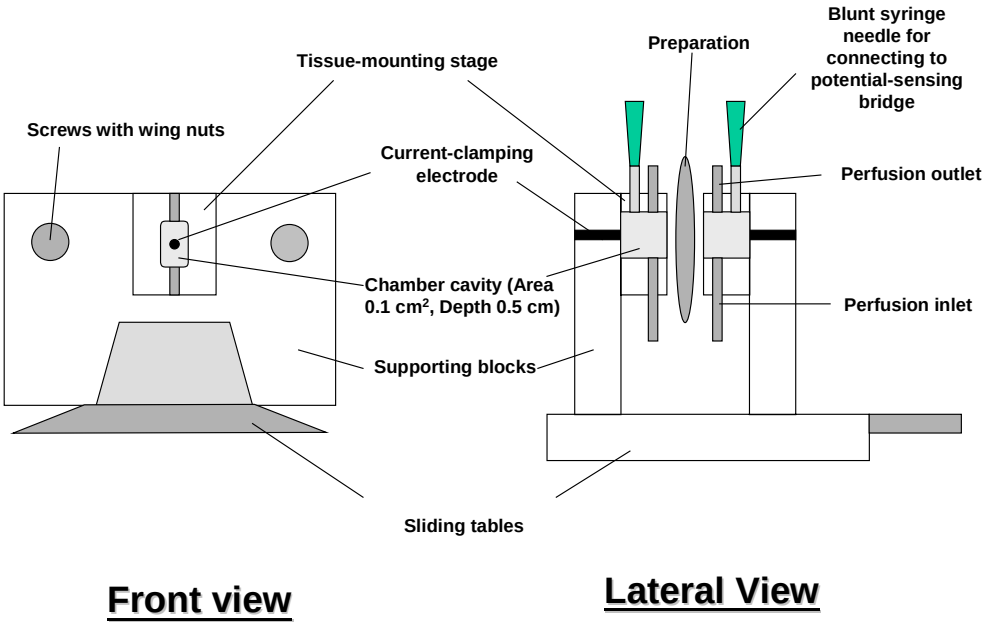

Figure 3-2 Illustrated diagram of a CP type chamber.

3.3.1.2 Tissue mounting in the CP chamber

Before mounting of tissue, a layer of silicone grease (Dow Corning Corporations, USA) was applied to the surface of the silicon plates on the two half-chambers. With silicon grease, a better seal can be obtained with minimal pressure applied on tissue, thus reduces tissue damage.

After that, the two half-chambers were laid flat, with the surface of the mounting stage horizontal to a tabletop. The perfusion to the chamber was implemented until the cavities were wetted with bathing solution. An isolated CBE was then transferred to the mounting stage with the aqueous side facing upward. The CBE was carefully positioned so that the aperture of the chamber was filled with the pars plicata region

only. The two half-chambers were assembled by tightening of wing nuts gently. Minimal pressure was applied until the chamber was leak-proof. The electrical circuit was connected as mentioned in Section 3.3.1.3.

3.3.1.3 Monitoring of the transepithelial electrical parameters in the CP chamber

The transepithelial electrical parameters were monitored by a dual voltage current clamp unit (DVC-1000; World Precision Instruments, Sarasota, FL, USA). The signal outputs were fed into dual-channel flatbed chart recorder for recording (BD-12E; Kipp & Zonen Inc., Saskatoon, Canada).

Typically the CBE gave a spontaneous *TEP*. A current (ΔI = 5μA) was passed across the tissue for 3 seconds in every 300 seconds via the two Ag / AgCl electrodes at the back of each half-chamber. The current applied (ΔI) induced changes in the potential difference (ΔPD) across the tissue. The "Fluid resistance compensation" mode was set to compensate for the blank resistance of the bathing medium (R_b) (predetermined in the absence of tissue) throughout the experiment and the real tissue resistance (R_t) was calculated by Ohm's law:

$$R_t = (\Delta PD / \Delta I) \times A$$

where A is the cross-sectional area of the chamber aperture (cm^2).

The short circuit current (I_{sc}) across a tissue was also calculated according to Ohm's law:

$$I_{sc} = TEP / R_t$$

For all experiments, *TEP*, I_{sc} and R_t were monitored until stable readings were obtained for at least 15 minutes. Then, interventions such as ion substitution, transport inhibitors were introduced. The effects of these interventions were monitored until re-stabilised readings were attained.

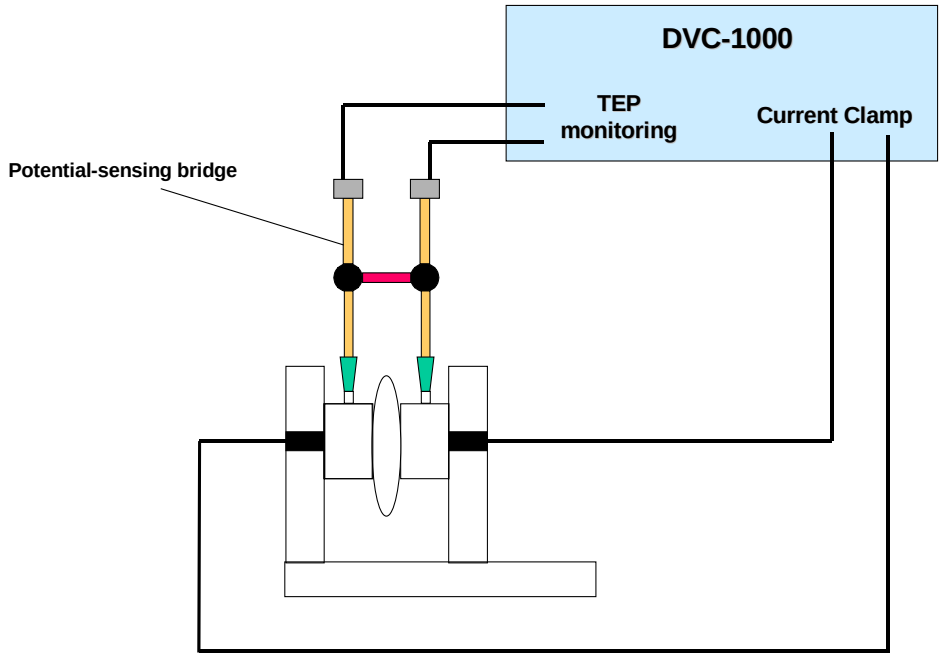

Figure 3-3 Connection of a CP chamber to DVC-1000 for monitoring of the *TEP*, I_{sc} and R_t. Noted that the components of the perfusion system have been omitted.

3.3.1.4 Study of isotopic Cl^- fluxes in the CP chamber

Only paired preparations from the same eye with comparable stable electrical parameters were enrolled for the study of isotopic Cl^- fluxes. Before the introduction of radiolabeled tracers, one sample of perfusates (2 ml in 12 minutes) from each of the bathing sides of the paired preparations were taken and immediately counted for radioactivity. These were the background radioactivity of the chamber. Isotopic Cl^- fluxes measurements were conducted if the background counts in all bathing sides were low indicating no contamination from previous experiments. In one of the paired preparations, radiolabeled [^{36}Cl] (0.5 μCi / ml Ringer solution) and [^{3}H] L-glucose (0.5 μCi / ml Ringer solution) were loaded on the stromal half-chamber for the study of the stromal-to-aqueous (J_{sa}) fluxes while in the conjugate preparation, the radiolabeled tracers of the same amount were loaded on the aqueous half-chamber for the study of the aqueous-to-stromal (J_{as}) fluxes. The net fluxes (J_{net}) were the differences between the J_{sa} and J_{as} from the paired preparations. After loading of radiolabeled tracers, preparations were allowed to equilibrate before short-circuiting and samples of perfusates taking. Sixty to seventy minutes were required for the equilibration of radioactivity so that stable radioactive counts can be obtained.

The preparations were short-circuited by the voltage clamp function in the DVC-1000. The I_{sc} required to clamp the *TEP* to zero was output to the chart-recorder. Usually, the tissues were short-circuited for at least 15 minutes before samples collection.

The procedures of sample collection were as follow. The bathing side with radioactive tracers loaded was designated the “hot” while that without was the “cold” side. Perfusates (2 ml) from the perfusion outlets of the “hot’ and “cold” sides were

collected with separate scintillation vials (986542; Wheaton, USA) in every 12 minutes. Totally 3 to 5 consecutive samples were collected in an experiment. Before transferring the outlet tubing to the next sample vial, the last drop of perfusates was dripped into the existing vial by gently touching the tip of tubing against the inner wall of the vial. This maneuver reduced the contamination of results between samplings. Each sample was then mixed well with 15 ml of scintillation cocktail (NBCS104; Amersham Radiochemicals, England). Finally, the radioactivity in all samples was counted by a liquid scintillation counter (Wallac 1414 Winspectral DSA; Wallac, Helsinki, Finland). In all experiments, measurement of [^{3}H] L-glucose fluxes act as an indicator of paracellular leakage.

Upon collection of data regarding the radioactivity in all samples, the unidirectional fluxes of both J_{sa} and J_{as} can be calculated by applying the equation below:

$$J = \frac{C \times I \times V}{H \times A \times T} \qquad (3.1)$$

where J = unidirectional flux of the studied ion

C = radioactivity in “cold” side samples (counts per minute)

H = radioactivity in “hot” side samples (counts per minute)

I = concentration of the studied ion in the Ringer solution (mM)

V = volume of perfusates collected in time “T” (ml)

A = cross-sectional area of the chamber aperture (cm^2)

T = collection time for each sampling (hr)

The unit of unidirectional Cl^- flux is $\mu Eqhr^{-1}cm^{-2}$. The mean unidirectional Cl^- flux across a preparation was averaged from consecutive samples.

3.3.2 Opened re-circulating type chamber (ORC)

3.3.2.1 Configuration of the ORC chamber

Figure 3-4 illustrates the basic configuration of an ORC chamber. The whole chamber was composed of four main parts: (1) tissue-mounting blocks, (2) tissue-bathing chambers, (3) chamber-mounting rack, and (4) re-circulating bath.

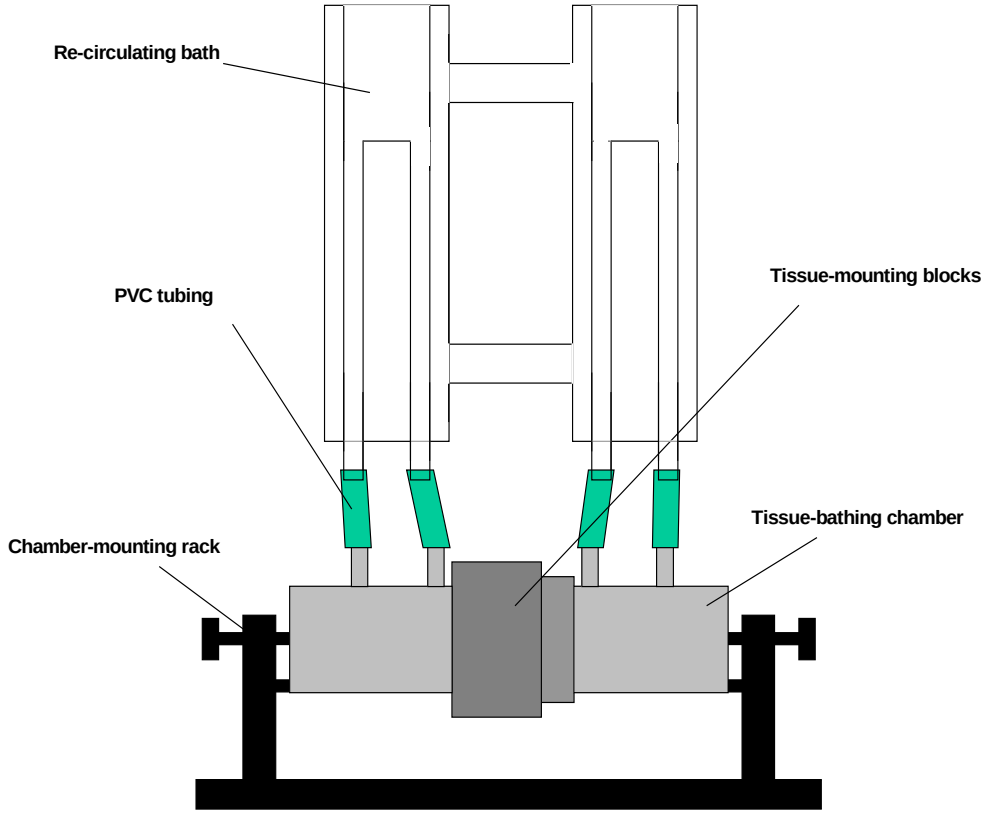

Figure 3-4 A simplified diagram showing the four components of an ORC type chamber. All ports connecting to gas pump, water re-circulator and electrodes have been omitted.

The configuration of the tissue-mounting blocks, which was made of Perspex, is shown in Figure 3-5a & b. The two blocks were made as a conjugate pair. The two stainless steel fixation rods, located at 6 and 12 o'clock positions, of the larger block were implanted in positions complementary to the two holes drilled in the smaller block. This fixation system allowed a quick and smooth assembly of the two blocks and greatly reduced damage of tissues caused by relative rotational movement of the two blocks. At the centre of the two tissue-mounting blocks, conjugate slotted apertures were made. Plastic O-rings fitted in place as shown provided a leak-proof condition during assembly. The aperture area, with O-ring in place, was 0.1 cm^2. The pins around the aperture of the larger block were conjugate to the holes drilled in the smaller block. These pins assisted in fixing the CBE preparation in position.

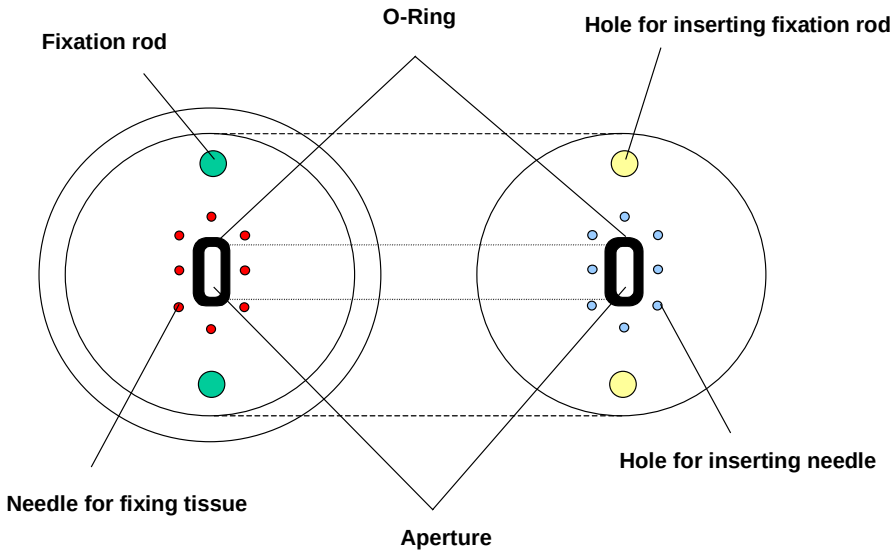

Figure 3-5a A front view of a conjugate pair of tissue-mounting blocks.

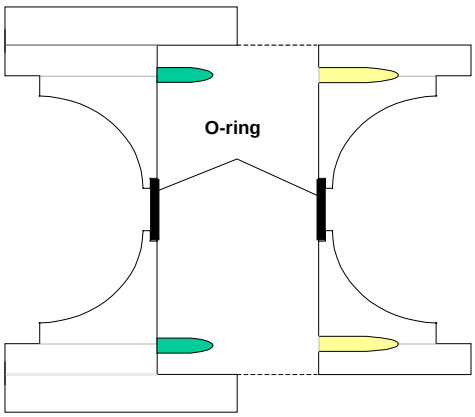

Figure 3-5b A side view of a conjugate pair of tissue-mounting blocks.

A conjugate pair of the tissue-bathing chambers was also made of Perspex. During assembly, this component was inserted into the back of the tissue-mounting block via a big O-ring situated just beyond its openings. Thus, a tissue-bathing chamber and a tissue-mounting block of the same side formed a half-chamber as shown in Figure 3-6a & b. The internal cavity of a tissue-bathing chamber was custom-made to a conical cylindrical shape as shown. On the ceiling of a tissue-bathing chamber, there were two ports that formed the inlet and outlet for the re-circulating bathing solution when connected to the re-circulating bath. There were another two ports located in the middle level of a tissue-bathing chamber. The one located at the back was to be connected to the current-clamping electrode. Another port, which was close to the surface of the CBE preparation, was connected to the potential-sensing bridge (details in Section 3.4) for the *TEP* measurement. The details of the connection of electrical circuit will be discussed later in Section 3.3.2.3.

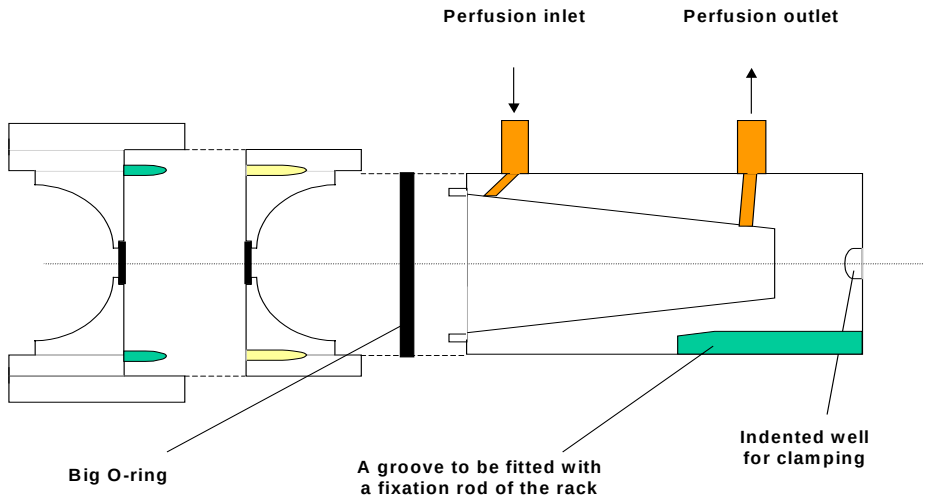

Figure 3-6a A tissue-bathing chamber viewed from the side. The assembly of the tissue-bathing chamber with the tissue-mounting block is as shown in the diagram. The ports for connecting to electric circuit have been omitted.

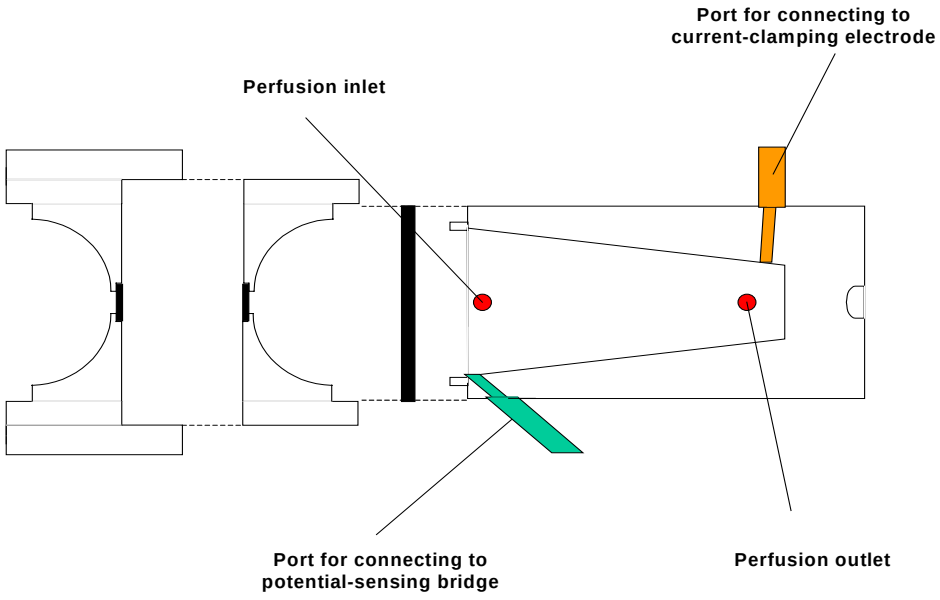

Figure 3-6b A tissue-bathing chamber viewed from the top. The assembly of the tissue-bathing chamber with the tissue-mounting block is as shown in the diagram.

A chamber-mounting rack is shown as Figure 3-7. The platform base was made of acrylic plastic while the other components were mainly metal. In the middle of the rack, there were stainless steel rods, one on each side. Each rod was conjugated to a groove on the bottom of a tissue-bathing chamber. These rods helped holding the chamber in place on assembly and avoided rotation of the whole chamber. The two screws on the opposite sides of the rack were used for clamping the whole chamber. During assembly, the two screws were advancing gently towards the shallow wells machined at the back of the tissue-bathing chamber. The screws, the shallow wells and the apertures of a chamber were all located at a horizontal level. This was important so that pressure imposing on the tissue was evenly distributed around the aperture during assembly.

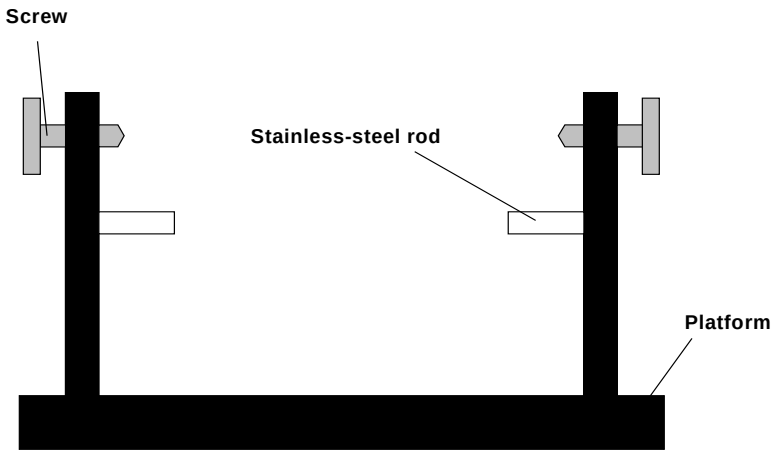

Figure 3-7 Illustrated diagram of a tissue-mounting rack.

Figure 3-8 shows the configuration of a re-circulating bath. The bath was custom-made of borosilicate glass. The bath was composed of two cavities. The outer cavity was connected, via polyvinyl chloride (PVC) tubing, to a temperature control water circulator (Freed Electronic; Haifa, Israel). The temperature of the circulated water and hence the whole bathing system was determined by the setting of the circulator. The inner cavity was filled with bathing solution and responsible for re-circulating the solution to nourish the CBE preparation. The tops of both inner cavities were opened for solution filling and interventions such as introduction of drugs, radiotracers. Stirring of bathing solution was accomplished by bubbling in the direction as shown in Figure 3.8. The gas used in the present work was atmospheric air and the flush of air was generated by air pump. PVC tubing (01-94-1583; AlteVin Laboratory PVC tubing, Altec, UK) completed the connection between the re-circulating bath and the tissue-bathing chamber.

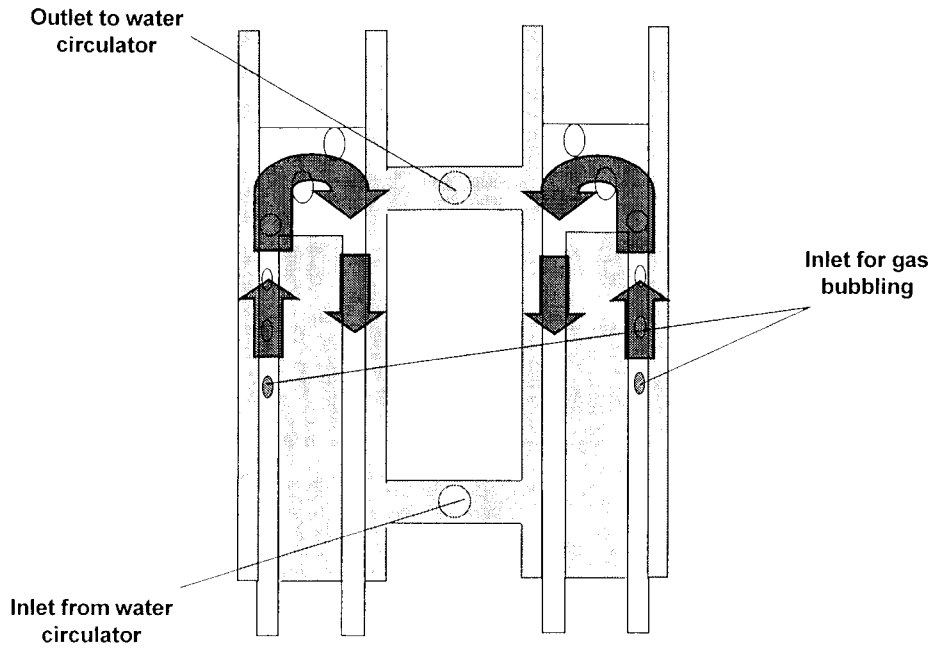

Figure 3-8 A simplified diagram of a re-circulating bath. The area in grey is the outer cavity while the area in white is the inner cavity. The circulation of bathing solution was in the direction as indicated by the arrows.

3.3.2.2 Tissue mounting in the ORC chamber

Before tissue mounting, a layer of silicone grease was applied on the surface of both mounting blocks with the O-ring in place in aperture. The smaller block was first laid flat on a table. An isolated CBE was then carefully transferred to the surface of the mounting block with the aqueous side facing upward. The CBE was positioned properly so that only the pars plicata region was included in the aperture. The bigger block was then gently applied from above, guided by the two fixation rods. Finally, the two mounting blocks were assembled. The assembled mounting blocks were then fitted

with the tissue-bathing chambers from both sides. The junctions between the tissue-mounting blocks and the tissue-bathing chambers were also filled with silicone grease to prevent leak.

The whole assembled chamber was transferred to the chamber-mounting rack. Firstly, it was sitting temporarily with the machined grooves fitted with the fixation rods on the rack. After proper positioning, the screws at the back of each side were advanced gradually. The PVC tubing adjoining the re-circulating bath and the tissue-bathing chamber were connected. Ringer solution was filled into the two half-chambers via the potential sensing ports until solution reached the top of the four L-shape connectors as shown in the inset of Figure 3-9. The screws would be tightened sufficiently if there was leakage of Ringer solution. The current-clamping electrodes and potential-sensing bridge were then connected as mentioned later in Section 3.3.2.3. Leakage was checked for again and Ringer solution was filled continuously via the openings of each re-circulating bath. Finally, the bathing solution was bubbled with the air pump connected. The final volume of each bath was 20 ml.

3.3.2.3 Monitoring of the transepithelial electrical parameters in the ORC chamber

The connections for the electrical measurement are showed in Figure 3-9. Connections between the tissue-bathing chamber and the electrodes / potential-sensing bridge were all via a component consisting of a L-shape plastic connector and PVC tubing (01-94-1596; AlteVin Laboratory PVC tubing, Altec, UK). Through this component, the ports near to the CBE on each side of the tissue-bathing chamber were connected to the potential-sensing bridge (details in Section 3.4). This circuit of potential-sensing bridge monitored the spontaneous *TEP*. The ports at the back of each

tissue-bathing chamber were connected to current-clamping electrodes (EKC; World Precision Instruments, Sarasota, USA) via the L-shape component. The current-clamping electrode was comprised of a Ag / AgCl electrode and a polyethylene cartridges filled with 154mM NaCl, 3% polyacrylamide gel as conducting medium. This circuit allowed an external current to pass through the preparation. The transepithelial electrical parameters were measured by a dual voltage current clamp (DVC-1000). The settings of DVC-1000 such as periodic current clamping and fluid resistance compensation were same as in the experiment of CP (Section 3.3.1.3). The effects of transport inhibitors were studied when the electrical parameters were stabled for over 15 minutes.

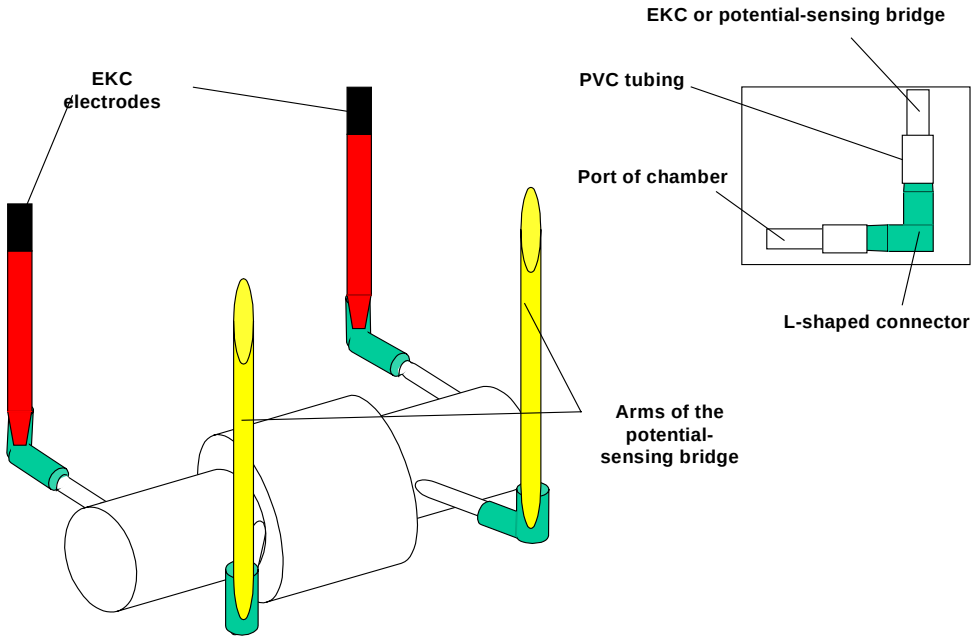

Figure 3-9 An illustrated diagram of the electrical circuit connection in an ORC chamber. Note that the tissue-mounting blocks have been simplified. The inset is an illustration of the connection bridged by the L-shaped connector and PVC tubing.

3.3.2.4 Study of isotopic Cl^- fluxes in the ORC chamber

As in the experiment of the CP, only paired preparations from the same eye attaining comparable electrical parameters were used for the study of isotopic fluxes. The measurements of unidirectional isotopic fluxes in both basal and drug-treated conditions were performed in the same preparation sequentially. This protocol allowed a direct comparison of the unidirectional ion fluxes in drug-treated condition to its own basal fluxes and therefore minimized the error due to variations among different preparations. The net fluxes (J_{net}) in both basal and drug-treated conditions were the differences between the two unidirectional fluxes: stromal-to-aqueous fluxes (J_{sa}) and aqueous-to-stromal fluxes (J_{as}).

Before the addition of radiolabeled tracers, the background radioactivity of all bathing sides was counted. Isotopic fluxes measurement would be conducted if the background counts were within the normal limit.

For the J_{sa} measurement, radiolabeled [^{36}Cl] (0.67 μCi / ml Ringer solution) and [^{3}H] L-glucose (0.6 μCi / ml Ringer solution) were pipetted into the stromal-side bath while for the study of J_{as}, radiolabeled tracers of equal amount were pipetted into the aqueous-side bath. The bathing side with radiolabeled tracers added was designated the "hot" side while the one without was the "cold" side. After 60 minutes of equilibration, the preparations were short-circuited by applying the voltage clamp function of the DVC-1000 as mentioned in the experiment of the CP. The first data sampling for determination of unidirectional ion fluxes was taken after around 20 minutes of short-circuiting. The I_{sc} changes were recorded throughout the whole experiment by a pen-recorder.

The procedures of samples taking for the “cold” and “hot” bath were different. For the “cold” side, samples were taken in every 20 minutes when the air bubbling was turned off. 2 ml of the bathing solution in the “cold” side was pipetted into a blank scintillation vial (986542; Wheaton, USA). Concurrently, 2 ml of the bathing solution in the “hot” side was withdrawn into a 2.5 ml plastic syringe (Plastipak®; Becton Dickinson, Dublin, Ireland). This manoeuvre reduced the effect of unequal hydrostatic pressure on the tissue due to unequal volume in the two baths. As the sampling finished, 2 ml of fresh Ringer solution was refilled into the “cold” side. In the “hot” side, the bathing solution in the plastic syringe was re-introduced into the re-circulating bath simultaneously. For drug-treated condition, the refilled solution would contain the same concentration of the drugs as in the bath. Bubbling of the bathing solution was resumed until the next sampling. Altogether, 4 samples were taken from the “cold” side before the incubation of drugs and 7 to 8 samples were collected thereafter.

For the “hot” side, samples were taken at the start and in the end of both the basal and drug-treated conditions. Each sample of 20 μl was taken by a pipette. As the amount was small (about 0.1% of total), no refill of fresh bathing solution was required. The 20 μl sample was injected into 1980 μl fresh Ringer solution preloaded in a scintillation vial to become 2 ml. The radioactive counts of the 2 samples collected from the “hot” bath would indicate if there was leakage during the experiment, in both basal and drug-treated conditions.

All samples collected were mixed well with 15 ml of scintillation cocktail (NBCS104; Amersham Radiochemicals, England) and the radioactivity in each sample was counted by a liquid scintillation counter (Wallac 1414 Winspectral DSA; Wallac, Helsinki, Finland). Some drugs used in the present work exerted quenching effect on scintillation counting. The extent of the quenching effect was predetermined by

comparing the total count in two groups of Ringer solution samples containing equal amount of radiotracers. One group contained no drug while another group contained the same concentration of the drug as used in the isotopic fluxes experiment. The differences found between the two groups were used for correcting the error due to the quenching effect. The [^{3}H] L-glucose fluxes concurrently monitored would again indicate if there was substantial paracellular leakage during experiment.

For the samples from the "cold" bath, the difference in radioactivity between 2 consecutive samples was first translated into the increase of radioactivity (ΔC) in the whole "cold" bath during the period (T) between the 2 samplings. On the other hand, the radioactivity in the 2 samples taken in the same condition from the "hot" bath were averaged and converted to the average total radioactivity (H) in the "hot" bath during that condition. The unidirectional ion fluxes were calculated by the following equation:

$$J = \frac{\Delta C \times I \times V}{H \times T \times A} \qquad (3.2)$$

where J = unidirectional flux of the studied ion

ΔC = increase in radioactivity in "cold" bath during period T (counts per minute)

H = average total radioactivity in "hot" bath (counts per minute)

I = concentration of the studied ion in the bathing solution (mM)

V = volume of "cold" sample taken (ml)

A = cross-sectional area of the chamber aperture (cm^2)

T = period between 2 consecutive samples (hr)

The 4 samples taken from the "cold" side during the basal condition were therefore translated into unidirectional ion fluxes in 3 consecutive 20 minutes period while the 7 to 8 samples taken during the drug-treated condition were translated into

fluxes data of 6 to 7 consecutive 20 minutes period. The mean unidirectional Cl^- flux across a preparation during the basal and drug-treated condition was averaged from these consecutive samples. The unit of unidirectional Cl^- flux is $\mu Eqhr^{-1}cm^{-2}$.

3.4 The potential-sensing bridge

Figure 3-10 is an illustrated diagram of a potential-sensing bridge. This device was comprised of 5 PVC tubing (Nalgene®180; Nalge Nunc International Corp., Rochester, NY, USA), 2 three-ways stopcocks, and 2 Ag / AgCl electrodes (EKV; World Precision Instruments, Sarasota, USA). The polyethylene cartridges of both EKV were filled with 154mM NaCl, 3% polyacrylamide gel as conducting medium. The male luer tip of the EKV was then fitted into the upper PVC tube, one on each side. The inside of the two upper PVC tube were filled with 154mM NaCl solution. In the beginning of an experiment, the two lower PVC tubes and the horizontal PVC tube were filled with fresh Ringer solution used for tissue bathing. The two lower PVC tubes were then fitted into the connectors for the *TEP* measurement in either the CP or ORC types chamber.

This device has two main advantages. First, there was no direct contact between electrodes and bathing solution. Thus, possible trace elements leak from electrode to bathing solution and tissue were minimized. Second, electrical drift between the two electrodes can be easily nullified by manipulating the two 3-ways stopcocks as shown in Figure 3-10a & b.

In Figure 3-10a, the two 3-ways stopcocks were so adjusted that the preparation was included in the circuit and the electrodes via the potential-sensing bridge measured the *TEP* across the tissue. From time to time, the two 3-ways stopcocks were switched to the position as shown in Figure 3-10b. Under this setting, the tissue was excluded from the circuit. Instead, the potential difference between the two ends of the horizontal PVC tube was measured. Any difference found in this situation must be due to electrical drift and was nullified by adjusting the “input offset” knob on the panel of

DVC-1000. This function was important that the real changes of the electrical properties across the preparation could be distinguished from the electrical drift of the two electrodes.

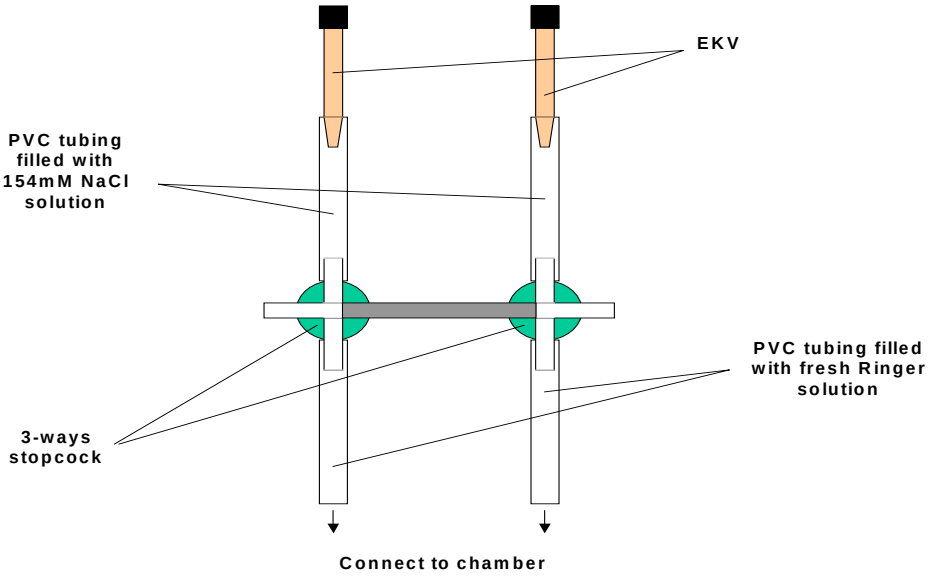

Figure 3-10a The potential-sensing bridge with its 3-ways stopcocks set for measurement of the *TEP*.

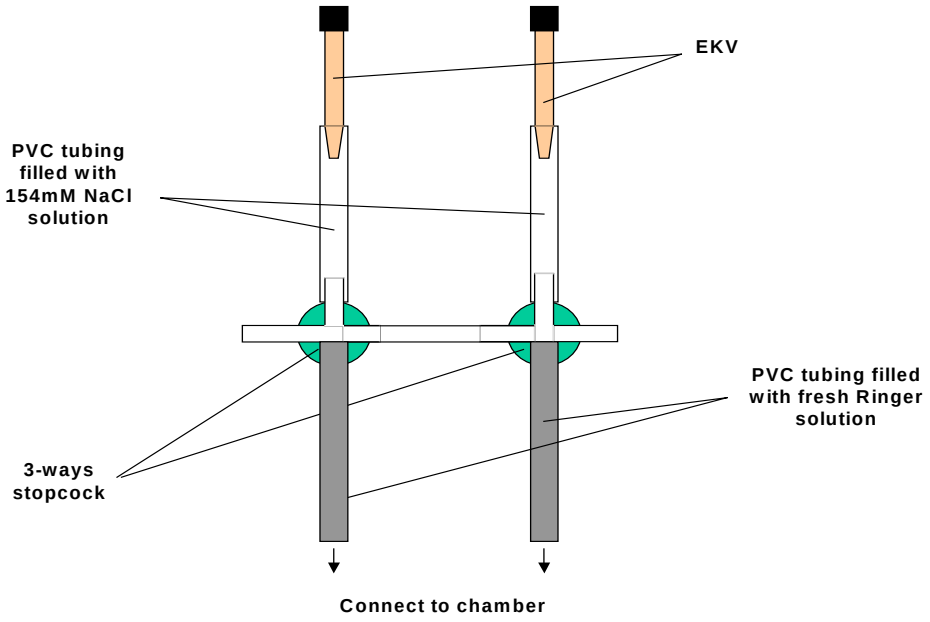

Figure 3-10b The potential-sensing bridge with its 3-ways stopcocks set for monitoring the electrical drift between the two EKV electrodes.

3.5 Relationship between the net ion fluxes (J_{net}) and short-circuit current (I_{sc}).

The current attributes to the active transport of a specific ion (I_{ion}) can be converted from the average J_{net} found under short-circuited condition according to the equation below:

$$I_{ion} = J_{net} \times z \times F \tag{3.3}$$

where z is the valence of the ion and F is the Faraday's constant.

Theoretically, if there is only one specific ion undergoing transepithelial active transport, the measured I_{sc} would be equal to the I_{ion}. For instance, the I_{sc} across frog skin was almost equal to the sole transport of sodium ions (Ussing and Zerahn, 1951).

3.6 Bathing solution and preparation of pharmacological agents

All chemical reagents were obtained from Sigma-Aldrich, Inc., USA unless otherwise stated. The bathing solution in the present experiment was standard Normal Ringer (NRR) solution contains (mM): NaCl 113.0, KCl 4.56, $NaHCO_3$ 21.0, $MgSO_4$ 0.6, D-glucose 7.5, Reduced glutathione 1.0, Na_2HPO_4 1.0, HEPES 10.0, $CaCl_2$ 1.4. The pH was adjusted to 7.4.

In the ion substitution experiment, the ion was substituted with equimolar gluconate or cyclamate.

Most reagents used were freshly dissolved in the respective solvent on the day of experiment. Ouabain and sodium nitroprusside (SNP) were freshly dissolved in double distilled water (DDH_2O). Bumetanide (BMT), furosemide (FSM), heptanol, niflumic acid (NFA), 4,4'-diisothiocyanatostilbene-2,2'-disulfonic acid disodium salt (DIDS) and 5-nitro-2-(3-phenylpropylamino)-benzoic acid (NPPB) were dissolved in dimethyl sulfoxide (DMSO).

Other chemicals were prepared as stock solution and diluted to the required concentration for use. These included: 8-(4-chlorophenylthio)guanosine 3':5'-cyclic monophosphate sodium (8-pCPT-cGMP) in DDH_2O, S-nitroso-N-acetylpenicillamine (SNAP) and 1H-[1,2,4]Oxadiazolo[4,3-a]quinoxalin-1-one (ODQ) in DMSO, 1-aminobenzotriazole (ABT) in ethanol. These stock solutions were stored for no more than a month.

The final concentration of the above stated solvents in the bathing solution were: DDH_2O (< 1%), DMSO (< 0.15%) and ethanol (< 0.3%).

Radiolabeled Cl^- [^{36}Cl] in the form of hydrochloric acid (HCl) was obtained from PerkinElmer, Inc., USA and Risø National Laboratory, Denmark.

3.7 Statistical analysis

All data are presented as the mean ± S.E.M. Statistical analyses were performed by GraphPad InStat version 3.00, GraphPad Software, San Diego California USA, www.graphpad.com. Student's t-test was used to compare the mean values of two groups. For cases with multiple comparisons, ANOVA were applied. Significance was considered as $P < 0.05$.

CHAPTER 4

RESULTS

4.1 Viability of the isolated porcine CBE

As mentioned in Section 3.3, two different types of modified Ussing-Zerahn-type chamber, namely the CP and ORC, were used in this study. The viability of the *in vitro* porcine CBE in both types of chamber has been assessed according to three criteria. These criteria aimed to ascertain that the preparations were functionally and structurally intact in the chambers. The three criteria were: (1) maintenance of stable transepithelial electrical parameters, (2) presence of characteristic electrical responses by ouabain, and (3) small diffusional L-glucose leak. Over 80% of the preparations mounted achieved stable electrical parameters. In these preparations, the characteristic ouabain-induced electrical responses and small diffusional L-glucose leak were also evident.

4.1.1 Maintenance of the transepithelial electrical parameters

Once an isolated porcine CBE was mounted in the chamber with bathing solution on both sides and electrical circuit completed, electrical parameters including the spontaneous *TEP* and R_t were continuously monitored. The electrical parameters were usually stable after an equilibration period of about 45 to 60 minutes and could be maintained for at least 3 hours in the CP chamber and at least 5 hours in the ORC

chamber. The duration was adequate for our investigation. Figure 4-1 shows typical transepithelial electrical parameters with time of the isolated porcine CBE in our modified Ussing chamber. Our preliminary data have shown that preparations with steady-state *TEP* smaller than -0.20 mV or R_t smaller than 50 Ωcm^2 were usually less responsive to various pharmacological agents and the electrical parameters deteriorated quickly as well.

4.1.2 Characteristic electrical responses by ouabain

Ouabain is a specific inhibitor of the Na^+,K^+-ATPase. As shown in Figure 4-1, bilateral (BS) ouabain produced typical biphasic responses of the *TEP* and I_{sc}. Ouabain transiently hyperpolarized the *TEP* and I_{sc} that peaked at about 30 minutes. The peak I_{sc} was on average 136% of the baseline value (Student's paired t-test, $p < 0.01$, $n = 32$). Both the *TEP* and I_{sc} depolarized gradually towards zero subsequently. This characteristic biphasic response indicated that the two populations of Na^+,K^+-ATPases on the basolateral membranes of the PE and NPE cells were functionally intact even after 5 hours in the chamber. In addition to its effects on the *TEP* and I_{sc}, ouabain (1mM, BS) also significantly reduced the R_t slightly by about 5% (Student's paired t-test, $p < 0.01$, $n = 32$).

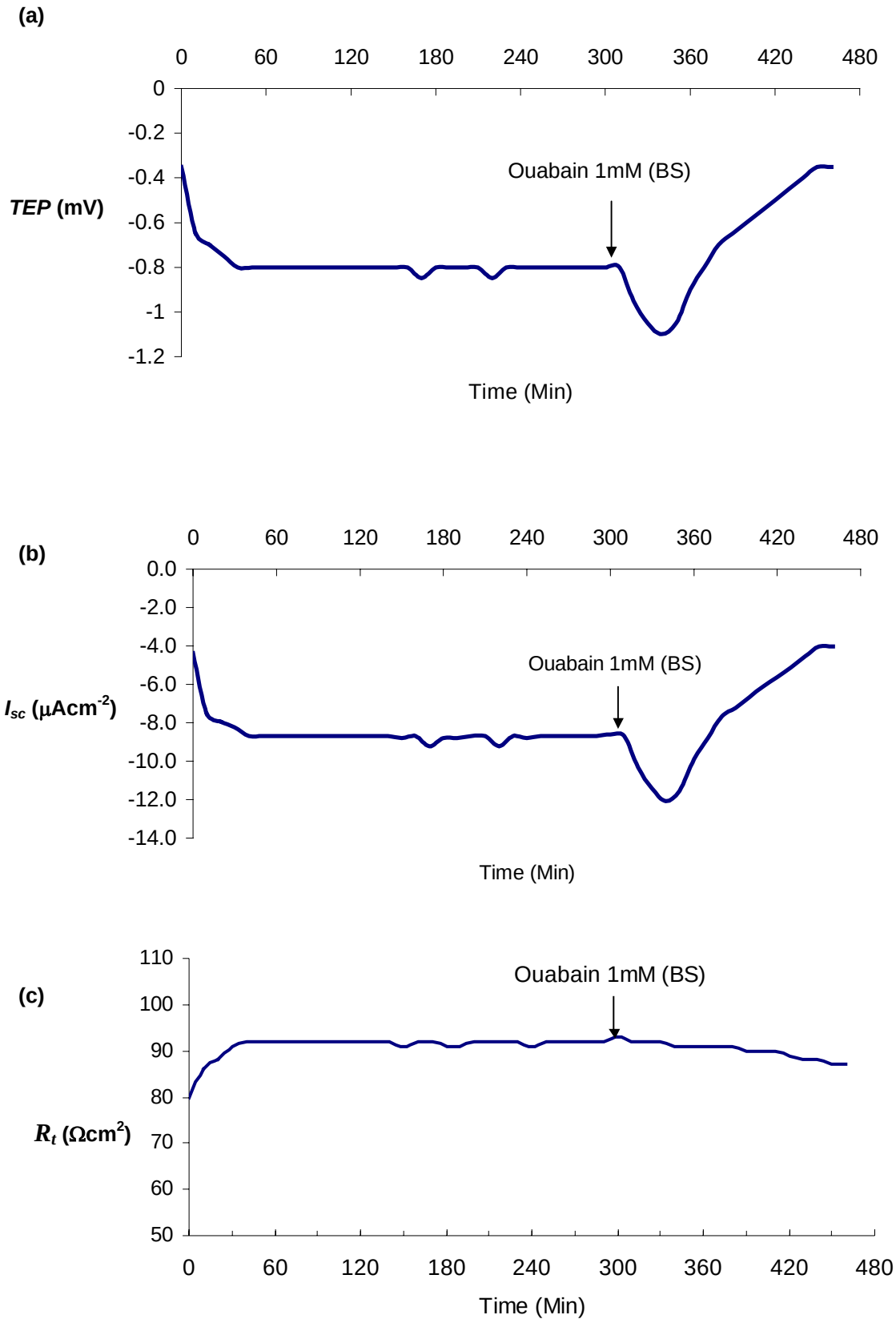

Figure 4-1 A typical time-course of the (a) *TEP*, (b) I_{sc}, and (c) R_t across the isolated porcine CBE. Ouabain (1mM) was introduced into the bathing solution bilaterally (BS) as indicated by the arrow.

4.1.3 Diffusional L-glucose leak

Quantitative analysis of the unidirectional L-glucose leak across an epithelial layer is a way to study its structural integrity. The rationale of this application is that most cells do not transport L-glucose and therefore the movement of L-glucose across an epithelium is paracellular either via the intercellular junctions or the induced edge damages (DiMattio and Streitman, 1986). Table 4-1 is a summary of the unidirectional L-glucose leak across the porcine CBE mounted in our modified Ussing chambers. The average unidirectional L-glucose leak was about 48 $\eta molh^{-1}cm^{-2}$ with the CP chamber (n = 12) and 54 $\eta molh^{-1}cm^{-2}$ with the ORC chamber (n = 218). The small paracellular leak of L-glucose suggested that the *in vitro* porcine CBE were structural intact in the chambers. This small paracellular leak of L-glucose also indicated that the porcine CBE should be categorized as tight epithelia.

		Stromal-to-aqueous (J_{sa})		**Aqueous-to-stromal (J_{as})**	
Chamber type	**n**	**L-glucose leak ($\eta molh^{-1}cm^{-2}$)**	**R_t (Ωcm^2)**	**L-glucose leak ($\eta molh^{-1}cm^{-2}$)**	**R_t (Ωcm^2)**
CP	6	52 ± 7	82 ± 10	43 ± 5	82 ± 8
ORC	109	54 ± 1	84 ± 1	53 ± 1	85 ± 1

Table 4-1 A summary of the unidirectional [^{3}H]-L-glucose leak measured under short-circuited condition in both CP and ORC types modified Ussing chambers. Values are given as mean ± SEM.

4.2 Steady-state basal transepithelial electrical parameters

Steady-state basal transepithelial electrical parameters in our experiments are summarized in Table 4-2. The spontaneous *TEP* found was approximately 1 mV with the aqueous side of the isolated porcine CBE consistently negative with respect to the stromal side. This polarity indicated that either there was a net transport of anion in the direction of stromal-to-aqueous or a net transport of cation in the opposite direction or both. However, in view of the direction of AHF in the eye, the existence of a net anionic transport from the stroma to aqueous is a more logical and plausible deduction.

The transepithelial electrical parameters of the isolated porcine CBE in both CP and ORC chambers were comparable and the changes induced by various pharmacological agents in both chamber types were qualitatively similar. The higher average R_t in the preparations in the ORC chamber may be due to the implementation of O-rings around the mounting apertures that had effectively reduced mechanically induced edge damages.

Chamber type	**n**	***TEP* (mV)**	**I_{sc} (μAcm^{-2})**	**R_t (Ωcm^2)**
CP	226	-1.17 ± 0.03	-15.77 ± 0.44	75 ± 1
ORC	448	-1.03 ± 0.02	-12.36 ± 0.24	85 ± 1

Table 4-2 Steady-state basal transepithelial electrical parameters of the isolated porcine CBE in the CP and ORC chambers. Values are given as mean ± SEM.

4.3 Effects of ion substitution on the transepithelial electrical parameters

As mentioned in section 4.2, the aqueous-negative *TEP* across the isolated porcine CBE probably indicated a net anionic transport from the stroma to aqueous. Therefore, we investigated the effects of anion substitution in the bathing solution on the transepithelial electrical parameters. These experiments were performed in the CP chamber. In that, anions in the bathing solution were substituted by equimolar gluconate or cyclamate whilst the pH and the osmolarity of the bathing solution were maintained.

4.3.1 Bilateral chloride (Cl^-) substitution

In this experiment, equimolar gluconate or cyclamate was used to replace the Cl^- ion in the normal bathing solution (120mM Cl^-). The effects were the same when either gluconate or cyclamate used. Upon perfusion of low Cl^- solution to the preparation, a transient hyperpolarization of the *TEP* and I_{sc} was first noted which was followed by a steady-state depolarization of the *TEP* and I_{sc}. Figure 4-2 shows a typical I_{sc} response with time across the isolated porcine CBE preparation in Cl^- substitution experiment. For the time being, we will focus the discussion on the steady-state effects and discuss the transient changes later on in Section 5.4. Table 4-3 is a summary of the steady-state electrical parameters in bathing solution of different Cl^- concentrations. Our results showed that the I_{sc} across the porcine CBE was dependent on the bathing Cl^- concentration. On average, the I_{sc} depolarized by 35% and 63% from its own basal

when the bathing Cl^- concentration was reduced to 60mM and 30mM respectively. Moreover, it was also noted that the R_t increased in low bathing Cl^- conditions.

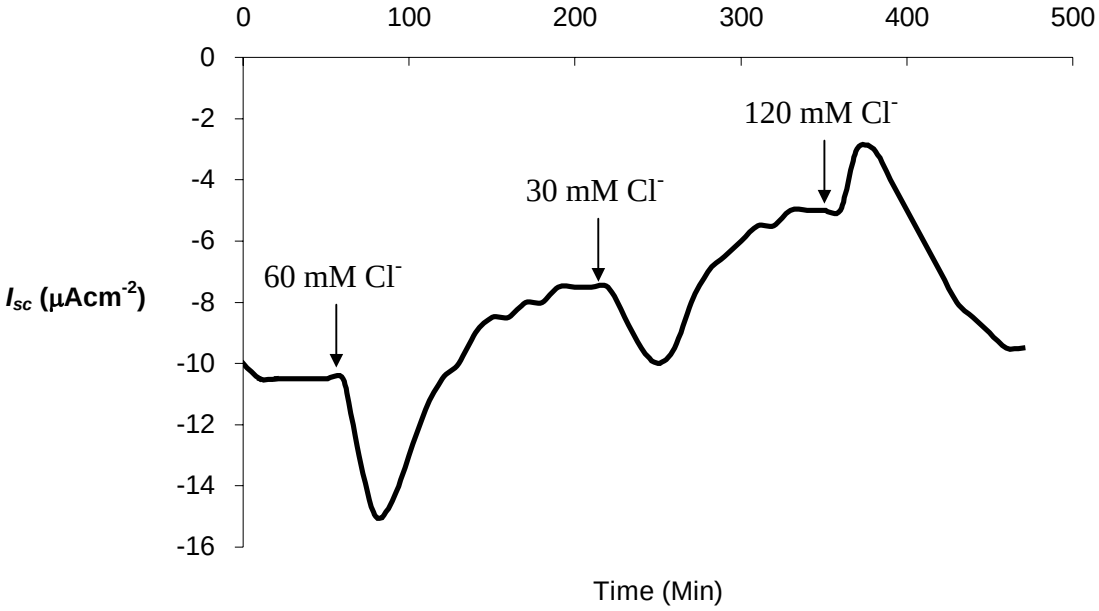

Figure 4-2 A typical time-course of the I_{sc} across the isolated porcine CBE when the bathing Cl^- concentration was changed sequentially as indicated by the arrows.

		***TEP* (mV)**		**I_{sc} (μAcm^{-2})**		**R_t (Ωcm^2)**	
	n	**Basal**	**Low Cl^-**	**Basal**	**Low Cl^-**	**Basal**	**Low Cl^-**
60mM Cl^-	15	-1.36 ±0.09	-0.95** ±0.09	-17.43 ±1.23	-11.25** ±1.14	79 ±4	87* ±8
30mM Cl^-	6	-1.18 ±0.25	-0.48** ±0.23	-15.63 ±2.91	-5.86** ±2.66	76 ±9	88* ±9

Table 4-3 Effects of bathing Cl^- concentration on the steady-state electrical parameters across the isolated porcine CBE in the CP chamber. Values are given as mean ± SEM.

* $p < 0.05$, ** $p < 0.01$ (Student's paired t-test compared with basal)

4.3.2 Bilateral bicarbonate (HCO_3^-) substitution

The bathing HCO_3^- (21mM) was substituted by equimolar gluconate to produce bicarbonate-free (BCF) solution. Our results showed that the BCF bathing environment abolished the *TEP* and I_{sc}, and reduced the R_t by approximately 8%. Table 4-4 is a summary of the effects of BCF condition on the transepithelial electrical parameters.

	***TEP* (mV)**		**I_{sc} (μAcm^{-2})**		**R_t (Ωcm^2)**	
n	**Basal**	**BCF**	**Basal**	**BCF**	**Basal**	**BCF**
6	-1.52 ±0.07	0.00** ±0.10	-18.88 ±1.85	-0.30** ±1.41	84 ±6	77** ±6

Table 4-4 Effects of BCF condition on the transepithelial electrical parameters across the isolated porcine CBE in the CP chamber. Values are given as mean ± SEM.

** $p < 0.01$ (Student's paired t-test compared with basal)

4.4 Chloride (Cl^-) transport across the isolated porcine CBE

The Cl^- transport was studied with both CP and ORC chambers. In all isotopic fluxes experiments, paired preparations attaining comparable electrical parameters were used. Each of the paired preparations was used for the study of the unidirectional Cl^- fluxes of stromal-to-aqueous (J_{sa}Cl) and aqueous-to-stromal (J_{as}Cl) respectively. The steady-state basal Cl^- fluxes across the porcine CBE are summarized in Table 4-5. With either chamber type, the J_{sa}Cl were significantly larger than the J_{as}Cl. Thus there was a net Cl^- transport of about 1.0 $\mu Eqh^{-1}cm^{-2}$ in the stromal-to-aqueous direction (J_{net}Cl) in the steady-state basal condition.

		Stromal-to-aqueous (J_{sa})			**Aqueous-to-stromal (J_{as})**			**Net Cl^- flux (J_{net})**
	n	**Cl^- flux**	**R_t**	**LG**	**Cl^- flux**	**R_t**	**LG**	**($\mu Eqh^{-1}cm^{-2}$)**
CP	6	3.70 ±0.23	82 ±10	52 ±7	2.70 ±0.18	82 ±8	43 ±5	1.00** ±0.18
ORC	109	5.15 ±0.09	84 ±1	54 ±1	4.14 ±0.07	85 ±1	53 ±1	1.01*** ±0.08

Table 4-5 Steady-state basal Cl^- fluxes across the isolated porcine CBE. Values are given as mean ± SEM. LG stands for L-glucose leak. The unit of Cl^- flux, R_t and LG is $\mu Eqh^{-1}cm^{-2}$, Ωcm^2 and $\eta molh^{-1}cm^{-2}$, respectively. The R_t and LG of the J_{sa} preparations were not significantly different from that of the J_{as} preparations.

** $p < 0.01$; *** $p < 0.001$ (Student's paired t-test, J_{sa} compared with J_{as})

4.5 Effects of transport inhibitors on the transepithelial electrical parameters and Cl^- transport across the isolated porcine CBE

The effects of various transport inhibitors on the transepithelial electrical parameters and Cl^- transport were obtained with the ORC chamber. In the Cl^- transport experiments with the ORC chamber, the steady-state basal Cl^- transport across a preparation was studied in the first hour. After that, the tested reagent was introduced and the drug-treated steady-state Cl^- transport was determined. Therefore, the pre- and post-drug Cl^- transport can be directly compared within the same preparation. This intra-preparation comparison would minimize the problem due to inter-preparation variations. Paired preparations attaining comparable transepithelial electrical parameters are essential for meaningful comparison of the unidirectional Cl^- fluxes of opposite directions (J_{sa} and J_{as}). The detailed steady-state basal electrical parameters of the paired preparations used for each experiment are summarized in the Appendix.

4.5.1 Effects of time and DMSO on the transepithelial electrical parameters and Cl^- transport

Possible decay with time and DMSO may complicate the analysis of the effects of the reagents used in our experiment. Therefore, it is crucial to determine their effects. Results from the two control experiments below suggested that the transepithelial electrical parameters and Cl^- transport across the isolated porcine CBE were not affected by time and DMSO. As a consequence, the changes induced in our later experiments of various transport inhibitors can be attributed to the drugs solely.

4.5.1.1 Effects of time

As the steady-state basal and drug-treated Cl^- transport were to be studied sequentially in the same preparation, the stability of the Cl^- transport throughout the study period would be important for meaningful comparison. Therefore, the effects of time on the transepithelial electrical parameters and Cl^- transport were studied for 3 hours. It was the duration required for studying the basal and drug-treated Cl^- transport sequentially. Figure 4-3 is a summary of the transepithelial electrical parameters across the porcine CBE after stabilization and at the end of experiment (3 hours later). There was no significant change in the transepithelial electrical parameters during the course of experiment. The hourly average basal Cl^- fluxes are summarized in Figure 4-4 and all the unidirectional and net Cl^- fluxes were stable during the study period. A statistically significant ($p < 0.05$) steady-state net Cl^- flux in the stromal-to-aqueous direction was evident at about 1.0 $\mu Eqh^{-1}cm^{-2}$. The fluxes data are summarized in Table 4-6.

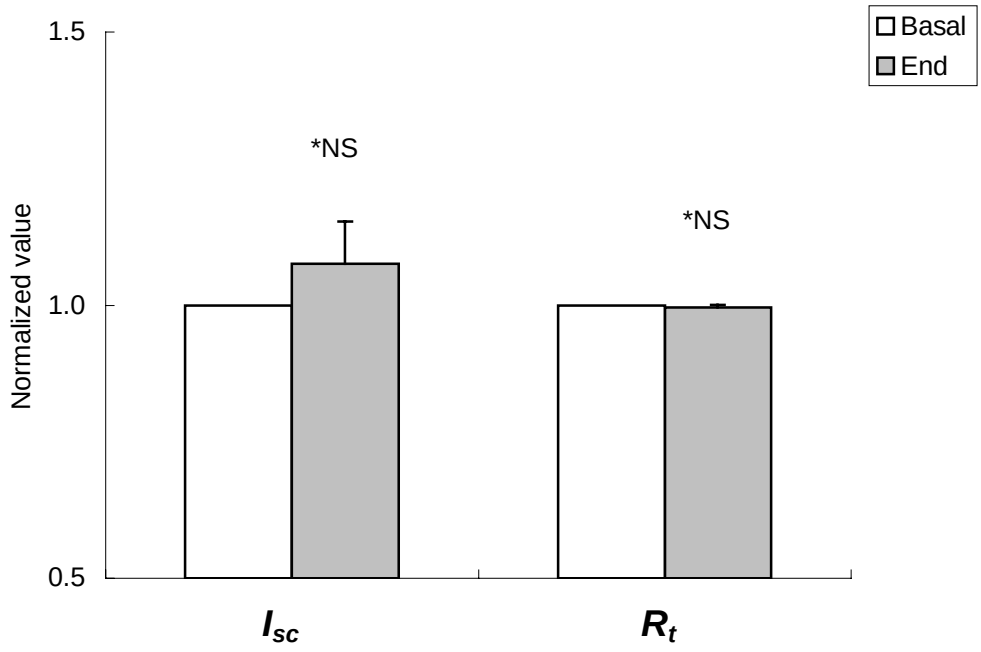

Figure 4-3 The transepithelial electrical parameters across the isolated porcine CBE upon stabilization (Basal) and 3 hours later (End) in the ORC chamber. The results are normalized and given as mean ± SEM that is denoted by the error bars (n = 22).

*NS Not significant (Student's paired t-test, End compared with Basal)

	n	Stromal-to-aqueous (J_{sa})	Aqueous-to-stromal (J_{as})	Net Cl^- flux (J_{net})
Basal average		4.97±0.24	3.97±0.23	1.00±0.33**
1st Hr average	11	5.23±0.30	4.21±0.24	1.02±0.34**
2nd Hr average		5.17±0.27	4.22±0.22	0.95±0.35*

Table 4-6 Hourly average basal Cl^- fluxes across the isolated porcine CBE. Values are given as mean ± SEM (n = 11). The unit of Cl^- flux is $\mu Eqh^{-1}cm^{-2}$.

* $p < 0.05$; ** $p < 0.01$ (Student's paired t-test, J_{sa} compared with J_{as})

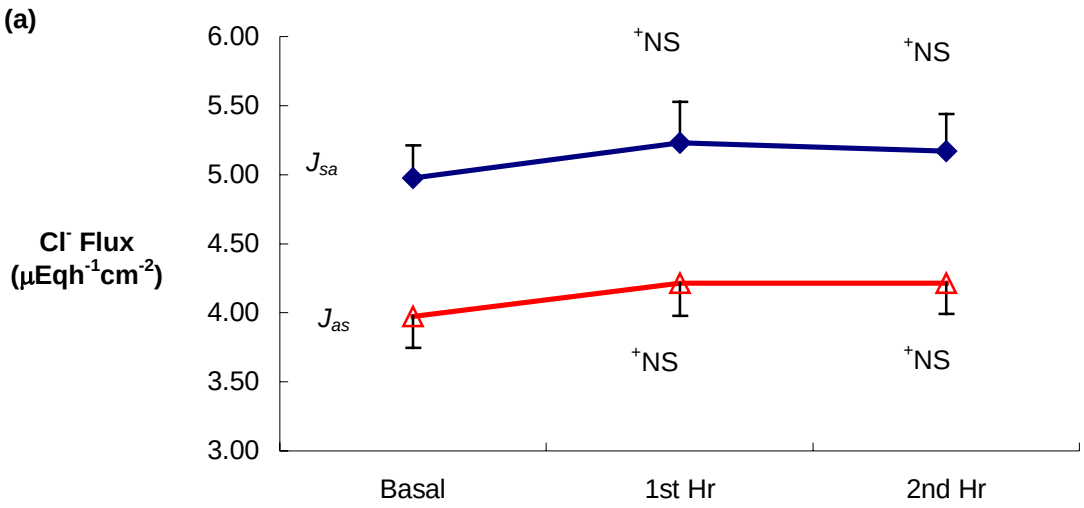

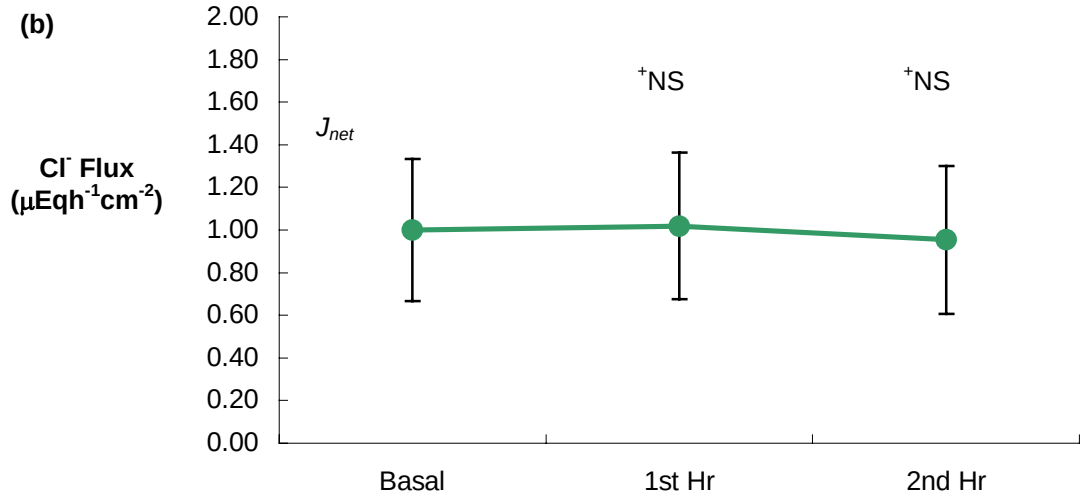

Figure 4-4 Hourly average basal (a) unidirectional, and (b) net Cl^- fluxes across the isolated porcine CBE. Values are given as mean ± SEM that is denoted by the error bars (n = 11).

$^+$NS Not significant from basal (Repeated measure ANOVA, followed by Tukey-Kramer multiple comparison test)

4.5.1.2 Effects of DMSO

DMSO were used in several occasions in our experiment for dissolving drugs. The maximum concentration of DMSO used did not exceed 0.15%. As a control, the effects of bilateral (BS) 0.15% DMSO on the preparation were studied. Figure 4-5 is a summary of the transepithelial electrical parameters before and after DMSO was added. It showed that DMSO has no effect on the I_{sc} and R_t. The effects of DMSO 0.15% (BS) on the Cl^- transport are summarized in Figure 4-6 and Table 4-7. Again, it showed that DMSO 0.15% (BS) has no effect on the Cl^- transport and a significant net Cl^- flux of about 1.3 $\mu Eqh^{-1}cm^{-2}$ was maintained throughout the course of experiment.

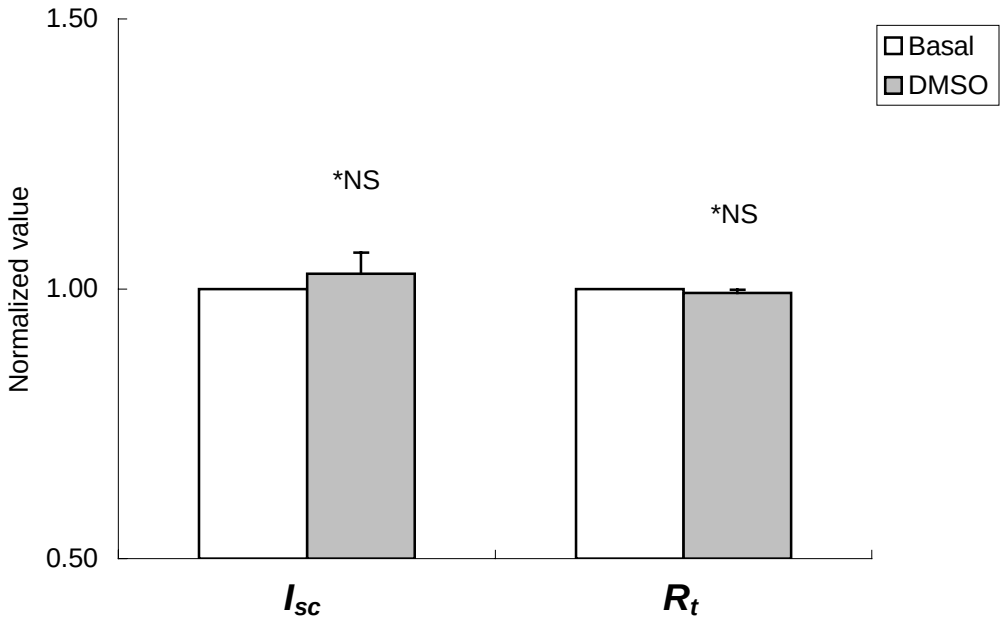

Figure 4-5 The transepithelial electrical parameters across the isolated porcine CBE before and 140 min after the addition of DMSO (BS, 0.15%). The results are normalized and given as mean ± SEM that is denoted by the error bars (n = 18).

*NS Not significant (Student's paired t-test, DMSO compared with Basal)

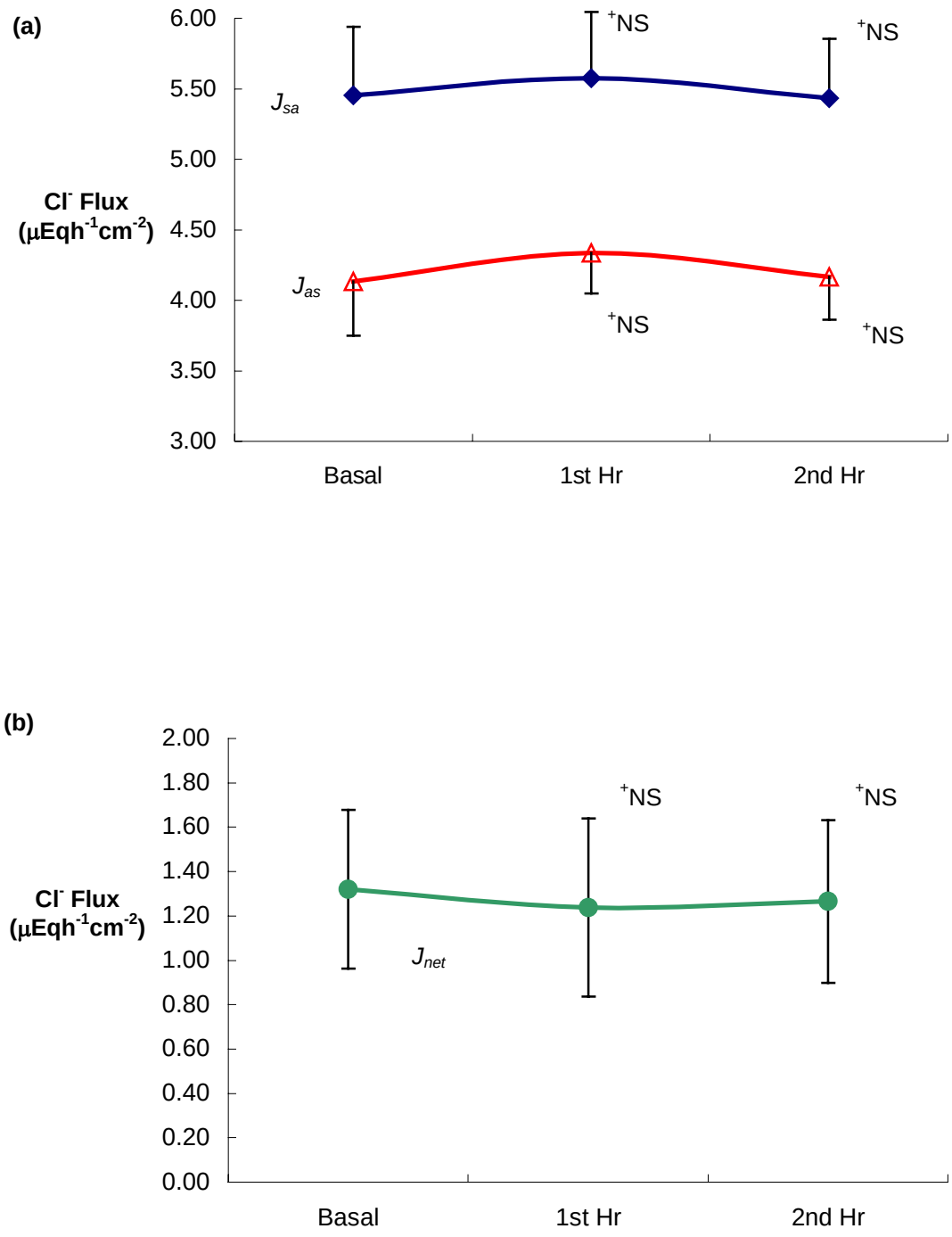

Figure 4-6 Hourly average (a) unidirectional, and (b) net Cl^- fluxes across the isolated porcine CBE in control experiment of DMSO. The basal fluxes data were obtained before DMSO added while the subsequent fluxes data were obtained after DMSO added. Values are given as mean ± SEM (n = 5). $^+$NS Not significant from basal (Repeated measure ANOVA, followed by Tukey-Kramer multiple comparison test)

	n	Stromal-to-aqueous (J_{sa})	Aqueous-to-stromal (J_{as})	Net Cl^- flux (J_{net})
Basal average		5.46±0.49	4.14±0.39	1.32±0.36*
1st Hr average	5	5.58±0.47	4.34±0.29	1.24±0.40*
2nd Hr average		5.43±0.42	4.17±0.30	1.27±0.37*

Table 4-7 Hourly average Cl^- fluxes across the isolated porcine CBE with DMSO (0.15%, BS) incubated after an hour of basal fluxes study. Values are given as mean ± SEM (n = 5). The unit of Cl^- flux is $\mu Eqh^{-1}cm^{-2}$.

* $p < 0.05$ (Student's paired t-test, J_{sa} compared with J_{as})

4.5.2 Effects of loop diuretics (FSM and BMT) on the transepithelial electrical parameters and Cl^- transport

FSM and BMT are loop diuretics commonly used as inhibitors of $Na^+/K^+/2Cl^-$ cotransporter (NKCC). In this experiment, the effects of these loop diuretics on the transepithelial electrical parameters and Cl^- transports were investigated in an attempt to test the role of NKCC on the ion transport across the porcine CBE.

4.5.2.1 Effects of FSM and BMT on the transepithelial electrical parameters

Figure 4-7 summarizes the effects of FSM (0.1mM) and BMT (0.1mM) on the I_{sc} across the porcine CBE. The effects of the two reagents were similar. Both reagents consistently depolarized the I_{sc} irrespective of the side of their addition. The inhibitory effects on the I_{sc} were smaller when the loop diuretics were added to the stromal side. Stromal (ST) FSM and BMT depolarized the I_{sc} by 15% and 32% respectively,

whereas aqueous (AQ) FSM and BMT depolarized the I_{sc} by 59% and 52% respectively. Bilateral (BS) BMT produced a slightly larger depolarization of the I_{sc} (56%) than its unilateral addition. The effects of FSM and BMT on the electrical parameters are summarized in Table 4-8.

Typical time-courses of the I_{sc} before and after BMT addition are shown in Figure 4-8. BMT (ST) depolarized the I_{sc} gradually, with the new steady state arrived at about 80 minutes while BMT (AQ) produced a much quicker depolarization that stabilized at around 40 minutes. The smaller and slower I_{sc} changes induced by the ST loop diuretics may be due to the fact that the ciliary stroma may have retarded the diffusion of the reagents to its molecular target - the NKCC.

		TEP **(mV)**		I_{sc} **(μAcm^{-2})**		R_t **(Ωcm^2)**	
Experiment	**n**	**Basal**	**Drug**	**Basal**	**Drug**	**Basal**	**Drug**
FSM (ST)	4	-0.88 ±0.14	-0.71* ±0.15	-11.60 ±1.79	-9.82* ±1.93	76 ±5	73** ±5
FSM (AQ)	4	-1.00 ±0.23	-0.40** ±0.23	-12.68 ±3.07	-5.25** ±3.17	81 ±11	77* ±9
BMT (ST)	22	-1.02 ±0.07	-0.64** ±0.07	-12.45 ±1.04	-8.44** ±1.06	85 ±4	80** ±3
BMT (AQ)	26	-0.94 ±0.08	-0.44** ±0.06	-11.35 ±0.98	-5.48** ±0.71	85 ±2	80** ±2
BMT (BS)	24	-0.96 ±0.06	-0.40** ±0.05	-11.15 ±0.72	-4.85** ±0.59	87 ±3	81** ±3

Table 4-8 Effects of FSM (0.1mM) and BMT (0.1mM) on the transepithelial electrical parameters across the isolated porcine CBE. Values are given as mean ± SEM. ST, AQ and BS stand for stromal, aqueous and bilateral addition of the tested reagent, respectively.

* $p < 0.05$; ** $p < 0.01$ (Student's paired t-test, compared with basal)

(a)

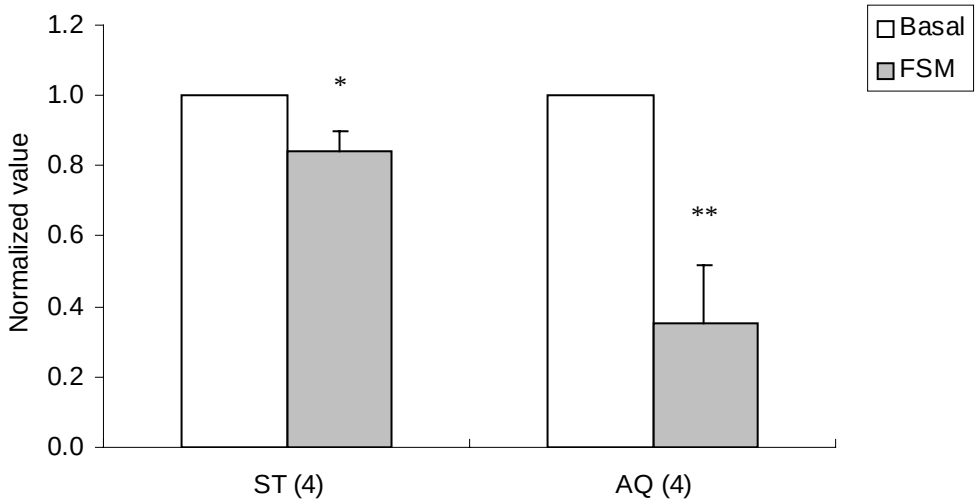

(b)

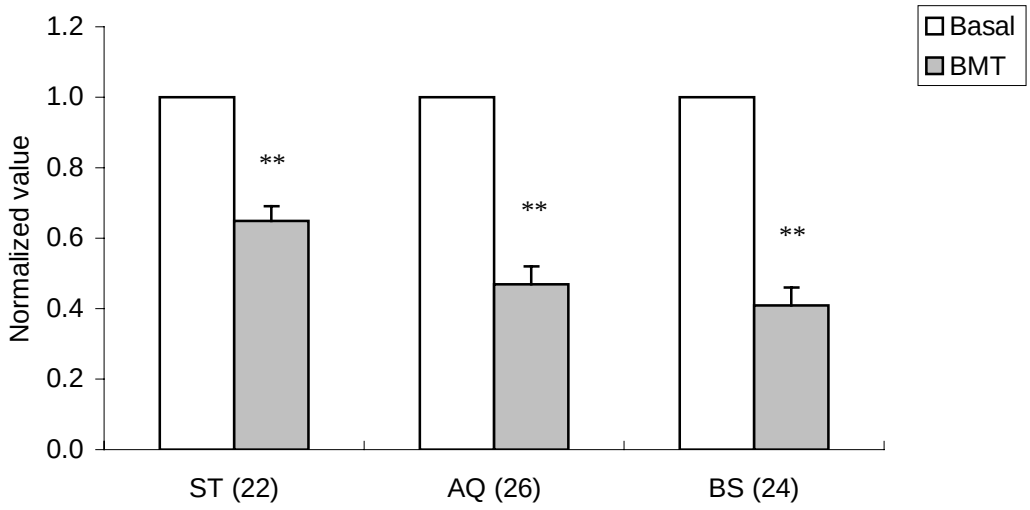

Figure 4-7 Effects of 0.1mM (a) FSM, and (b) BMT on the I_{sc} across the isolated porcine CBE. Results are normalized and given as mean ± SEM that is denoted by the error bars. The number of experiments performed is indicated as in parenthesis. ST, AQ and BS stand for stromal, aqueous and bilateral addition of the tested reagent, respectively.

* p <0.05; ** p <0.01 (Student's paired t-test, compared with basal)

(a)

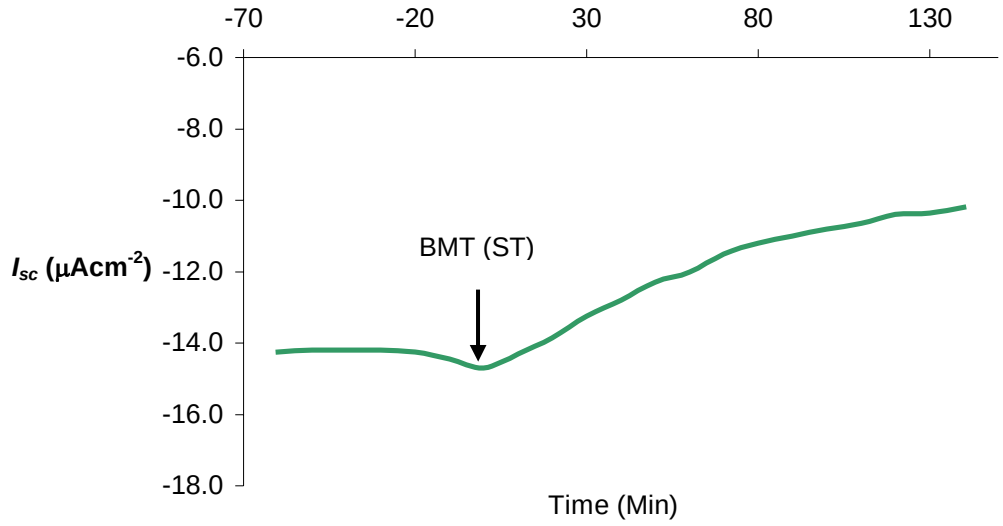

(b)

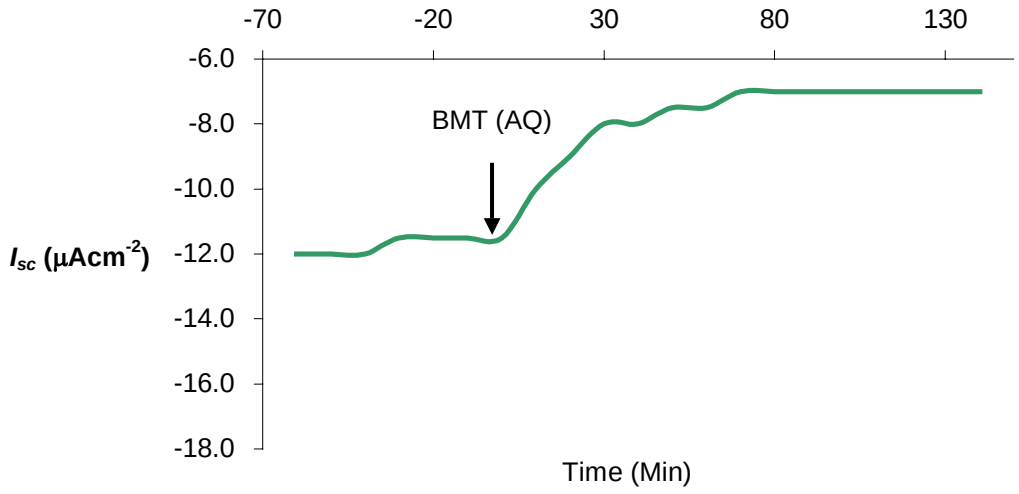

Figure 4-8 A typical time-course of the I_{sc} response of the isolated porcine CBE with (a) ST and (b) AQ BMT (0.1mM).

4.5.2.2 Effects of BMT on the Cl^- transport

The effects of BMT (0.1mM) on the net Cl^- transport in the stromal-to-aqueous direction ($J_{net}Cl$) across the porcine CBE are illustrated in Figure 4-9. BMT significantly reduced the $J_{net}Cl$ by 36% ($p < 0.05$, $n = 5$) and 46% ($p < 0.05$, $n = 8$) when it was introduced to the stromal (ST) and aqueous (AQ) side, respectively. When BMT was incubated bilaterally (BS), the $J_{net}Cl$ was reduced by 57% ($p < 0.01$, $n = 7$). Similar to its effect on the I_{sc}, the effects of unilateral incubation of BMT on the Cl^- transport were not completely additive to the bilateral effects. Instead, they were only partly additive. Table 4-9 summarizes the effects of BMT on the Cl^- transport. It should be noted that the aqueous-to-stromal Cl^- transport ($J_{as}Cl$) were significantly increased in all cases indicating that the inhibitory effects of BMT on the $J_{net}Cl$ may be partly attributed to increases in the $J_{as}Cl$, the backflux across the CBE. The increase in the $J_{as}Cl$ may be a result of increased paracellular leak since the R_t was also significant reduced by BMT treatment (Table 4-8).

(a)

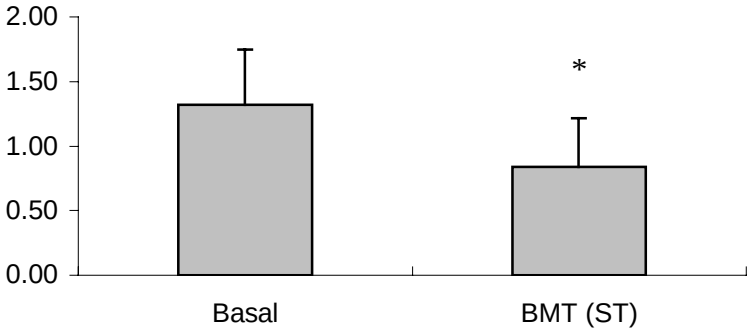

(b)

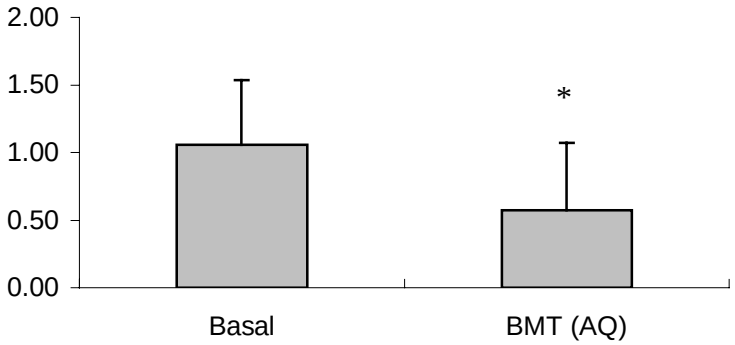

(c)

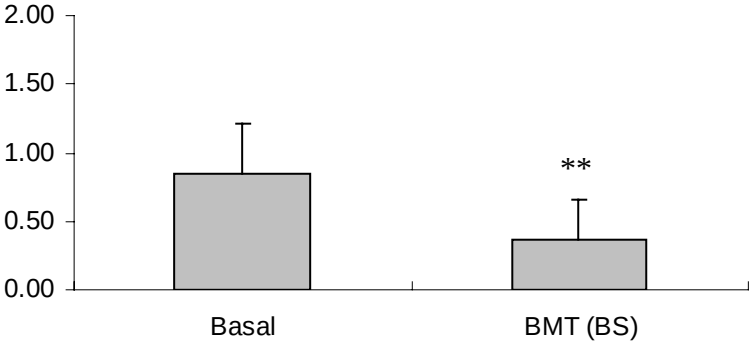

Figure 4-9 Effect of (a) ST (n = 5), (b) AQ (n = 8) and (c) BS (n = 7) BMT (0.1mM) on the J_{net}Cl across the isolated porcine CBE. Values are given as mean ± SEM. The unit of the J_{net}Cl is $\mu Eqh^{-1}cm^{-2}$. * $p < 0.05$; ** $p < 0.01$ (Student's paired t-test, BMT compared with basal)

	BMT (ST)			BMT (AQ)			BMT (BS)		
n	**5**			**8**			**7**		
Cl^-	**Basal**	**BMT**	**Δ%**	**Basal**	**BMT**	**Δ%**	**Basal**	**BMT**	**Δ%**
J_{sa}	5.35 ±0.77	5.40 ±0.80	$+1^{*NS}$	4.91 ±0.36	4.88 ±0.40	-1^{*NS}	5.56 ±0.34	5.41 ±0.35	-3^{*}
J_{as}	4.03 ±0.43	4.56 ±0.49	$+13^{*}$	3.86 ±0.27	4.32 ±0.37	$+12^{*}$	4.71 ±0.34	5.05 ±0.38	$+7^{*}$
J_{net}	$1.32^{\#}$ ±0.43	$0.84^{\#}$ ±0.38	-36^{*}	$1.06^{\#}$ ±0.48	$0.57^{\#NS}$ ±0.50	-46^{*}	$0.85^{\#}$ ±0.36	$0.37^{\#NS}$ ±0.29	-57^{**}

Table 4-9 Effects of BMT (0.1mM) on the Cl^- transport across the isolated porcine CBE. Values are given as mean ± SEM. The unit of the Cl^- transport is $\mu Eqh^{-1}cm^{-2}$.

*NS Not significant; * $p < 0.05$; ** $p < 0.01$ (Student's paired t-test, BMT compared with basal)

#NS Not significant; # $p < 0.05$ (Student's paired t-test, J_{sa} compared with J_{as})

4.5.3 Effects of DIDS on the transepithelial electrical parameters and Cl^- transport

Disulfonic stilbene DIDS is an inhibitor of Cl^-/HCO_3^- anion exchanger (AE). We studied the DIDS effects and aimed to elucidate the role of AE in the ion transport across the porcine CBE.

4.5.3.1 Effects of DIDS on the transepithelial electrical parameters

Figure 4-10 illustrates the steady-state effects of DIDS (0.1mM) on the I_{sc} across the porcine CBE and Figure 4-11 show typical time-courses of the I_{sc} response by stromal (ST) and aqueous (AQ) DIDS. DIDS (ST) did not alter the *TEP* and I_{sc} but significantly reduced the R_t by 1.5% ($p < 0.01$, $n = 18$). DIDS (AQ) produced a biphasic response of the I_{sc}. The I_{sc} was depolarized slightly within the first 10 minutes and a gradual and sustained hyperpolarization of I_{sc} was observed which

stabilized at a value 80% higher than the basal I_{sc} at about 100 minutes post-drug. Besides, the R_t was also significantly decreased by 2% ($p < 0.01$, $n = 18$). The detailed steady-state effects of DIDS on the transepithelial electrical parameters are summarized in Table 4-10.

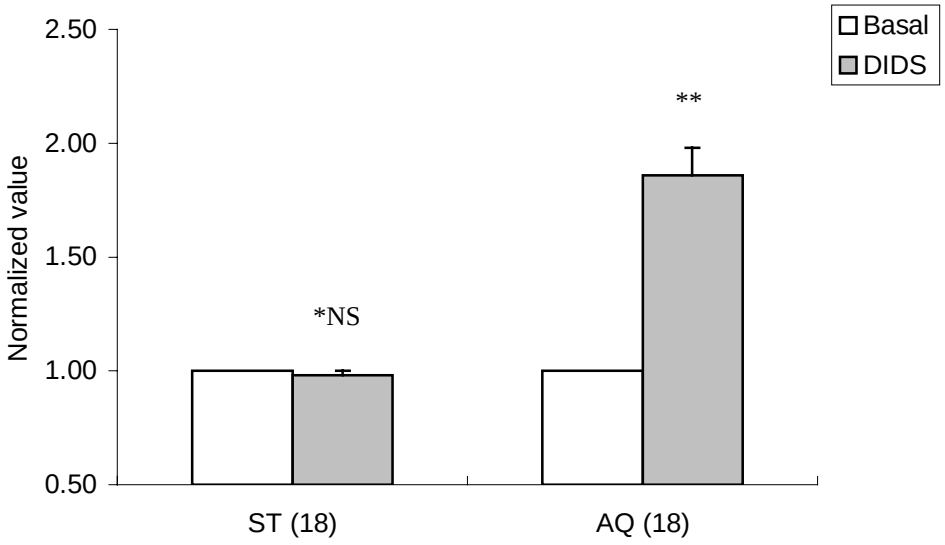

Figure 4-10 Steady-state effects of DIDS (0.1mM) on the I_{sc} across the isolated porcine CBE. Results are normalized and given as mean ± SEM that is denoted by the error bars. The number of experiments performed is indicated as in parenthesis. ST and AQ stand for stromal and aqueous DIDS, respectively. *NS Not significant; ** $p < 0.01$ (Student's paired t-test, DIDS compared with basal)

(a)

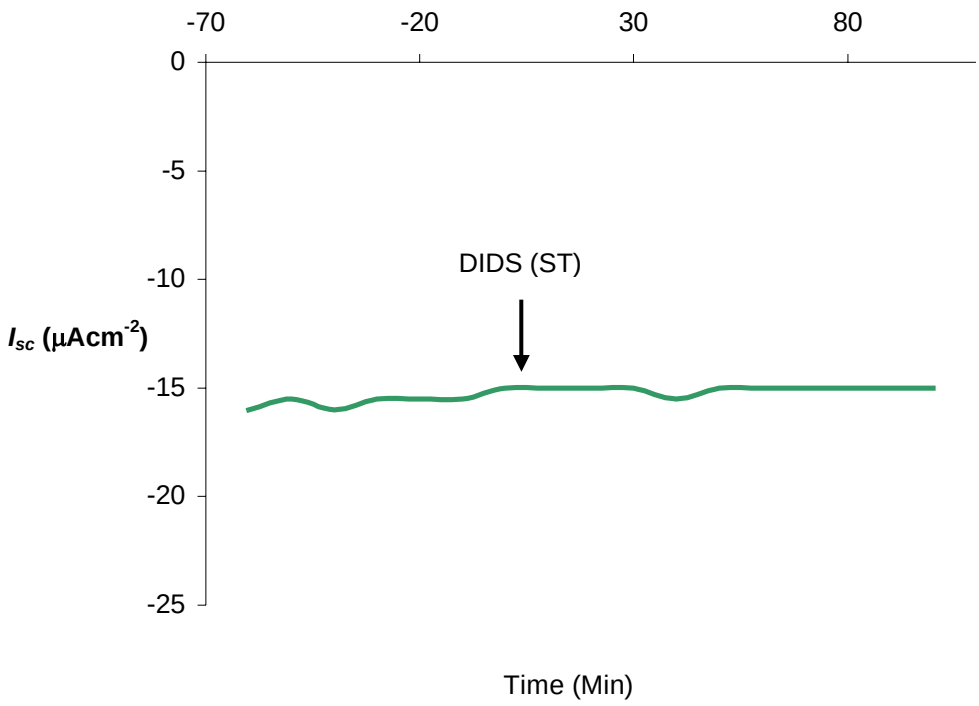

(b)

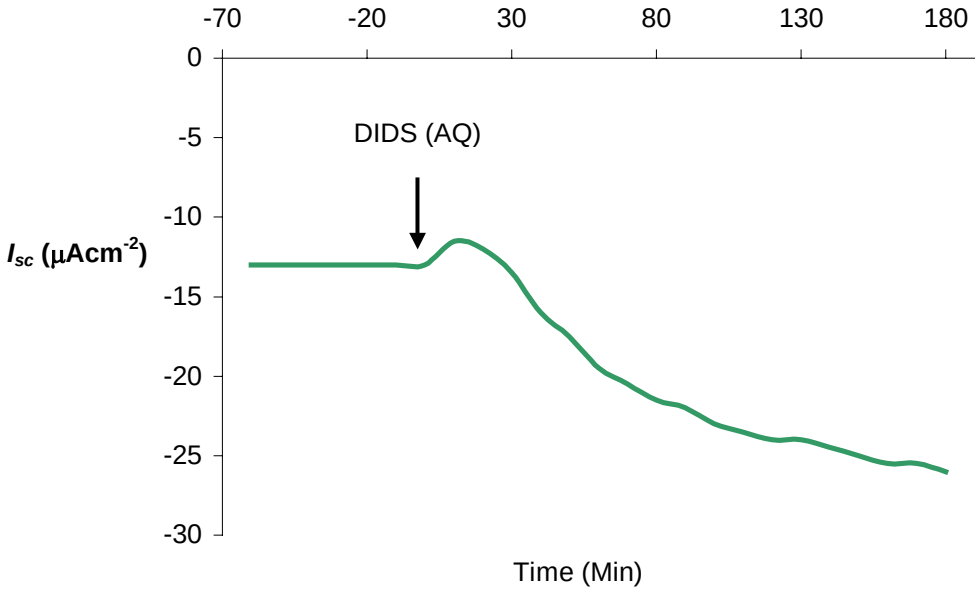

Figure 4-11 A typical time-course of the I_{sc} response of the isolated porcine CBE with (a) ST and (b) AQ DIDS (0.1mM).

		TEP **(mV)**		I_{sc} **(μAcm^{-2})**		R_t **(Ωcm^2)**	
Experiment	**n**	**Basal**	**Drug**	**Basal**	**Drug**	**Basal**	**Drug**
DIDS (ST)	18	-1.32 ±0.11	-1.29^{*NS} ±0.11	-14.44 ±1.15	-14.16^{*NS} ±1.18	96 ±5	94** ±5
DIDS (AQ)	18	-1.35 ±0.08	-2.42** ±0.16	-15.22 ±0.87	-28.51** ±2.35	89 ±3	87** ±3

Table 4-10 Steady-state effects of DIDS (0.1mM) on the transepithelial electrical parameters across the isolated porcine CBE. Values are given as mean ± SEM. ST and AQ stand for stromal and aqueous DIDS, respectively.

*NS Not significant; ** $p < 0.01$ (Student's paired t-test, DIDS compared with basal)

4.5.3.2 Effects of DIDS on the Cl^- transport

The effects of DIDS (0.1mM) on the net Cl^- transport in the stromal-to-aqueous direction (J_{net}Cl) across the porcine CBE are shown in Figure 4-12. Stromal (ST) DIDS did not change the J_{net}Cl. However, aqueous (AQ) DIDS significantly increased the J_{net}Cl, by 59% on average ($p < 0.05$, $n = 5$). The effects of DIDS on the transepithelial electrical parameters and J_{net}Cl did not indicate an important role of AE for the Cl^- uptake into the PE, which should have otherwise reduced the I_{sc} and/or J_{net}Cl. Instead, DIDS (AQ) increased both the I_{sc} and J_{net}Cl. The detailed effects of DIDS on the Cl^- transport are summarized in Table 4-11. Our unidirectional fluxes data appeared to indicate that the stimulated J_{net}Cl with DIDS (AQ) was a result of increases (11%) in the stromal-to-aqueous Cl^- transport (J_{sa}Cl). However, it should be noted that the aqueous-to-stromal Cl^- transports (J_{as}Cl) was also slightly reduced although the reduction was not significant. The insignificancy of the J_{as}Cl reduction may be due to the fact that DIDS has also increased the unidirectional fluxes by

reducing the R_t as shown in Table 4-11. Therefore, a combination of the increase in the J_{sa}Cl and the decrease in the J_{as}Cl may actually be the cause of increase in the J_{net}Cl induced by DIDS (AQ)**.**

(a)

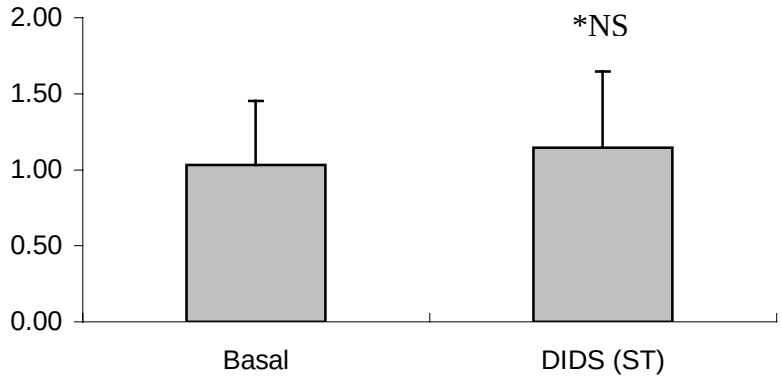

(b)

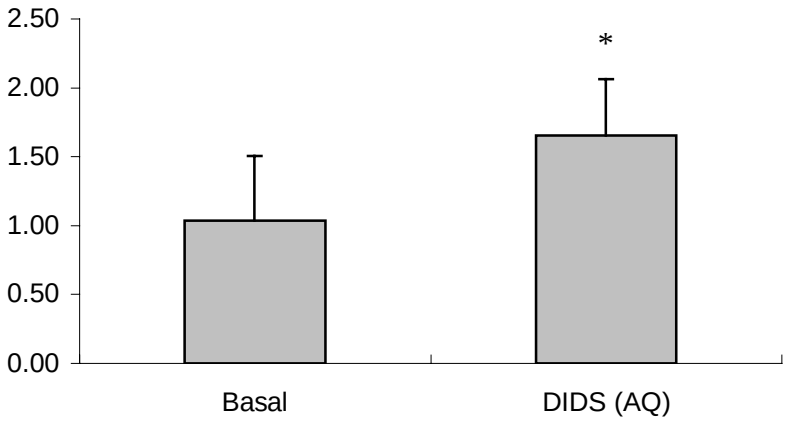

Figure 4-12 Effect of (a) ST (n = 5) and (b) AQ (n = 5) DIDS (0.1mM) on the J_{net}Cl across the isolated porcine CBE. Values are given as mean ± SEM. The unit of the J_{net}Cl is $\mu Eqh^{-1}cm^{-2}$.
*NS Not significant; * $p < 0.05$ (Student's paired t-test, DIDS compared with basal)

	DIDS (ST)			DIDS (AQ)		
n		**5**			**5**	
Cl^-	**Basal**	**DIDS**	**Δ%**	**Basal**	**DIDS**	**Δ%**
J_{sa}	5.15 ±0.59	5.46 ±0.58	$+6^{*NS}$	4.89 ±0.52	5.40 ±0.53	$+11^{**}$
J_{as}	4.11 ±0.37	4.29 ±0.29	$+5^{*NS}$	3.85 ±0.27	3.75 ±0.25	-3^{*NS}
J_{net}	$1.03^{\#}$ ±0.42	$1.14^{\#}$ ±0.50	$+11^{*NS}$	$1.04^{\#}$ ±0.47	$1.65^{\#\#}$ ±0.41	$+59^{*}$

Table 4-11 Effects of DIDS (0.1mM) on the Cl^- transport across the isolated porcine CBE. Values are given as mean ± SEM. The unit of the Cl^- transport is $\mu Eqh^{-1}cm^{-2}$. ST and AQ stand for stromal and aqueous DIDS, respectively.

*NS Not significant; * $p < 0.05$ (Student's paired t-test, DIDS compared with basal)

# $p< 0.05$; # # $p < 0.01$ (Student's paired t-test, J_{sa} compared with J_{as})

4.5.4 Effects of heptanol on the transepithelial electrical parameters and Cl^- transport

The effects of heptanol, a gap junction inhibitor on the ionic transport properties were studied. This experiment studied the role of gap junctions in the ionic transport process across the porcine CBE.

4.5.4.1 Effects of heptanol on the transepithelial electrical parameters

Figure 4-13 shows the effect of bilateral (BS) heptanol (3.5mM) on the I_{sc} across the porcine CBE. Upon its addition, heptanol virtually abolished the *TEP* and I_{sc} ($p < 0.01$, $n = 18$). Figure 4-14 shows a typical time-course of the heptanol effect on the I_{sc}. On average, maximum inhibition on the I_{sc} was seen at about 50 minutes. Detailed effects of heptanol on the transepithelial electrical parameters are

summarized in Table 4-12. As noted from the data, the R_t was also significantly reduced by 11% ($p < 0.01$, $n = 18$).

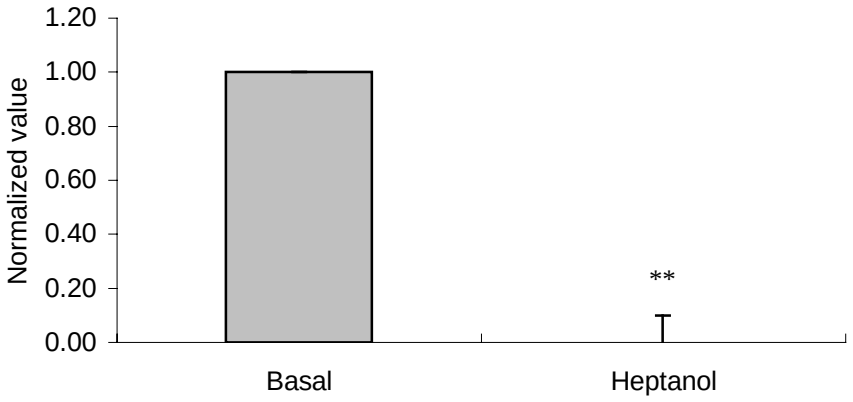

Figure 4-13 Effect of heptanol (BS, 3.5mM) on the I_{sc} across the isolated porcine CBE. Results are normalized and given as mean ± SEM that is denoted by the error bars (n = 18).
** $p < 0.01$ (Student's paired t-test, compared with basal)

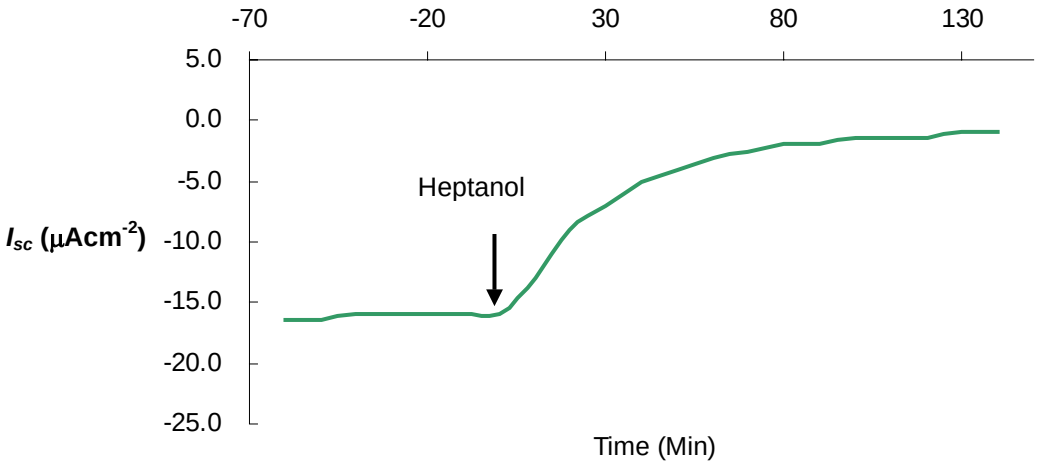

Figure 4-14 A typical time-course of the I_{sc} response with heptanol (BS, 3.5mM) on the isolated porcine CBE.

		TEP **(mV)**		I_{sc} **(μAcm^{-2})**		R_t **(Ωcm^2)**	
Experiment	**n**	**Basal**	**Drug**	**Basal**	**Drug**	**Basal**	**Drug**
Heptanol (BS)	18	-1.18 ±0.12	-0.11** ±0.07	-15.00 ±1.62	-1.50** ±0.88	80 ±3	71** ±2

Table 4-12 Effects of heptanol (BS, 3.5mM) on the transepithelial electrical parameters across the isolated porcine CBE. Values are given as mean ± SEM.

** $p < 0.01$ (Student's paired t-test, heptanol compared with basal)

4.5.4.2 Effects of heptanol on the Cl^- transport

Figure 4-15 summarizes the effect of bilateral (BS) heptanol (3.5mM) on the net Cl^- transport in the stromal-to-aqueous direction ($J_{net}Cl$) across the porcine CBE. Heptanol treatment significantly reduced the $J_{net}Cl$ by 82% ($p < 0.01$, $n = 6$). Table 4-13 summarizes the detailed fluxes data with heptanol. When the unidirectional fluxes data were considered alone, heptanol appeared to reduce the stromal-to-aqueous Cl^- transport ($J_{sa}Cl$) by 19% ($p < 0.01$, $n = 6$) and rendered the aqueous-to-stromal Cl^- transport ($J_{as}Cl$) unaltered. However, if the reduction of the R_t by heptanol (Table 4-12) was also taken into consideration, heptanol might actually have reduced the $J_{as}Cl$ but the effect had been masked by the increase in paracellular leak as indicated by the reduction of the R_t. In the same way, the heptanol effect on $J_{sa}Cl$ might have been underestimated. Nevertheless, our results showed that heptanol has effectively interrupted the Cl^- transport across the porcine CBE and it has also indicated that gap junctions may serve a major role in the regulation of the net Cl^- transport.

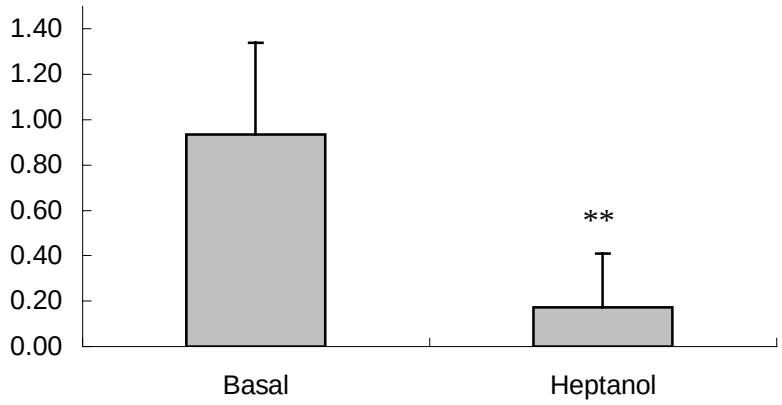

Figure 4-15 Effect of heptanol (BS, 3.5mM) on the $J_{net}Cl$ across the isolated porcine CBE. Values are given as mean ± SEM (n = 6). The unit of the $J_{net}Cl$ is $\mu Eqh^{-1}cm^{-2}$.

** $p < 0.01$ (Student's paired t-test, heptanol compared with basal)

		Heptanol (BS)	
n		**6**	
Cl^-	**Basal**	**Heptanol**	**Δ%**
J_{sa}	5.15 ±0.37	4.19 ±0.23	-19**
J_{as}	4.21 ±0.19	4.02 ±0.12	-5*NS
J_{net}	0.94 # ±0.40	0.17 #NS ±0.24	-82**

Table 4-13 Effects of heptanol (BS, 3.5mM) on the Cl^- transport across the isolated porcine CBE. Values are given as mean ± SEM. The unit of the Cl^- transport is $\mu Eqh^{-1}cm^{-2}$.

*NS Not significant; ** $p < 0.01$ (Student's paired t-test, heptanol compared with basal)

#NS Not significant; # $p < 0.05$ (Student's paired t-test, J_{sa} compared with J_{as})

4.5.5 Effects of Cl^- channel inhibitors (NPPB and NFA) on the transepithelial electrical parameters and Cl^- transport

NPPB and NFA are common Cl^- channel inhibitors and the effects of them on the porcine CBE were tested. Our results indicated that the Cl^- channel on the porcine CBE, which may be responsible for the Cl^- efflux from the NPE into the aqueous was NFA-sensitive but NPPB-insensitive.

4.5.5.1 Effects of NPPB and NFA on the transepithelial electrical parameters

The effects of aqueous (AQ) NPPB (0.1mM) and NFA (1.0mM) on the I_{sc} across the porcine CBE are summarized in Figure 4-16. Our results showed that NPPB has no effect on the I_{sc} across the porcine CBE while NFA almost completely abolished the I_{sc} ($p < 0.01$, $n = 18$). The detailed results of NPPB (AQ, 0.1mM) and NFA (AQ, 1.0mM) on the electrical parameters are summarized in Table 4-14. Both Cl^- channel inhibitors have no apparent effect on the R_t of the tissue.

Typical I_{sc} changes with NPPB and NFA are shown in Figure 4-17. In the experiment of NFA, 80% of the maximum I_{sc} inhibition occurred at around 60 minutes after incubation.

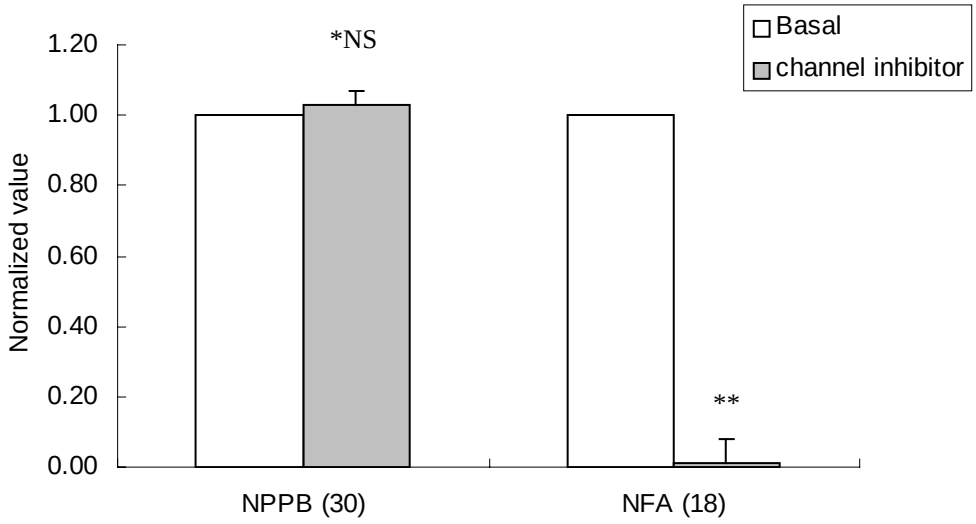

Figure 4-16 Effects of NPPB (AQ, 0.1mM) and NFA (AQ, 1.0mM) on the I_{sc} across the isolated porcine CBE. Results are normalized and given as mean ± SEM that is denoted by the error bars. The number of experiments performed is in parenthesis.

*NS Not significant; ** p <0.01 (Student's paired t-test, compared with basal)

		***TEP* (mV)**		**I_{sc} (μAcm^{-2})**		**R_t (Ωcm^2)**	
Experiment	**n**	**Basal**	**Drug**	**Basal**	**Drug**	**Basal**	**Drug**
NPPB (AQ)	30	-1.05 ±0.06	-1.06^{*NS} ±0.06	-12.60 ±0.70	-12.93^{*NS} ±0.81	84 ±2	83^{*NS} ±2
NFA (AQ)	18	-1.18 ±0.13	-0.03** ±0.07	-15.08 ±1.79	-0.33** ±0.90	82 ±4	82^{*NS} ±4

Table 4-14 Effects of NPPB (AQ, 0.1mM) and NFA (AQ, 1.0mM) on the electrical parameters across the isolated porcine CBE. Values are given as mean ± SEM.

*NS Not significant; ** p < 0.01 (Student's paired t-test, compared with basal)

(a)

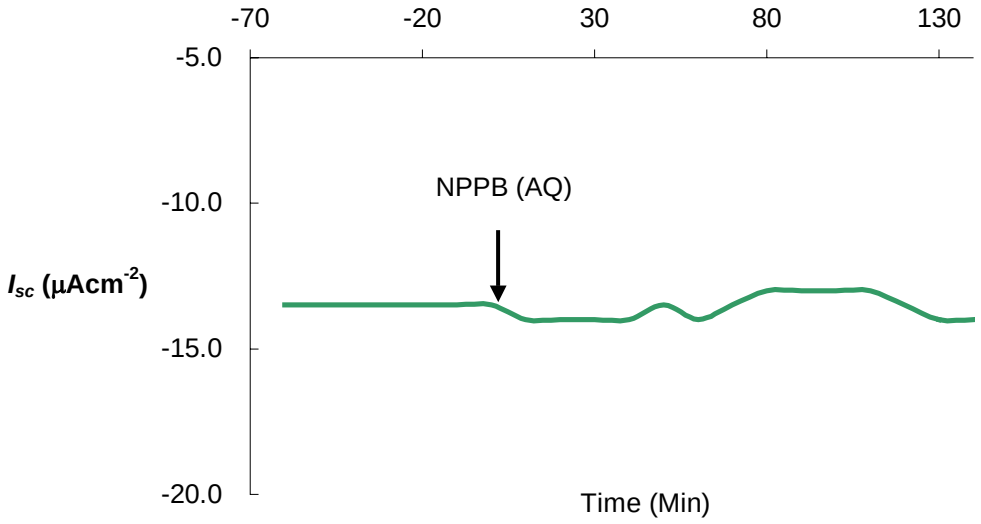

(b)

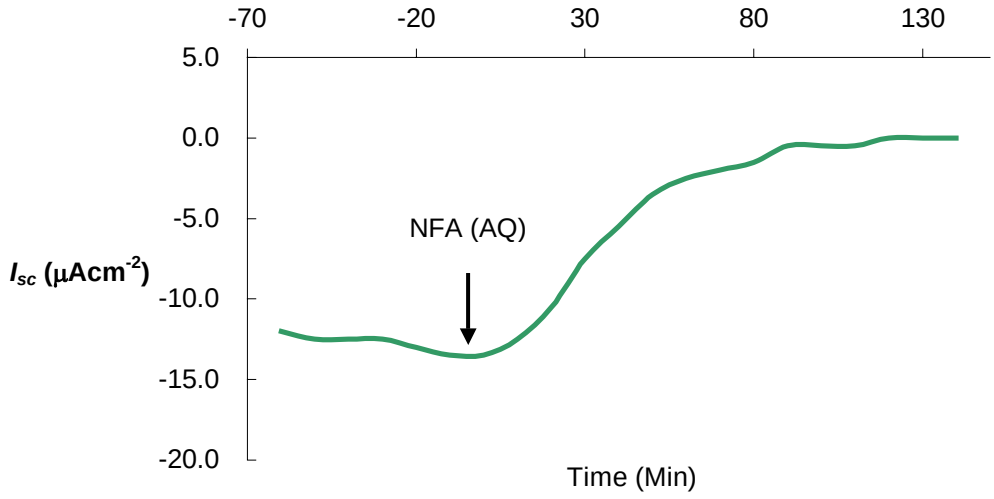

Figure 4-17 A typical time-course of the I_{sc} responses across the isolated porcine CBE with (a) NPPB (AQ, 0.1mM) and (b) NFA (AQ, 1.0mM).

4.5.5.2 Effects of NPPB and NFA on the Cl^- transport

The effects of aqueous (AQ) NPPB (0.1 mM) and NFA (1.0 mM) on the net Cl^- transport in the stromal-to-aqueous direction ($J_{net}Cl$) across the porcine CBE are summarized in Figure 4-18. Our results showed that the $J_{net}Cl$ across the porcine CBE was unaltered by NPPB (n = 7) while it was abolished by NFA ($p < 0.01$, n = 4). In addition, NFA also significantly reduced the unidirectional Cl^- transport of both directions as shown in Table 4-15. The explanation for the reduction on the stromal-to-aqueous Cl^- transport ($J_{sa}Cl$) was likely due to the blockage of the NFA-sensitive Cl^- channel, which in turn inhibited the efflux of Cl^- from the NPE into the aqueous. On the other hand, the reason for the reduction of the aqueous-to-stromal Cl^- transport ($J_{as}Cl$) was less certain.

	NPPB (AQ, 0.1 mM)			**NFA (AQ, 1.0 mM)**		
n		**7**			**4**	
Cl^-	**Basal**	**NPPB**	**Δ%**	**Basal**	**NFA**	**Δ%**
J_{sa}	4.92 ±0.48	4.72 ±0.34	-4 *NS	5.43 ±0.20	3.17 ±0.12	-42 **
J_{as}	3.73 ±0.37	3.57 ±0.28	-4 *NS	4.14 ±0.55	3.20 ±0.05	-23 **
J_{net}	1.19 # ±0.44	1.15 # ±0.28	-3 *NS	1.29 # ±0.44	-0.03 #NS ±0.15	-102 *

Table 4-15 Effects of NPPB (AQ, 0.1mM) and NFA (AQ, 1.0mM) on the Cl^- transport across the isolated porcine CBE. Values are given as mean ± SEM. The unit of the Cl^- transport is $\mu Eqh^{-1}cm^{-2}$.
*NS Not significant; * $p < 0.05$; ** $p < 0.01$ (Student's paired t-test, compared with basal)
#NS Not significant; # $p < 0.05$ (Student's paired t-test, J_{sa} compared with J_{as})

(a)

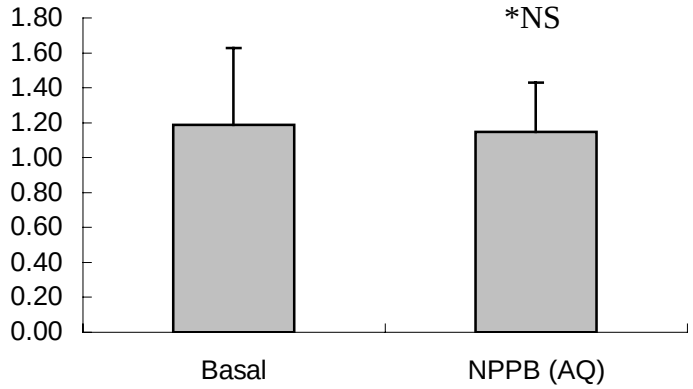

(b)

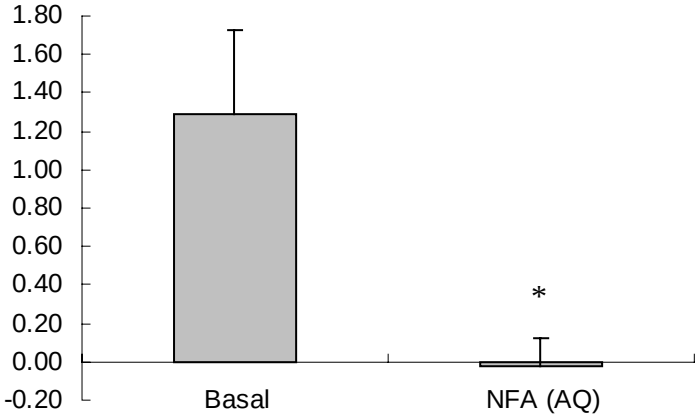

Figure 4-18 Effect of (a) NPPB (AQ, 0.1mM, n = 7) and (b) NFA (AQ, 1.0mM, n = 4) on the J_{net}Cl across the porcine CBE. Values are given as mean ± SEM. The unit of the J_{net}Cl is $\mu Eqh^{-1}cm^{-2}$.
*NS Not significant; * $p < 0.05$ (Student's paired t-test, compared with basal)

4.6 Modulation of the transepithelial electrical parameters and Cl^- transport by nitric oxide (NO) related reagents

Results in previous sections have demonstrated that in our *in vitro* porcine CBE, there was a net Cl^- transport in the stromal-to-aqueous direction ($J_{net}Cl$) that may drive the fluid transport in the process of aqueous humor formation (AHF). The involvement of various entities such as NKCC, AE, gap junction and Cl^- channel on the ion transport across the porcine CBE has also been characterized.

In the following section, the modulation of the transepithelial electrical parameters and Cl^- transport by several nitric oxide (NO) related reagents was studied. NO is a simple reactive molecule involves in a wide variety of biological functions and physiological signalling is one of its diverse functions. Recent studies have suggested that NO may modulate AHF via the classical NO-sGC-cGMP pathway. Therefore, we studied whether and how the NO related compounds regulated the ionic transport mechanism across the porcine CBE.

4.6.1 Effects of 8-pCPT-cGMP, SNP and SNAP on the transepithelial electrical parameters and Cl^- transport

In these experiments, the effects of a membrane permeable cGMP analog, 8-pCPT-cGMP and two NO donors, SNP and SNAP on the transepithelial electrical parameters and Cl^- transport were studied.

4.6.1.1 Effects of 8-pCPT-cGMP, SNP and SNAP on the transepithelial electrical parameters

Figures 4-19 show typical time-courses of the I_{sc} changes induced by 8-pCPT-cGMP, SNP and SNAP. The data of aqueous (AQ) 8-pCPT-cGMP and SNAP were shown only, as the stromal (ST) addition of the two reagents did not alter the I_{sc} across the porcine CBE significantly. In the case of SNP, unilateral addition of the reagent to either side gave qualitatively similar I_{sc} responses of different extents and therefore the effect of bilateral (BS) SNP was studied in an attempt to trigger the maximum effect. As shown in Figure 4-19a, 8-pCPT-cGMP (AQ, 0.1mM) caused a rapid and sustained hyperpolarization of the I_{sc} that reached its maximum within 20 minutes. However, the I_{sc} responses induced by NO donors (SNP and SNAP) were biphasic as shown in Figure 4-19b & c. Upon addition, NO donors triggered transient hyperpolarization of the I_{sc}, which peaked at about 6 to 7 minutes. The transient hyperpolarization of the I_{sc} were then reversed and finally stabilized at approximately 60 minutes post-drug. Figures 4-20 are the summary of the average I_{sc} changes induced by 8-pCPT-cGMP, SNP and SNAP. The sustained I_{sc} induced by 8-pCPT-cGMP was on average 102% ($p < 0.01$, $n = 20$) larger than its basal value. Although SNP and SNAP produced similar biphasic changes of the I_{sc}, the extents of changes were different. Firstly, SNP produced a larger transient I_{sc} hyperpolarization than SNAP. SNP triggered a transient I_{sc} hyperpolarization by an average of 129% ($p < 0.01$, $n = 22$) while SNAP only produced average changes of 89% ($p < 0.01$, $n = 20$). Secondly, the final steady-state I_{sc} were different. SNP depolarized the final steady-state I_{sc} from its basal value by 46% ($p < 0.01$, $n = 22$) while SNAP produced no significant depolarization. The detailed results of their effects on the steady-state

electrical parameters are summarized in Table 4-16. All three reagents significantly reduced the R_t slightly.

		***TEP* (mV)**		**I_{sc} (μAcm^{-2})**		**R_t (Ωcm^2)**	
Experiment	**n**	**Basal**	**Drug**	**Basal**	**Drug**	**Basal**	**Drug**
8-pCPT-cGMP (AQ, 0.1mM)	20	-0.90 ±0.10	-1.77** ±0.11	-9.50 ±1.13	-19.18** ±1.42	96 ±3	94** ±3
SNP (BS, 0.1mM)	22	-0.92 ±0.06	-0.45** ±0.05	-12.84 ±0.97	-6.91** ±0.93	74 ±3	70** ±3
SNAP (AQ, 0.1mM)	22	-1.01 ±0.07	-0.94*NS ±0.08	-12.36 ±1.24	-12.12*NS ±1.48	86 ±4	84** ±4

Table 4-16 Steady-state changes of the electrical parameters induced by 8-pCPT-cGMP, SNP and SNAP. Values are given as mean ± SEM. AQ and BS stand for aqueous and bilateral addition of the tested reagent, respectively.

*NS Not significant; ** $p < 0.01$ (Student's paired t-test, compared with basal)

(a)

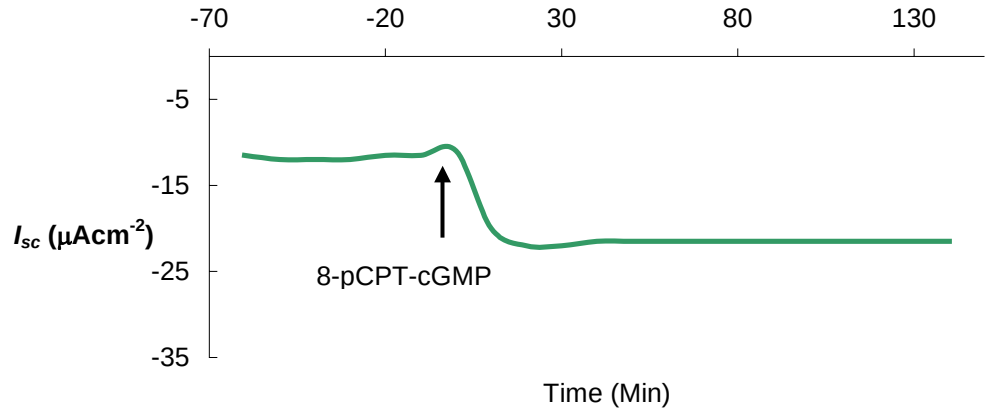

(b)

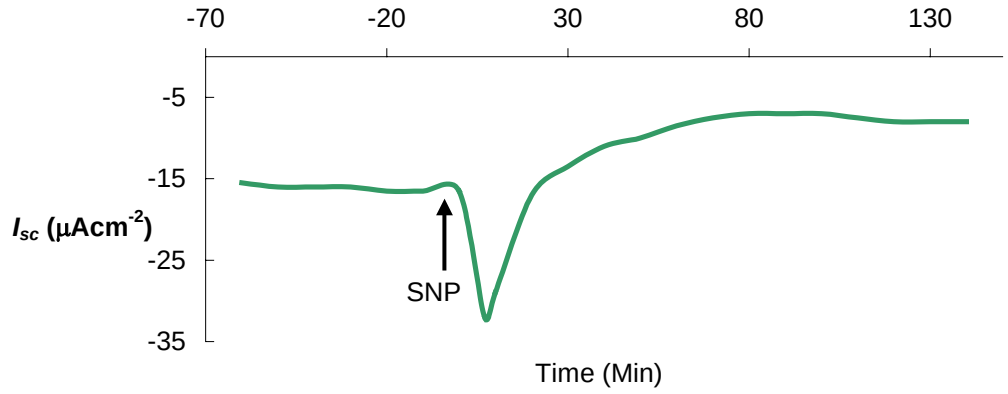

(c)

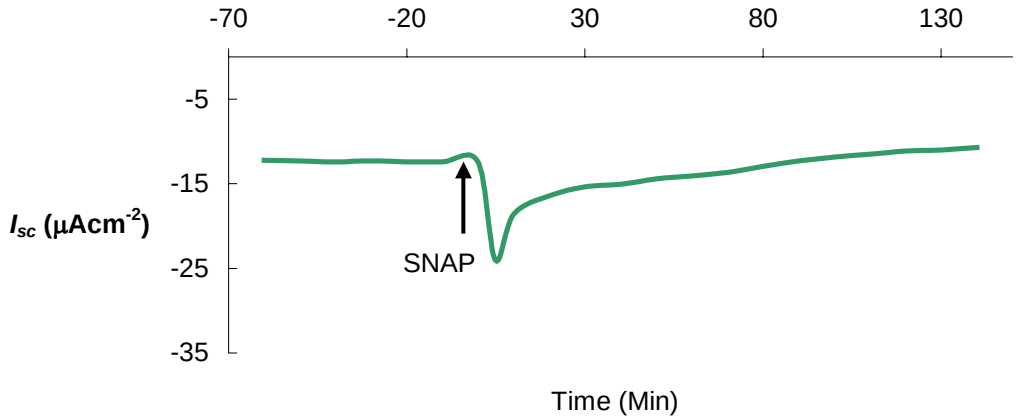

Figure 4-19 A typical time-course of the I_{sc} changes induced by (a) 8-pCPT-cGMP (AQ, 0.1mM), (b) SNP (BS, 0.1mM) and (c) SNAP (AQ, 0.1mM). AQ and BS stand for aqueous and bilateral addition of the reagent, respectively.

(a)

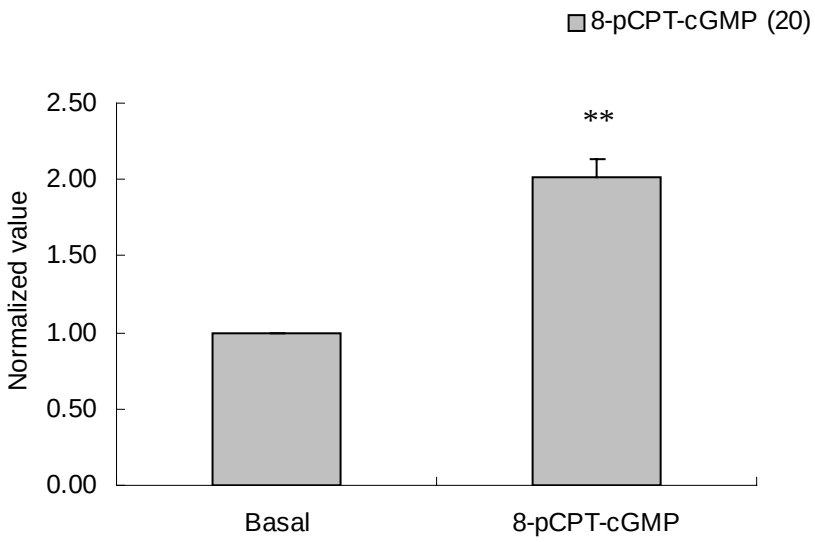

(b)

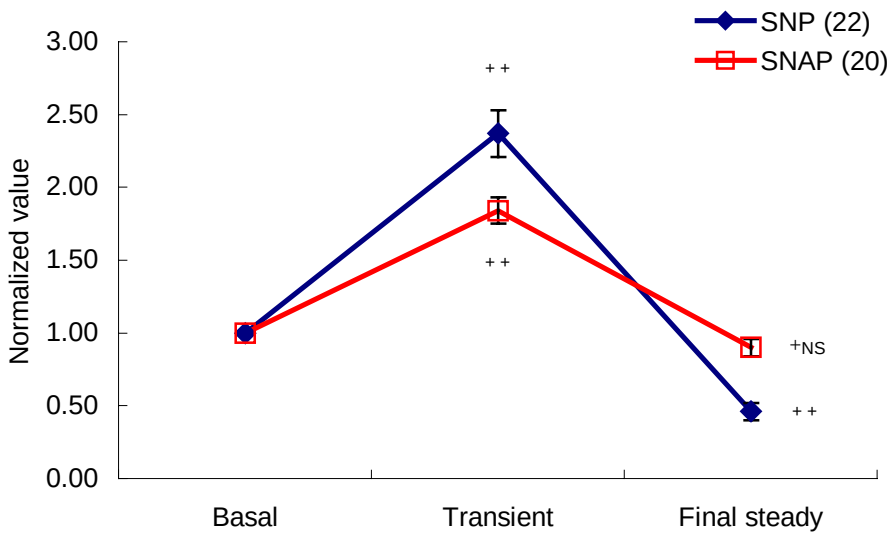

Figure 4-20 Average I_{sc} changes induced by (a) 8-pCPT-cGMP (AQ, 0.1mM), and (b) SNP (BS, 0.1mM) and SNAP (AQ, 0.1mM). Results are normalized and given as mean ± SEM (error bars). The number of experiments performed is in parenthesis.

** $p < 0.01$ (Student's paired t-test, compared with basal)

+NS Not significant; + + $p < 0.01$ (Repeated measure ANOVA, followed by Tukey-Kramer multiple comparison test; Value at the specified condition compared with basal).

4.6.1.2 Effects of 8-pCPT-cGMP, SNP and SNAP on the Cl^- transport

The effects of 8-pCPT-cGMP, SNP and SNAP on the net Cl^- transport in the stromal-to-aqueous direction (J_{net}Cl) across the porcine CBE are illustrated in Figure 4-21. The steady-state fluxes were averaged data after the steady-state I_{sc} has reached. Therefore, the data did not account for the changes in the Cl^- transport during the transient hyperpolarization of the I_{sc}. As shown in the figures, 8-pCPT-cGMP (AQ, 0.1mM) significantly increased the J_{net}Cl by an average of 31% ($p < 0.01$, $n = 10$). However, SNP (BS, 0.1mM) significantly reduced the J_{net}Cl by an average of 44% ($p < 0.05$, $n = 6$) while another NO donor, SNAP (AQ, 0.1mM) did not alter the J_{net}Cl. The detailed unidirectional Cl^- fluxes data are summarized in Table 4-17.

	8-pCPT-cGMP (AQ)			**SNP (BS)**			**SNAP (AQ)**		
n		**10**			**6**			**7**	
Cl^-	**Basal**	**Drug**	**Δ%**	**Basal**	**Drug**	**Δ%**	**Basal**	**Drug**	**Δ%**
J_{sa}	4.75 ±0.36	5.19 ±0.34	$+9^{**}$	5.51 ±0.27	5.29 ±0.21	-4^{*NS}	5.36 ±0.31	5.46 ±0.36	$+2^{*NS}$
J_{as}	3.75 ±0.13	3.88 ±0.10	$+4^{*}$	4.58 ±0.31	4.77 ±0.27	$+4^{*NS}$	4.30 ±0.33	4.44 ±0.32	$+3^{*}$
J_{net}	$1.00^{\#}$ ±0.36	$1.31^{\#\#}$ ±0.35	$+31^{**}$	$0.93^{\#}$ ±0.15	$0.52^{\#}$ ±0.25	-44^{*}	$1.06^{\#\#}$ ±0.32	$1.02^{\#}$ ±0.37	-4^{*NS}

Table 4-17 Effects of 8-pCPT-cGMP (AQ, 0.1mM), SNP (BS, 0.1mM) and SNAP (AQ, 0.1mM) on the Cl^- transport across the isolated porcine CBE. Values are given as mean ± SEM. The unit of the Cl^- transport is $\mu Eqh^{-1}cm^{-2}$.

*NS Not significant; * $p < 0.05$; ** $p < 0.01$ (Student's paired t-test, compared with basal)

# $p < 0.05$; # # $p < 0.01$ (Student's paired t-test, J_{sa} compared with J_{as})

(a)

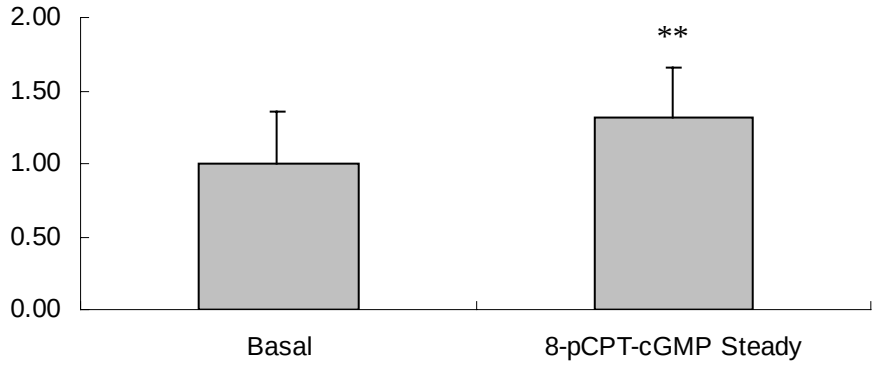

(b)

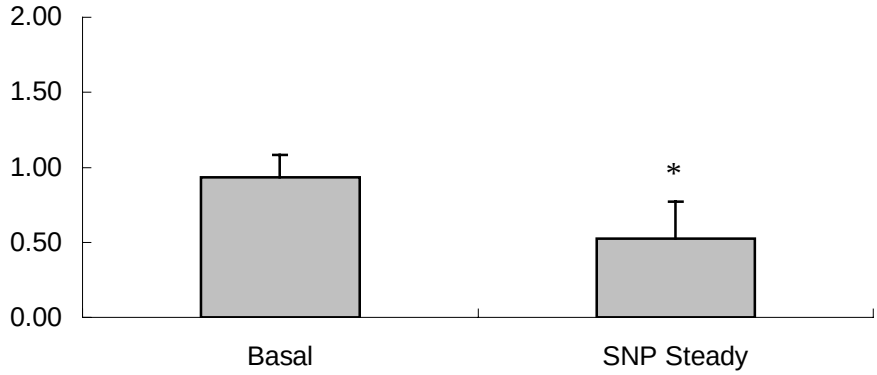

(c)

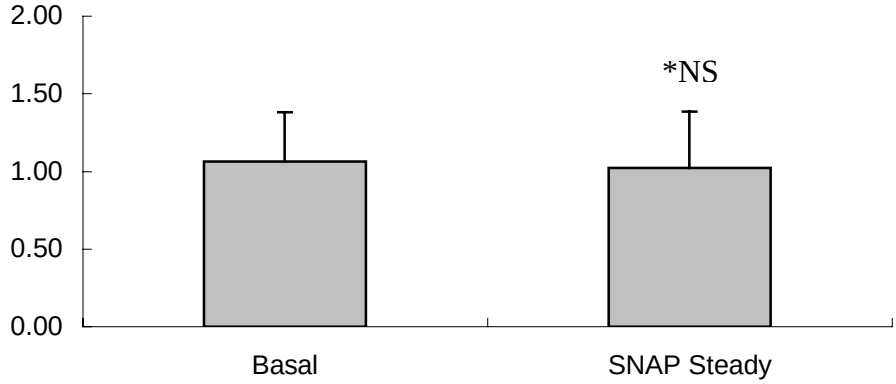

Figure 4-21 Effect of (a) 8-pCPT-cGMP (AQ, 0.1mM, n = 10), (b) SNP (BS, 0.1mM, n = 6) and (c) SNAP (AQ, 0.1mM, n = 7) on the J_{net}Cl across the isolated porcine CBE. Values are given as mean ± SEM. The unit of the J_{net}Cl is $\mu Eqh^{-1}cm^{-2}$.

*NS Not significant; * $p < 0.05$; ** $p < 0.01$ (Student's paired t-test, compared with basal)

4.6.2 Effects of ODQ pre-treatment on the transepithelial electrical parameters and the Cl^- transport changes induced by 8-pCPT-cGMP, SNP and SNAP

Results in the previous section showed that the effects of NO donors on the ion transport properties across the porcine CBE were different from that of the cGMP-analog. It suggested that NO may have exerted unknown cGMP-independent effects on its modulation of the ion transport across the porcine CBE. The final NO effect may therefore be a result of the interplay of both the cGMP-dependent and -independent effects. In order to elucidate the exact mechanism, the effects of pre-treatment of a sGC inhibitors, ODQ (BS, 10μM) on the subsequent responses induced by 8-pCPT-cGMP, SNP and SNAP were studied. Presumably, ODQ pre-treatment would block the NO-cGMP-dependent effect and reveal the cGMP-independent effect.

4.6.2.1 Effects of ODQ pre-treatment on the transepithelial electrical parameters changes induced by 8-pCPT-cGMP, SNP and SNAP

ODQ (BS, 10μM) was incubated for 20 minutes before cGMP-analog or NO donor was added to the bathing solution. Figure 4-22 summarizes the average I_{sc} changes induced by 8-pCPT-cGMP, SNP and SNAP with the pre-treatment of ODQ. As expected, pre-treatment of ODQ have no effect on the subsequent I_{sc} changes induced by 8-pCPT-cGMP as the effect exerted by the cGMP-analog does not require the stimulation of sGC (which is the target of inhibition by ODQ). The sustained stimulated I_{sc} was still on average 106% ($p < 0.01$, $n = 18$) larger than its basal value. That was similar to the changes induced by 8-pCPT-cGMP alone (102%). However, although the biphasic responses of the I_{sc} induced by SNP and SNAP were preserved, the magnitudes of the transient hyperpolarization of the I_{sc} were dramatically reduced

with the pre-treatment of ODQ. SNP and SNAP transiently hyperpolarized the I_{sc} by an average of 41% ($p < 0.05$, $n = 12$) and 45% ($p < 0.01$, $n = 18$) respectively. In addition, the final steady-state I_{sc} re-established with either SNP or SNAP was both significantly depolarized from their basal values. SNP depolarized the I_{sc} by 89% on average ($p < 0.01$, $n = 12$) while SNAP depolarized the I_{sc} by an average of 15% ($p < 0.05$, $n = 18$). Clearly, the depolarizations of the I_{sc} were larger than that with the NO donors alone (Section 4.6.1.1). These results reinforced our postulation that the transient hyperpolarization of the I_{sc} was cGMP-dependent while the subsequent depolarization of the I_{sc} was cGMP-independent. The detailed effects of the three reagents on the steady-state electrical parameters with ODQ pre-treatment are summarized in Table 4-18.

		***TEP* (mV)**		**I_{sc} (μAcm^{-2})**		**R_t (Ωcm^2)**	
Experiment	**n**	**Basal**	**Drug**	**Basal**	**Drug**	**Basal**	**Drug**
8-pCPT-cGMP (AQ, 0.1mM)	18	-0.93 ±0.09	-1.84** ±0.14	-10.86 ±1.18	-22.39** ±2.12	89 ±4	87* ±4
SNP (BS, 0.1mM)	12	-0.70 ±0.06	-0.08** ±0.06	-8.30 ±0.81	-0.95** ±0.75	88 ±4	83** ±3
SNAP (AQ, 0.1mM)	18	-0.81 ±0.07	-0.67** ±0.07	-9.75 ±0.92	-8.29** ±0.92	84 ±4	82* ±4

Table 4-18 Steady-state changes of the electrical parameters induced by 8-pCPT-cGMP, SNP and SNAP with ODQ (BS, 10μM) pre-treatment. Values are given as mean ± SEM. AQ and BS stand for aqueous and bilateral addition of the tested reagent, respectively.

* $p < 0.05$; ** $p < 0.01$ (Student's paired t-test, compared with basal)

(a)

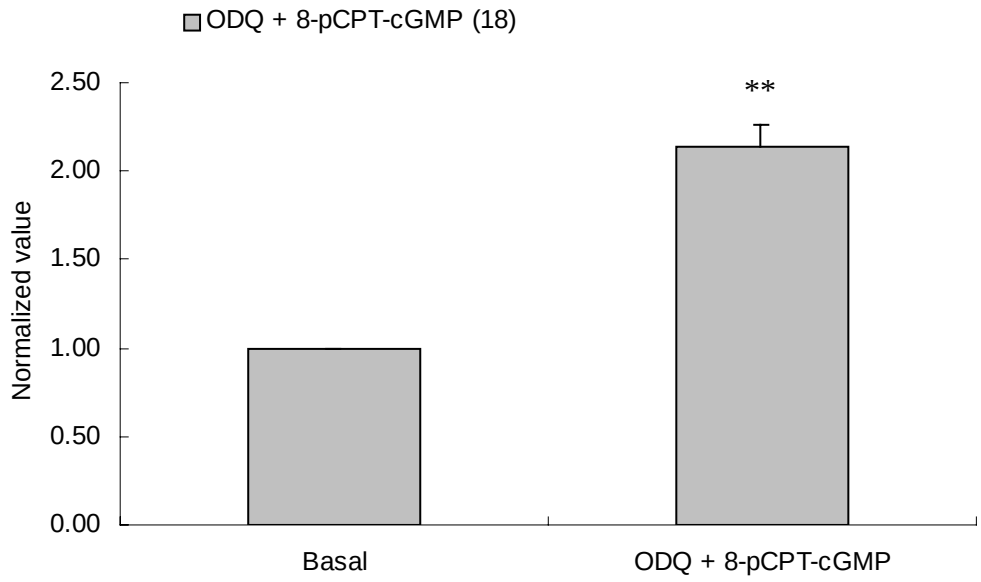

(b)

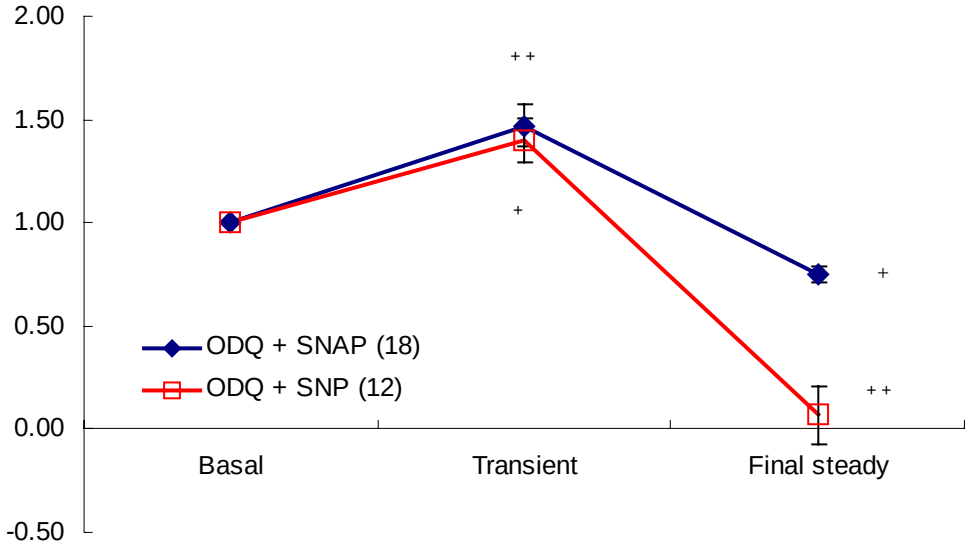

Figure 4-22 Average I_{sc} changes induced by (a) 8-pCPT-cGMP (AQ, 0.1mM) and (b) SNP (BS, 0.1mM) and SNAP (AQ, 0.1mM) with ODQ (BS, 10μM) pre-treatment. Results are normalized and given as mean ± SEM that is denoted by the error bars. The number of experiments performed is indicated as in parenthesis.

** $p < 0.01$ (Student's paired t-test, compared with basal)

+ $p < 0.05$; + + $p < 0.01$ (Repeated measure ANOVA, followed by Tukey-Kramer multiple comparison test; Value at the specified conditions compared with basal).

4.6.2.2 Effects of ODQ pre-treatment on the Cl^- transport changes induced by 8-pCPT-cGMP, SNP and SNAP

The effects of ODQ (BS, 10μM) pre-treatment on the changes of the net Cl^- transport in the stromal-to-aqueous direction ($J_{net}Cl$) induced by 8-pCPT-cGMP, SNP and SNAP are demonstrated in Figure 4-23. Again, the steady-state fluxes data were the average fluxes obtained after the respective steady state of the I_{sc} has reached. With ODQ pre-treatment, the increase in the $J_{net}Cl$ stimulated by 8-pCPT-cGMP (AQ, 0.1mM) was still amounted to 32% ($p < 0.05$, $n = 5$). This increase was similar to that without ODQ pre-treatment (31%). In addition, the steady-state inhibition of NO donors on the $J_{net}Cl$ was enhanced by ODQ pre-treatment. With ODQ pre-treatment, both SNP (BS, 0.1mM) and SNAP (AQ, 0.1mM) significantly reduced the $J_{net}Cl$ by an average of 63% ($p < 0.05$, $n = 4$) and 25% ($p < 0.05$, $n = 4$) respectively. While SNP alone only reduced the $J_{net}Cl$ by 44% and SNAP alone produced no significant reduction of the $J_{net}Cl$ (Section 4.6.1.2). The detailed unidirectional Cl^- transport data are summarized in Table 4-19.

In summary, the cGMP-analog and NO donors used in our experiments did not produce identical effects on the transepithelial electrical parameters and Cl^- transport. The cGMP-analog produced sustained hyperpolarization of the I_{sc} and increased the steady-state net Cl^- transport in the stromal-to-aqueous direction ($J_{net}Cl$) while NO donors triggered only transient hyperpolarization of the I_{sc} and reduced (in case of SNP) and did not affect (in case of SNAP), rather than stimulated the $J_{net}Cl$. The NO donors-induced transient hyperpolarization of the I_{sc} and its alleviation by ODQ pre-treatment suggested the involvement of the NO-sGC-cGMP pathway. The fact that NO donors produced different effects on the steady-state I_{sc} and $J_{net}Cl$ from that of the cGMP analog, together with the observation that such effects were further

aggravated by ODQ pre-treatment strongly suggested the presence of NO-cGMP-independent pathway. This NO-cGMP-independent pathway produced an opposite and yet a more dominating effect as compared to the cGMP-dependent pathway on the modulation of the Cl^- transport across the porcine CBE.

	8-pCPT-cGMP (AQ)			**SNP (BS)**			**SNAP (AQ)**		
n		**5**			**4**			**4**	
Cl^-	**Basal**	**Drug**	**Δ%**	**Basal**	**Drug**	**Δ%**	**Basal**	**Drug**	**Δ%**
J_{sa}	5.38 ±0.35	5.68 ±0.31	$+6^{*}$	5.06 ±0.48	4.80 ±0.44	-5^{*}	5.16 ±0.60	5.35 ±0.66	$+4^{*}$
J_{as}	4.44 ±0.22	4.45 ±0.15	0^{*NS}	4.19 ±0.31	4.48 ±0.34	$+7^{*NS}$	4.33 ±0.46	4.74 ±0.47	$+9^{**}$
J_{net}	$0.93^{\#}$ ±0.30	$1.23^{\#\#}$ ±0.30	$+32^{*}$	$0.87^{\#}$ ±0.30	$0.32^{\#NS}$ ±0.19	-63^{*}	$0.83^{\#\#}$ ±0.16	$0.61^{\#}$ ±0.19	-25^{*}

Table 4-19 Effects of 8-pCPT-cGMP (AQ, 0.1mM), SNP (BS, 0.1mM) and SNAP (AQ, 0.1mM) on the Cl^- transport across the isolated porcine CBE pre-treated with ODQ (BS, 10μM). Values are given as mean ± SEM. The unit of the Cl^- transport is $\mu Eqh^{-1}cm^{-2}$.

*NS Not significant; * $p < 0.05$; ** $p < 0.01$ (Student's paired t-test, compared with basal)

#NS Not significant; # $p < 0.05$; # # $p < 0.01$ (Student's paired t-test, J_{sa} compared with J_{as})

(a)

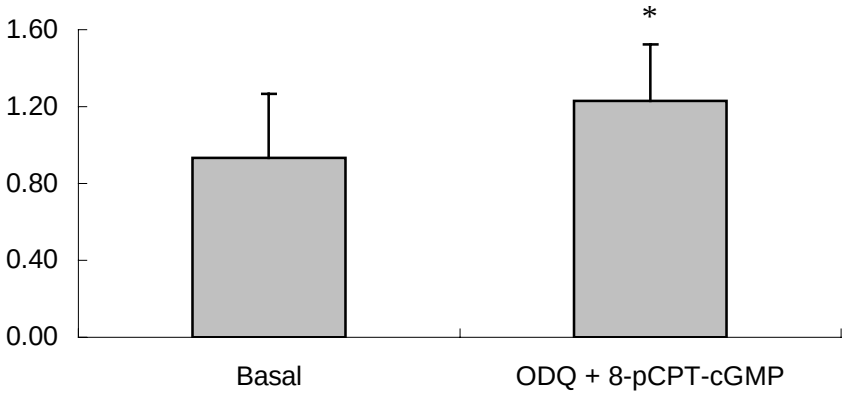

(b)

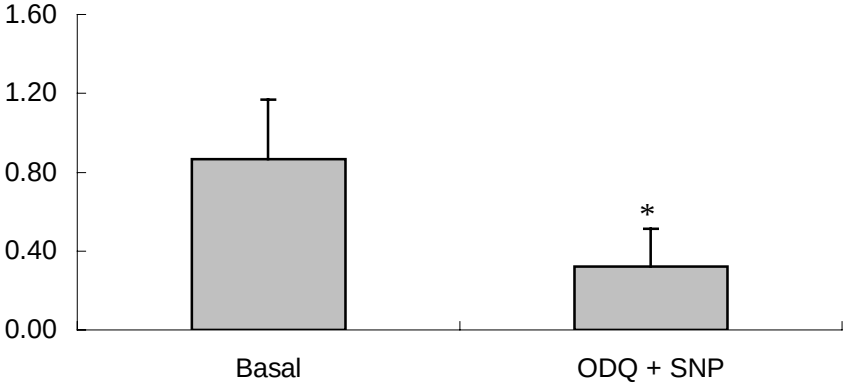

(c)

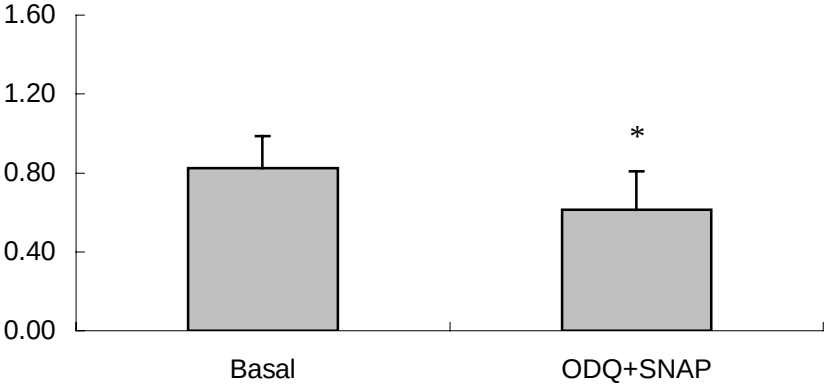

Figure 4-23 Effect of (a) 8-pCPT-cGMP (AQ, 0.1mM, n = 5), (b) SNP (BS, 0.1mM, n = 4) and (c) SNAP (AQ, 0.1mM, n = 4) on the J_{net}Cl across the isolated porcine CBE pre-treated with ODQ (BS, 10μM). Values are given as mean ± SEM that is denoted by the error bars. The unit of the J_{net}Cl is $\mu Eqh^{-1}cm^{-2}$.

* $p < 0.05$ (Student's paired t-test, compared with basal)

4.6.3 Effects of ABT pre-treatment on the subsequent I_{sc} changes induced by SNP and SNAP

Results in the previous section suggested the possible involvement of NO-cGMP-independent pathway in modulating the ion transport across the porcine CBE. We sought to study the details of this unknown pathway with the following experiment. Cytochrome P-450 enzyme (Cyt P450) is also a direct molecular target of NO as it is a heme-containing protein. This enzyme, along with cyclooxygenase and lipoxygenase, are involved in the metabolism of arachidonic acid (AA) and produced active cell signalling products, eicosanoid. For instance in renal epithelial cells, NO stimulated the production of an epoxyeicosatrienoic acid (EET) via a Cyt P450-dependent pathway and that EET inhibited NKCC (He et al., 2003).

In the present experiment, the effects of a Cyt P450 enzyme inhibitor, 1-aminobenzotriazole (ABT) pre-treatment on the subsequent NO donors-induced I_{sc} responses were studied. It was to examine whether the NO-induced I_{sc} depolarization was mediated via Cyt P450-dependent pathway. The preparations were randomly assigned as experimental and control groups. For the experimental group, ABT (BS, 1mM) was incubated for 1 hour before SNP (BS, 0.1mM) and 2 hours before SNAP (AQ, 0.1mM) addition. The control group only received the vehicle (BS, 0.3% ethanol (ETOH)) without ABT before the addition of NO donors. It was noted that neither ABT nor ethanol altered the transepithelial electrical parameters. The subsequent I_{sc} responses induced by NO donors with and without pre-treatment of ABT or ethanol are summarized in Figure 4-24 and were illustrated with two ratios in the respective conditions. The two ratios were: (1) Transient hyperpolarization of the I_{sc} : Basal I_{sc} (H:B), and (2) Steady-state re-established I_{sc} : Basal I_{sc} (S:B). Our results showed that the transient increases in the I_{sc} induced by NO donors were not affected

by the ABT nor ethanol pre-treatment as the H:B ratios were the same in the conditions of NO donors alone, pre-treatment of ABT and pre-treatment of ETOH. However, the S:B ratios in both cases of SNP and SNAP with ABT pre-treatment were significant larger than those with NO donors alone and ETOH pre-treatment. The larger S:B ratios reflected that the NO-induced depolarization of the steady-state I_{sc} could be alleviated by ABT pre-treatment. These results implied that NO might, at least in part, modulate the ion transport across the porcine CBE via an ABT-sensitive Cyt P450 pathway, in addition to the classical NO-sGC-cGMP pathway.

(a)

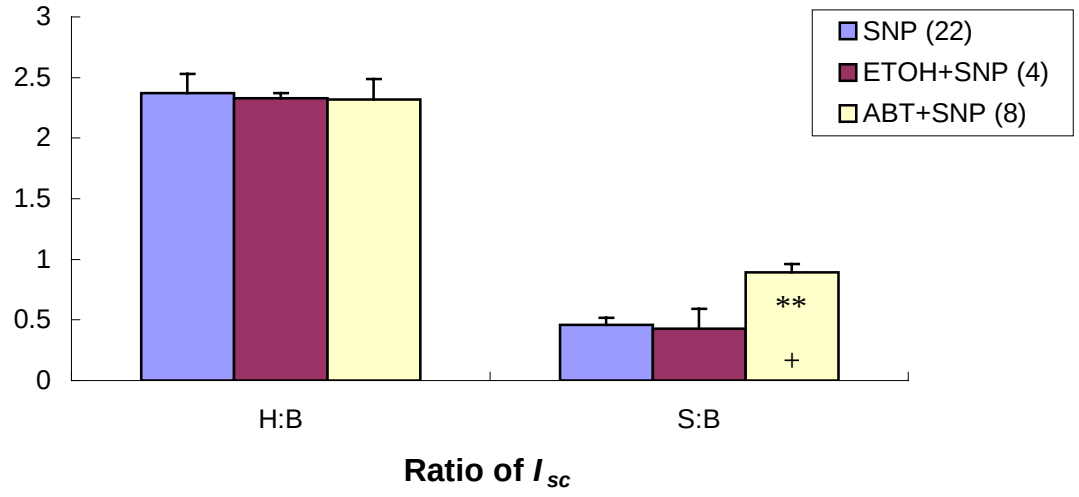

(b)

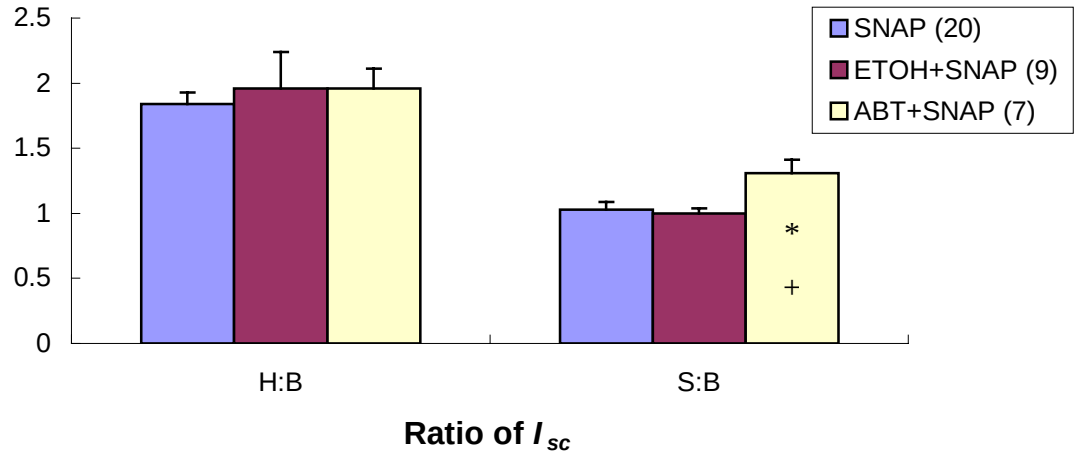

Figure 4-24 Summary of the biphasic I_{sc} changes induced by (a) SNP (BS, 0.1mM), and (b) SNAP (AQ, 0.1mM) in conditions with and without ABT (BS, 1mM) or ethanol (ETOH, BS, 0.3%) pre-treatment. Results were translated into the ratios of H : B and S : B as mentioned in the text and given as mean ± SEM that is denoted by the error bars. The number of experiments performed is indicated as in parenthesis.

* $p < 0.05$; ** $p < 0.01$ (ANOVA, followed by Tukey-Kramer multiple comparison test as compared with NO donors alone)

+ $p < 0.05$ (ANOVA, followed by Tukey-Kramer multiple comparison test as compared with ETOH pre-treatment)

All the other comparisons were statistical insignificant.

CHAPTER 5

DISCUSSION

5.1 Design of the modified Ussing-Zerahn-type chambers

Throughout this work, two types of modified Ussing-Zerahn-type chambers were used, namely the continuous perfusion type (CP) and opened re-circulating type (ORC). The CP and ORC chambers were similar in many aspects. Basically, both of them were composed of two half-chambers of equal volume assembled together with electrodes and connections for monitoring the electrical parameters and responses generated by the mounted preparation. Equal volume of bathing solution was infused into the two half-chambers to nourish the preparation. The dimensions of the apertures for the exposed CBE preparations were identical in both types of chambers (0.1 cm^2). The small-sized slotted aperture helped in excluding the iris from the chamber aperture that may complicate the electrical responses. Similar methods have been employed in both chambers to reduce damages to the CBE preparations during mounting. In the CP chamber, a sliding table system was used to limit the sideway movements of the two half-chambers during assembly which could inflict tissue damage. A flat silicone plate on each mounting stage aided a good seal during chamber assembly and minimized the clamping pressure required in achieving leak-proof. In the ORC chamber, there were two stainless steel fixation rods and the holes on complementary mounting blocks that aided accurate alignment of the two half-chambers. The O-rings fitted in place around the slotted apertures of paired tissue-

mounting blocks also helped to optimize seal. Virtual probe electrodes, which do not involve real probe electrodes projecting into the chambers intersecting the path of the external current flow, were used in both chambers to monitor the electrical responses across the CBE. The use of virtual probe electrodes was advantageous to chamber of small aperture size (1-2 cm^2). If real probe electrodes were used, they may distort the externally applied current passing through the preparations and result in an erroneous estimation of the resistance of the chamber and tissue (Rehm, 1975). In our chambers, the aperture sizes were even smaller (0.1 cm^2) and therefore virtual probe electrodes were more appropriate.

Although the CP and ORC chambers were similar as stated above, they differed from each other in the way of bathing solution delivery for nourishing the tissue. In the CP chamber, fresh bathing solution was driven by external pump and was continuously perfusing the tissue on both half-chambers. The solution was drained either for disposal or collection via the perfusion outlets. As the perfusion inlet and outlet were placed in close proximity to the surface of the exposed tissue, vigorous stirring and good interchange of nutrients and metabolic wastes across the tissue were achieved. Moreover, as the bathing solution was being continuously replaced by fresh solution, the degradation of the bathing solution and pharmacological agents, and the accumulation of the metabolic wastes produced by the CBE were minimized. In the ORC chamber, fixed amount of bathing solution was bubbled and re-circulating in the bath during the whole course of experiment. The bubbling of fluid provided oxygen, good stirring and facilitated exchange of materials across the tissue. A large volume of bathing solution (20 ml per side) was contained in the bath in order to provide sufficient and relatively stable nutrient supply throughout the experiment.

5.2 Viability of the isolated porcine CBE

Although there were slight differences between the CP and ORC chambers (Section 5.1), viable porcine CBE were maintained in both chamber types. Three different aspects of the porcine CBE have been assessed to validate its viability.

First of all, the porcine CBE demonstrated stable electrical parameters including the spontaneous *TEP*, I_{sc} and R_t, since damaged tissue typically presented deteriorating electrical responses in our setup. According to our observations, those preparations attaining either steady-state *TEP* smaller than -0.2 mV or R_t smaller than 50 Ωcm^2 often showed minimal and inconsistent responses to pharmacological agents. Consequently, preparations were said to be viable and included in study only if they have *TEP* more negative than -0.2 mV and R_t larger than 50 Ωcm^2. It was noted that preparations mounted in the ORC chamber had a higher viability rate. It may be due to several reasons. Firstly, the dissection technique may have improved with time since the CP chambers were used during the early stage of this research. Secondly, the continuous bubbling of air in the ORC chamber may be more effective in oxygenating the tissue and maintaining its physiology. Thirdly, the small O-rings introduced in the ORC chamber may have been effective in reducing edge damages.

The second aspect in validating our *in vitro* porcine CBE was the normal functioning of the Na^+,K^+-ATPase. The Na^+,K^+-ATPase is ubiquitous in animal cells. It pumps 3 Na^+ ions out of the cells and 2 K^+ ions into the cells at the expense of an ATP molecule (Glynn, 1993). The sodium pump maintains a chemical and an electrical ionic gradient across the cell membrane that are vital for several cellular functions including regulation of osmotic balance, cell volume and intracellular pH, and generation of transmembrane electrical potential. It also allows cellular

excitability and provides driving forces for various secondary active transports (Balshaw et al., 2001). In the CE, the Na^+,K^+-ATPases were found along the basolateral infoldings and interdigitations of both the PE and NPE cells (Usukura et al., 1988; Mori et al., 1991). Previous works have suggested that the Na^+,K^+-ATPases of the PE and NPE cells are different in terms of their relative enzymatic activities (Riley and Kishida, 1986; Usukura et al., 1988), the quantities of the α-subunit (Dunn et al., 2001) and the isoforms expressed (Ghosh et al., 1991). Nevertheless, the enzyme is essential for the aqueous humor formation (AHF) since ouabain, its specific inhibitor, reduced the AHF in cat (Garg and Oppelt, 1970), rabbit (Kodama et al., 1985) and ox (Shahidullah et al., 2003). In our *in vitro* porcine CBE, bilateral (BS) ouabain (1 mM) consistently produced a biphasic electrical response as shown in Figure 4-1 with an initial hyperpolarization followed by a gradual depolarization. This characteristic electrical response can be explained by the sequential inhibition of the Na^+,K^+-ATPases at the NPE and PE cell layers. This biphasic response was also observed in bovine CBE (To et al., 1998a) and was consistent with a dual Na^+,K^+-ATPases model (Krupin et al., 1984; Wiederholt and Zadunaisky, 1987). The presence of biphasic response with ouabain implied that the Na^+,K^+-ATPases were functioning in our *in vitro* porcine CBE.

The third aspect in validating our *in vitro* porcine CBE was a quantitative analysis of L-glucose leak across the preparations. L-glucose leak was studied because glucose transport across epithelia is stereospecific with D-glucose transports transcellularly and L-glucose moves across the cell layer paracellularly (DiMattio and Streitman, 1986). Therefore, L-glucose diffusion can be used as an indicator of the paracellular permeability of a preparation, which in turn reflects its structural integrity. In our *in vitro* porcine CBE, the unidirectional L-glucose diffusion in either direction

was not different from each other. The magnitude of the unidirectional L-glucose diffusion ranged from 43 to 54 $\eta molh^{-1}cm^{-2}$. The amount was comparable to previous findings in ox (To et al., 1998b) and rabbit (Chu and Candia, 1987). In ox, the magnitude of the L-glucose diffusion was about 74 $\eta molh^{-1}cm^{-2}$, with the exposed area of 0.25 cm^2. In rabbit, mannitol (MW = 182.2), which has a similar molecular weight as glucose (MW = 180.2), was used as the diffusional control. The mannitol flux obtained across a flat surface area of 0.75 cm^2 of the isolated rabbit iris-ciliary body (ICB) preparation ranged from 54 to 63 $\eta molh^{-1}cm^{-2}$. Our data indicated that our *in vitro* porcine CBE was able to maintain a tight barrier similar to other species. However, it should be noted that the L-glucose diffusion obtained in the CBE was calculated by assuming the tissue was a flat sheet of epithelium. The true L-glucose diffusion per unit flat area is likely to be less if the highly convoluted anatomy of the CBE was taken into consideration. Cole (1966) has estimated that the total surface area of the rabbit ciliary epithelium was about 6 cm^2. Using this value, Chu and Candia (1987) arrived at a conversion factor of 8 for correcting the extensively folded area and gave a corrected mannitol flux of 9.7 $\eta molh^{-1}cm^{-2}$ in rabbit ciliary epithelium. In porcine eye, the total surface area of the ciliary epithelium is not known. If we assume the extent of convolution is similar between rabbit and pig ciliary epithelium, the corrected L-glucose diffusion in our porcine CBE will range from 5.4 to 6.8 $\eta molh^{-1}cm^{-2}$. The data are comparable to the mannitol diffusion in other “tight” epithelia (Dawson, 1977) and implied that the porcine CBE should be considered as a tight epithelium as well.

5.3 Steady-state basal transepithelial electrical parameters

In our study, the *in vitro* porcine CBE possessed a spontaneous *TEP* (about 1 mV) with its aqueous side consistently negative with respect to the stromal side. The aqueous-negative polarity is apparently typical as it was seen in almost all vertebrate ciliary preparations (Table 4-2 and 5-1) although the magnitudes of the *TEP* and I_{sc} found in different studies did vary. Earlier studies in ox and rabbit ciliary preparations reported positive potentials on the aqueous side (Cole, 1961b; Cole, 1961a; Cole, 1962) which have led to the speculation that active Na^+ transport was the driving force for AHF. However, the notion was later questioned by a number of electrophysiological studies that observed a negative *TEP* on the aqueous side in different species (Holland and Gipson, 1970; Watanabe and Saito, 1978; Kishida et al., 1981; Iizuka et al., 1984; Krupin et al., 1984; Chu et al., 1987; To et al., 1998b; Wu et al., 2003). Kishida et al. (1981) have suggested the positive potential observed by Cole may be due to the lack of bicarbonate in the bathing solution. Moreover, it was also suggested that the positive potential found by Cole (1961b) by inserting an electrode into the posterior part of the eye might actually come from the retinal pigment epithelium (Iizuka et al., 1984) which is positive on the retinal side (Steinberg et al., 1978; To and Hodson, 1998). Although the *TEP* appears to be negative on the aqueous side in most recent studies, interesting observations have been reported in studies on shark (Wiederholt and Zadunaisky, 1987) and pig (Wu et al., 2003). In the shark study, half of the preparations exhibited positive *TEP* whereas the other half was negative. The authors postulated that it was the relative activities of Na^+ and Cl^- transport across the cell membrane of the PE and NPE cells that determined the polarity and magnitude of the electrical parameters. In the pig study, it

was found that about 2/3 of the porcine tissues had aqueous-negative *TEP* while the rest showed positive *TEP* of comparable magnitude but the authors did not explain the observations. In our study, the isolated porcine CBE did not show aqueous-positive *TEP* of comparable magnitudes as those of aqueous-negative *TEP*. However, we noticed that the *TEP* depolarized to a value closed to zero if the bathing temperature was too high or if the perfusion in the CP chamber stopped in our preliminary works. Since we also found that preparations with low *TEP* were less responsive to various pharmacological reagents, we postulated that these preparations might not have been physiologically intact. As a result, we decided to perform all our later experiments in a lower temperature (23 to 27 °C). Presumably lower bathing temperature can reduce the accumulation of metabolic wastes and preserve the physiology better. The presence of characteristic electrical responses by ouabain (Section 4.1.2), active secretion of Cl^- (Section 4.4) and brisk responses to various pharmacological agents all indicated that our *in vitro* isolated porcine CBE were physiological intact.

As summarized in Table 5-1, the R_t of the ciliary epithelial preparations varied with species. The value ranged from about 30 Ωcm^2 in shark to 185 Ωcm^2 in monkey. The average R_t of our porcine CBE was about 80 Ωcm^2, which was slightly higher than that reported in another porcine study (Wu et al., 2003), but was generally comparable to those R_t in other species. As in the case for L-glucose diffusion (Section 5.2), the real R_t of our porcine CBE has to be corrected for the extensive foldings of the ciliary processes. By applying the same conversion factor (8x) as stated in section 5.2, the real R_t of our preparations was about 640 Ωcm^2 which also categorizes the porcine ciliary epithelium (CE) as tight epithelium (Fromter and Diamond, 1972). To summarize, the findings of high R_t and low L-glucose diffusion

implied that the *in vitro* porcine CBE have maintained a low leakage and high resistance barrier.

Investigators	**Year**	**Species**	***TEP*** **(mV)**	$\boldsymbol{I_{sc}}$ **(μAcm^{-2})**	$\boldsymbol{R_t}$ **(Ωcm^2)**
Cole	(1961a)	Ox	[3.80]	[62.0]	61
Cole	(1962)	Ox	[5.53]	[46.0]	116
		Rabbit	[3.83]	[29.5]	124
Holland & Gipson	(1970)	Cat	~ -1.3	~ -27	~ 49
Watanabe & Saito	(1978)	Toad	-3.7	-51	89
Kishida et al.	(1981)	Rabbit	-0.70	-13.3	48
Burstein et al.	(1984)	Rabbit	-0.66	-7.8	84
Krupin et al.	(1984)	Rabbit	-1.2	-7.9	152
Iizuka et al.	(1984)	Dog	-1.35	-23.6	57
Nagasubramanian & Poinoosawmy	(1986)	Rabbit	[4.04]	N/A	N/A
Wiederholt & Zadunaisky	(1987)	Shark	-0.51	-18.3	31
			[0.53]	[19.6]	28
Chu et al.	(1987)	Monkey	-2.5	-13.6	185
Sears et al.	(1991)	Rabbit CE bilayer	-0.65	-13.0	50
To et al.	(1998b)	Ox	-0.51	-5.43	94
Do & To	(2000)	Ox	-0.55	-8.0	72
Crook et al.	(2000)	Rabbit CE bilayer	-0.68	-18.5	40
Wu et al.	(2003)	Human	-1.18	-19.9	59
		Pig	-0.86	-15.6	57
			[0.81]	[16.3]	54

Table 5-1 Summary of the average electrical parameters across the ciliary preparation in previous investigations. CE stands for ciliary epithelium.

[ ] Aqueous positive *TEP* N/A Not available

5.4 Anions (Cl^-, HCO_3^-) dependent *TEP* and I_{sc}

The negative *TEP* found across our porcine CBE indicated that there is either anionic transport in the stromal-to-aqueous direction or cationic transport in the opposite direction or both. The predominance of anion transport is a more logical and plausible deduction since it is in the direction of AHF. The fact that reducing bathing Cl^- and depleting bathing HCO_3^- both substantially depolarized the *TEP* and I_{sc} further supported the importance of anionic transport in AHF.

In our Cl^- substitution experiment, the electrical parameters were depolarized by 35% and 63% when the bathing Cl^- concentration was reduced from 120mM to 60 mM and 30mM, respectively. The polarity of the *TEP* and I_{sc} across the CBE preparations have been demonstrated to be dependent on the bathing Cl^- concentration in various species including toad (Watanabe and Saito, 1978), rabbit (Kishida et al., 1981) and ox (Do and To, 2000) although the extent of dependence varied among the species. In toad, depletion of bathing Cl^- almost completely abolished the *TEP* to about 2% of its basal value (Watanabe and Saito, 1978). Contrasting data have been reported in rabbit studies. In one of the rabbit studies, the *TEP* was almost abolished when the bathing Cl^- concentration was reduced to 25.6 mM and a reverse in polarity was observed when the bathing Cl^- was depleted (Kishida et al., 1981). However, this Cl^- dependent *TEP* changes could not be reproduced in another electrophysiology study using rabbit (Krupin et al., 1984). In ox, reversed polarity of the *TEP* was seen when the bathing Cl^- concentration was reduced to 30mM (Do and To, 2000). In addition to the dependence of the steady-state electrical parameters on the bathing Cl^-, we have observed a transient hyperpolarization of the *TEP* and I_{sc} whenever the bathing Cl^- concentration was reduced. There are several possible explanations for

this transient phenomenon. Firstly, as the bathing Cl^- concentration was reduced, Cl^- in the NPE immediately flushed into the aqueous along its electrochemical gradient. This is the most direct explanation. Secondly, substitution of bathing Cl^- with the less permeant gluconate/cyclamate in our experiment may have reduced the paracellular shunting. As the *TEP* was shunted to a lesser extent, transient hyperpolarization would be observed. The fact that the R_t increased in low bathing Cl^- (Table 4-3) was consistent with this speculation of changes in paracellular shunting. Thirdly, reduction of bathing Cl^- decreased the exchange of extracellular Cl^- with intracellular HCO_3^- across a putative anion exchanger (AE) on the basolateral membrane of the NPE facing aqueous. As the intracellular HCO_3^- increases, intracellular pH (pH_i) increases and it may open up Cl^- conductive pathway on the basolateral membrane of the NPE and thus the Cl^- efflux is enhanced. The detailed observations led to our postulation of this putative AE will be discussed further in Section 5.5.1.2. It should be noted that the above possible explanations for the transient hyperpolarization were not mutually exclusive. Moreover, further investigation is needed to verify the origin of these transient responses.

In the HCO_3^- depletion experiment, the *TEP* and I_{sc} across the porcine CBE were virtually abolished. Removing HCO_3^- reversed the polarity of the *TEP* (Kishida et al., 1981; Krupin et al., 1984) in rabbit preparations while the same manoeuvre only inhibited the I_{sc} by about 30% in ox (Do and To, 2000). The extent of dependence of the *TEP* of the porcine CBE on the bathing HCO_3^- apparently fell in between the rabbit and ox. This result also implied that HCO_3^- may have a more important role in the AHF in pig than in ox, although recent findings of higher Cl^- concentrations in the AH than in the plasma in both species suggested a predominant role of Cl^- (Gerometta et al., 2005).

To summarize, our present findings indicated that ion transport across the porcine CBE showed a clear dependence on the bathing Cl^- and HCO_3^-. The findings signified the importance of the two anions in the mechanism of AHF in pig eye.

5.5 Cl^- transport across the isolated porcine CBE

Earlier studies in search of net Cl^- transport across the CBE preparations have been controversial. Statistical significant net Cl^- transport in the stromal-to-aqueous direction have been demonstrated in studies of cat (Holland and Gipson, 1970), toad (Saito and Watanabe, 1979), and rabbit (Kishida et al., 1982). However, other works found no net Cl^- transport across the preparations of rabbit (Pesin and Candia, 1982; Krupin et al., 1984). Recent demonstration of the net Cl^- transport across the CBE preparations of ox (To et al., 1998a; To et al., 1998b; Do and To, 2000) and CE bilayer of rabbit (Crook et al., 2000) rekindled the importance and attention of Cl^- transport in AHF.

In our study of the porcine CBE, we have detected a net stromal-to-aqueous Cl^- transport of about 1.0 $\mu Eqh^{-1}cm^{-2}$ across the isolated preparations under short-circuited condition with both CP and ORC chambers (Table 4-5). The magnitude of the net Cl^- transports across the porcine CBE was comparable to those in most other species (Table 5-2). The usual findings of the net Cl^- transport were in the range of 0.81 to 2.89 $\mu Eqh^{-1}cm^{-2}$. Exceptionally large net Cl^- transport (108.0 $\mu Eqh^{-1}cm^{-2}$) has been found in rabbit CE bilayer (Crook et al., 2000). The large net Cl^- transport amounted to 48 times of that reported in previous study using the same species (Kishida et al., 1982). The exact reason for the discrepancy remains obscure.

Using the net Cl^- transport (1.01 $\mu Eqh^{-1}cm^{-2}$, n = 109) found with the ORC chamber as most of the Cl^- flux studies were carried out in this chamber and by applying equation 3.3 (section 3.5), we converted the net Cl^- transport into its corresponding current flow (I_{Cl}) and the value was about 27.1 μAcm^{-2}. Such amount of I_{Cl} was about 2.2 times of the measured I_{sc} (about 12.4 μAcm^{-2}, Table 4-2) across

the porcine CBE mounted in the ORC chamber. The discrepancy between the I_{Cl} and the measured I_{sc} appeared to be a common finding among the CBE preparations of different species. The ratio between the I_{Cl} and measured I_{sc} (I_{Cl} / measured I_{sc}) was 2.7 in cat (Holland and Gipson, 1970), 1.5 in toad (Saito and Watanabe, 1979), 4.6 in rabbit (Kishida et al., 1982), and 3.5 in ox (Do and To, 2000). As the measured I_{sc} is the algebraic sum of all ions transport across the preparations, the above discrepancy may indicate the involvement of other ion transport processes accompanying with Cl^-. Cations (e.g. Na^+) transport along with Cl^- and anions transport (e.g. HCO_3^-) in the opposite direction are both possible reasons for our observations and they are not mutually exclusive. The existence of other active ions transport across the porcine CBE is yet to be determined. Nevertheless, our observation of the I_{sc} depolarization by HCO_3^- depletion (Section 4.3.2) did not suggest the presence of active aqueous-to-stromal HCO_3^- transport. It is because if there is an active HCO_3^- transport in such direction, depletion of bathing HCO_3^- should have led to a stimulation of the measured I_{sc}.

Investigators	Year	Species	J_{sa}Cl	J_{as}Cl	J_{net}Cl
Holland & Gipson	(1970)	Cat	12.28	9.39	2.89*
Saito & Watanabe	(1979)	Toad	7.67	4.12	2.60*
Kishida et al.	(1982)	Rabbit	15.69	13.44	2.25*
Pesin & Candia	(1982)	Rabbit	10.9	9.2	1.7
To et al.	(1998b)	Ox	4.50	3.69	0.81*
To et al.	(1998a)	Ox	6.32	5.20	1.12*
Do & To	(2000)	Ox	4.74	3.71	1.03*
Crook et al.	(2000)	Rabbit CE bilayer	180.3	72.3	108.0*

Table 5-2 Summary of the average Cl^- transport across the ciliary preparation under short-circuited condition in previous investigations. CE stands for ciliary epithelium.
The unit of the Cl^- transport is $\mu Eqh^{-1}cm^{-2}$. * Statistical significant net Cl^- secretion

5.5.1 Influx of Cl^- into the porcine PE

Influx of ions into the PE across its basolateral membrane facing the ciliary stroma is the first step of transepithelial ion transport across the CE (Section 1.5). Based on their observations in the cultured bovine PE cells, Wiederholt et al. (1991) proposed that there are two major influx pathways for loading of NaCl into the PE cells (Figure 1-2): (1) the bumetanide-sensitive $Na^+/K^+/2Cl^-$ cotransporter (NKCC), and (2) the Cl^-/HCO_3^- (AE) and Na^+/H^+ (NHE) double exchangers. Both pathways make use of the standing Na^+ gradient created by the Na^+,K^+-ATPases on the basolateral membrane of the PE to accumulate other ions in an electroneutral manner. The two mechanisms are not mutually exclusive and their dominance may vary among species (To et al., 2002). In our experiment, we have tested the contribution of

the two pathways on the Cl^- transport across the porcine CBE by studying the effects of their inhibitors on both electrical properties and Cl^- transport.

5.5.1.1 $Na^+/K^+/2Cl^-$ cotransporter (NKCC) in the porcine CBE

$Na^+/K^+/2Cl^-$ cotransporter (NKCC) is a class of membrane proteins which transports Na^+, K^+ and Cl^- ions in a coupled and electroneutral manner (Haas and Forbush, 2000; Russell, 2000). The cotransporter usually actively accumulates intracellular Cl^- concentration ($[Cl^-]_i$) above the predicted electrochemical equilibrium in most cells under physiological condition. The role of NKCC in salt-transporting epithelia is well characterized. In secretory epithelia such as intestine (Dharmsathaphorn et al., 1985), airway (Boucher and Larsen, 1988), and salivary gland (Nauntofte, 1992), Cl^- enters into the cells with Na^+ and K^+ via the basolateral NKCC and then diffuses into the lumen via the apical Cl^- channels, thus it results in a lumen-negative electrical potential. The negative potential then drives passive flow of Na^+ from the serosa into the lumen and finally bulk flow of water is driven by the NaCl chemical gradient.

The 5-sulfamoylbenzoic acid loop diuretics including furosemide (FSM), bumetanide (BMT), and benzmetanide are inhibitors of the transport of NKCC (O'Grady et al., 1987). In the CE, evidences supported the role of NKCC for solute uptakes into PE cells are substantial. Firstly, FSM decreased intracellular Cl^- activity of intact shark CE (Wiederholt and Zadunaisky, 1986). Secondly, uptake of $^{22}Na^+$ and $^{36}Cl^-$ in cultured bovine PE cells was blunted by BMT (Helbig et al., 1989a). Thirdly, a Na^+, K^+, and Cl^--dependent, BMT-inhibitable uptake activated by iso-osmotical shrinkage has been demonstrated on the freshly dissociated bovine PE cells (Edelman

et al., 1994). Later studies with Ussing chamber also found that BMT inhibited Cl^- secretion in rabbit CE bilayer (Crook et al., 2000) and bovine CBE preparation (To et al., 1998a; Do and To, 2000). Most recently, it has also been found that perfusion of BMT reduced the AHF by 35% in *in vitro* perfused bovine eye (Shahidullah et al., 2003). On the other hand, contradicting findings that did not support a major role of NKCC in solute uptake on PE cells have also been reported. For instance, it was found that BMT has no inhibitory effect on the intracellular Cl^- accumulation in isolated rabbit PE cells (McLaughlin et al., 1998).

Our findings supported a role of NKCC for the Cl^- uptake into PE cells as both FSM and BMT depolarized the I_{sc} across the porcine CBE (Figure 4-7 and Table 4-8) and BMT reduced the net Cl^- secretion in the stromal-to-aqueous direction ($J_{net}Cl$) (Figure 4-9 and Table 4-9). In that, bilateral (BS) BMT reduced the I_{sc} and $J_{net}Cl$ by 56% and 57%, respectively. BMT (BS) has produced at least 86% inhibition on the $J_{net}Cl$ in bovine CBE (To et al., 1998a; Do and To, 2000) and 52% inhibition on the PE-to-NPE Cl^- flux across the rabbit CE bilayer with no inhibition on the backflux (Crook et al., 2000). The inhibitory effect of BMT on the $J_{net}Cl$ across the porcine CBE was comparable to that of rabbit but smaller than that of ox. However, the fact that aqueous addition of both FSM and BMT produced a larger inhibition on the I_{sc} than their stromal (ST) addition, and BMT (AQ) (46%) showed a slightly higher inhibitory effect on the $J_{net}Cl$ than BMT (ST) (36%) was apparently inconsistent with the immunological studies revealed that NKCC were more abundant in PE cells than in NPE cells of rabbit (Crook et al., 2000) and ox (Dunn et al., 2001). Presumably, larger inhibition should be resulted by the loop diuretics with their ST addition if NKCC is more abundant on the basolateral membrane of PE cells. There are a number of possible explanations. There may be an unknown FSM/BMT-sensitive anion

transport system at the NPE cells for Cl^- efflux into AH. In addition, the presence of the ciliary stroma in our CBE might have hindered the diffusion of FSM/BMT to the NKCC at the PE. Therefore, aqueous FSM/BMT may have actually acted more easily on the NKCC at the PE cells and more directly on the unknown anion transport system at the NPE than their stromal addition. Further investigation is required to clarify the situation.

In Table 4-9, it was noted that the aqueous-to-stromal Cl^- fluxes ($J_{as}Cl$) were significantly increased in all cases of BMT treatment while the changes in the stromal-to-aqueous Cl^- fluxes ($J_{sa}Cl$) were minimal. It was apparent that the reduction on the net Cl^- secretion ($J_{net}Cl$) was due to the increase in the $J_{as}Cl$. However, given the R_t of the porcine CBE have also been reduced by BMT (Table 4-8), both unidirectional fluxes may have been increased by the increased paracellular leakage. Therefore, the inhibitory effect of BMT on the $J_{sa}Cl$ may have been underestimated while the stimulatory effect on the $J_{as}Cl$ may have been overestimated. As a result, it is still possible that BMT reduced the $J_{net}Cl$ by direct inhibition of the $J_{sa}Cl$ or combined effects of a reduced $J_{sa}Cl$ and an increased $J_{as}Cl$. In ox, BMT (ST) also stimulated the $J_{as}Cl$ (Do and To, 2000). The authors postulated that as the cotransporter in the PE cells is blocked, the solute uptake decreases and the intracellular Cl^- concentration drops accordingly. Afterwards, reabsorption of Cl^- increases to replenish the intracellular Cl^- and thus the $J_{as}Cl$ increases. The same proposition may also be applicable to the case in pig.

In additional to the PE cells, NKCC has also been detected in NPE cells (Dunn et al., 2001). The function of the NKCC in the NPE cells is less defined. In cultured human NPE cells, Civan et al. (1996) found that NKCC was one of the cotransporter responsible for the ion absorption from AH leading to regulatory volume increase

(RVI) while in freshly dissociated bovine NPE cells, no RVI activity have been detected after exposing the cells to osmotic shrinkage (Edelman et al., 1994). Based on the observations with electron probe X-ray microanalysis (EPMA) that measured the intracellular ion contents of isolated CE (Bowler et al., 1996; McLaughlin et al., 1998), Macknight et al. (2000) developed an interesting new model of AHF. In that model, NKCC was proposed to be responsible for the net outward movement of ions (Na^+, K^+ and Cl^-) from the CE to both the stroma and aqueous, with the cotransporter on the NPE cells being the major conduit for solutes efflux into the aqueous. However, our data did not support such outwardly directed NKCC on both PE and NPE layers as the effects of unilateral BMT on both the I_{sc} and Cl^- transport were overlapped and concerted. Moreover, our data argued against the proposition that NKCC being the major conduit for solutes efflux from the NPE cells into the aqueous, since if it is the case, inhibition of NKCC with BMT (AQ) should reduce the J_{sa}Cl drastically. Instead, no significant inhibition of the J_{sa}Cl was found (Table 4-9) while a Cl^- channel inhibitor, NFA (AQ) can reduce the J_{sa}Cl by 42% (Table 4-15).

5.5.1.2 Cl^-/HCO_3^- exchanger (AE) in the porcine CBE

Cl^-/HCO_3^- exchanger (AE) and Na^+/H^+ exchanger (NHE) are primarily physically independent entities that exist virtually in all cells and they are crucial for a number of physiological functions including regulation of intracellular pH (pH_i), cell volume, and transepithelial transport (Lowe and Lambert, 1982; Wakabayashi et al., 1997). In the ciliary epithelium (CE), AE and NHE have been functionally demonstrated in both PE (Helbig et al., 1988a; Helbig et al., 1988b; Helbig et al., 1988c; Helbig et al., 1989c) and NPE cells (Wolosin et al., 1991; Matsui et al., 1996; Wu et al., 1998). Wiederholt (1991) proposed that AE and NHE could work in concert to constitute a NaCl uptake mechanism on the PE cells by functionally coupling to carbonic anhydrase (CA). Subsequent investigations by electron probe X-ray microanalysis (EPMA) supported the mechanism as the key pathway of NaCl uptake (McLaughlin et al., 1998; Macknight et al., 2000).

In the present study, we have tested the role of AE by investigating the effects of an AE inhibitor, DIDS. Our results did not support AE as a major uptake pathway of Cl^- at the PE cells as DIDS showed no inhibitory effects on both the I_{sc} (Figure 4-10 and Table 4-10) and net Cl^- secretion in the stromal-to-aqueous direction (J_{net}Cl) (Figure 4-12 and Table 4-11). Instead, aqueous (AQ) DIDS (0.1 mM) unexpectedly induced a hyperpolarization of the I_{sc} (80%) and an increase in the J_{net}Cl (59%) across the porcine CBE while DIDS (ST) did not altered these two parameters.

The effects of DIDS on the CE were variable among previous studies. In monkey CE, DIDS (AQ, 0.1mM) reduced the I_{sc} while stromal (ST) DIDS has no effect. In rabbit CE bilayer, DIDS inhibited the I_{sc} regardless the side of addition but was more potent at low concentrations (< 0.1mM) when added to the NPE side and more potent at higher concentrations (> 0.1mM) when added to the PE side (Crook et

al., 2000). In ox, bilateral (BS) DIDS (0.1mM) reduced the I_{sc} by half but did not alter the J_{net}Cl in CBE preparations (Do and To, 2000) while DIDS (ST, 0.1mM) reduced the AHF rate by 56% in *in vitro* perfused eye (Shahidullah et al., 2003). The variations may be due to considerable species differences.

The unexpected DIDS (AQ) stimulatory effects on the I_{sc} and J_{net}Cl were intriguing. The unidirectional fluxes data have apparently revealed that the increase in J_{net}Cl was predominantly due to a stimulated stromal-to-aqueous Cl^- transport (J_{sa}Cl) of 11% (Table 4-11). The increase in J_{sa}Cl (0.51 $\mu Eqh^{-1}cm^{-2}$) corresponded to an equivalent electrical current increase of about 13.7 μAcm^{-2}, which was almost equal to the average I_{sc} increase induced by DIDS (AQ) (13.3 μAcm^{-2}). This result indicated that the I_{sc} hyperpolarization with DIDS (AQ) could be attributed solely to its stimulation on the J_{sa}Cl. The phenomenon was seldom seen with other pharmacological agents. Among other possibilities, we proposed that the phenomenon could be explained by a putative, highly selective Cl^- channel on the basolateral membrane of the NPE. This putative Cl^- channel may be opened by alkaline intracellular pH (pH_i) but closed by acidic pH_i. DIDS (AQ) may inhibit a putative AE on the basolateral membrane of the NPE that exchanges intracellular HCO_3^- ($[HCO_3^-]_i$) with extracellular Cl^- ($[Cl^-]_o$). Operation of such AE has been observed in rabbit NPE and it was proposed as one of the major determinants of the pH_i of the NPE (Wolosin et al., 1991). Inhibition of the putative AE increases $[HCO_3^-]_i$ and thus pH_i. This alkalization then causes the opening of the putative Cl^- channel. As a result, both the I_{sc} and J_{sa}Cl increased.

Ion substitution experiments in the present study were consistent with the above proposition. Firstly, bathing Cl^- substitution showed a transient I_{sc} hyperpolarization (Section 4.3.1) that might be attributed to the reduction of bathing

Cl^- that retarded the exchange by the putative AE. $[HCO_3^-]_i$ and pH_i thus increased and caused the opening of the putative Cl^- channel. Secondly, HCO_3^- depletion abolished the I_{sc} (Section 4.3.2). In this case, depletion of bathing HCO_3^- favoured HCO_3^- efflux via the putative AE and the pH_i reduced subsequently so that the putative Cl^- channel was closed. Regardless of the mechanism, pH_i reduction due to HCO_3^- depletion has been detected in cultured rabbit NPE cells (Wu et al., 1998). Acidification caused by HCO_3^- (AQ) depletion has also been proposed as a mechanism of Cl^- channel closure that reduced the I_{sc} and $J_{net}Cl$ in a recent study in bovine CBE (To et al., 2001). Although direct evidence regarding the regulation of Cl^- channels on the NPE cells by pH_i is yet to be available at present, it has been shown in parotid (Arreola et al., 1995) and lacrimal acinar cells (Park and Brown, 1995) that Ca^{2+}-dependent Cl^- channel can be modulated by pH_i. In addition, the strong inhibitory effects of niflumic acid (NFA) on the I_{sc} and $J_{net}Cl$ across our porcine CBE may also pointed to the dominance of Ca^{2+}-activated Cl^- channel (Section 5.5.3).

5.5.2 Cl^- transport between the PE and NPE in the porcine CBE

Once Cl^- was taken up into the PE cells, the ions can freely diffuse between the PE and NPE cells via the gap junctions which are well demonstrated by structural (Raviola and Raviola, 1978), immunological (Coca-Prados et al., 1992; Coffey et al., 2002) and functional studies (Green et al., 1985; Edelman et al., 1994; Bowler et al., 1996). In the present study, gap junction inhibitor, heptanol, abolished the I_{sc} (Figure 4-13 and Table 4-12) and inhibited the net Cl^- secretion ($J_{net}Cl$) by 82% (Figure 4-15 and Table 4-13). Our results are comparable to previous findings that heptanol

inhibited the I_{sc} (85-90%) across rabbit ICB (Wolosin et al., 1997) and both I_{sc} (80%) and J_{net}Cl (80%) in bovine CBE (Do and To, 2000). Our results further confirmed an important role of gap junction in the ion transfer between the PE and NPE cells. Furthermore, the strong inhibition on the J_{net}Cl also confirmed the transcellular nature of the Cl^- secretion detected in our isolated porcine CBE. Heptanol also reduced the R_t across the porcine CBE by an average of 11% (Table 4-12), suggesting the reagent may have loosened the tight junctions of the paracellular pathway. A similar R_t reduction (7-8%) was also noticed in bovine CBE (Do and To, 2000).

5.5.3 Efflux of Cl^- from the porcine NPE

Cl^- channels reside both in membrane and in intracellular organelles and are responsible for a wide range of physiological functions including ion homeostasis, cell volume regulation, transepithelial transport, and regulation of electrical excitability (Jentsch et al., 2002). In the ciliary epithelium (CE), the final step of the transepithelial Cl^- transport is probably through the Cl^- channels on the basolateral membrane of the NPE cells (Jacob and Civan, 1996). The Cl^- channel has also been proposed as the rate-limiting step of AHF (Coca-Prados et al., 1995; Civan et al., 1997). The driving force of the Cl^- efflux through the channels is provided by its electrochemical gradient built up by the accumulation of Cl^- ions above its equilibrium potential as has been detected in isolated shark (Wiederholt and Zadunaisky, 1986) and rabbit (Bowler et al., 1996) CE.

NPPB is a commonly used Cl^- channel blocker that has shown inhibitory effect on the Cl^- channels activity in a number of CE studies. For instance, NPPB inhibited

the regulatory volume decrease (RVD) in cultured human NPE cells (Civan et al., 1992; Coca-Prados et al., 1996) and prevented the activation of hypotonic-induced Cl^- channels activity in bovine PE and NPE cells (Zhang and Jacob, 1997). Moreover, it also slightly reduced the AHF rate (25%) in *in vitro* perfused bovine eye (Shahidullah et al., 2003) and recently it has also been shown to inhibit a cAMP-activated maxi-Cl^- channel in native bovine PE cells (Do et al., 2004).

In an Ussing chamber study, NPPB dramatically reduced the I_{sc} and net Cl^- secretion (J_{net}Cl) across the bovine CBE preparation by over 90% (Do and To, 2000). However, we did not observe any inhibitory effect of NPPB on the I_{sc} (Figure 4-16 and Table 4-14) and J_{net}Cl (Figure 4-18 and Table 4-15) across the porcine CBE. The results indicated either there is no Cl^- channel on the porcine NPE or its Cl^- channel is not NPPB-inhibitable. As a result, we tried another Cl^- channel inhibitors, niflumic acid (NFA) and found that NFA abolished the I_{sc} (Figure 4-16 and Table 4-14) and J_{net}Cl (Figure 4-18 and Table 4-15). Therefore, our results suggested that the Cl^- efflux from the NPE of the porcine CE into the aqueous went through a NFA-sensitive but NPPB-insensitive Cl^- channel. At present, the molecular identity of the Cl^- channel on the NPE is still unknown although several candidates have been proposed from a number of RVD studies (Coca-Prados et al., 1995; Coca-Prados et al., 1996; Wu et al., 1996). Drastic NFA effects on the I_{sc} and J_{net}Cl in our study suggested that the Cl^- channel on the porcine NPE may be a calcium-activated Cl^- channel (CaCC) since NFA is the most common and potent blocker of native CaCC in *Xenopus* oocytes (White and Aylwin, 1990). However, the concentration used in the present study was relatively high and therefore, it is possible that NFA may have also affected other unknown molecular identities (reviewed in Hartzell et al. (2005)). To date, the presence of CaCC in CE is yet to be demonstrated (Jacob and Civan, 1996)

but it warrants further investigation as this channel clearly plays a significant role in other secretory epithelia (reviewed in Begenisich & Melvin, (1998)). In additional to Cl^- channel, $Na^+/K^+/2Cl^-$ cotransporter (NKCC) has also been proposed as the dominant pathway for Cl^- releases from the NPE in rabbit (McLaughlin et al., 1998). Therefore, dramatic species differences may exist in the Cl^- efflux pathway in the CE.

5.6 Regulation of the net Cl^- secretion ($J_{net}Cl$) by nitric oxide (NO)

NO is a simple diatomic molecule and it has multifaceted biological effects including protective, regulatory and deleterious functions (Wink and Mitchell, 1998). In biological system, NO is produced from the conversion of L-arginine into L-citrulline by nitric oxide synthase (NOS) (Moncada et al., 1991). In normal physiology, NO has emerged as a prototype molecule that signals by its chemistry, instead of its special configuration as in case of traditional signalling molecules (Lane and Gross, 1999).

NOS activity has been demonstrated in porcine (Haufschild et al., 1996) and bovine (Geyer et al., 1997) ciliary processes and NOS has also been localised in porcine CE (Meyer et al., 1999). These observations have indicated the involvement of NO on the physiology of AHF. Later in an electrophysiological study, activation of the classical nitric oxide (NO)-guanylate cyclase (GC)-3',5'-cyclic guanosine monophosphate (cGMP) pathway stimulated a transmembrane anionic current in porcine CE, which can be inhibited by Cl^- channel inhibitors (Fleischhauer et al., 2000). This finding provided the first evidence that NO has a direct modulatory role on the ionic transport across the CE. Very recently, a transient hyperpolarization of the I_{sc} across the porcine CBE, which depended on bathing Cl^- and HCO_3^- and inhibited by Cl^- channel inhibitors, were triggered by activation of the same NO-sGC-cGMP pathway (Wu et al., 2004). Based on the transient changes of the I_{sc}, the authors concluded that NO could stimulate anion secretion that implied an increase in AHF via the NO-sGC-cGMP pathway. However, such conclusion will need to be substantiated by the presence of transepithelial ion transport. Furthermore the I_{sc} changes were only transient, further information regarding the regulatory role of NO

on AHF is required. Therefore, we aimed to study whether and how NO signalling affects the steady-state net Cl^- secretion in the stromal-to-aqueous direction ($J_{net}Cl$).

In the present study, the effects of a stable and cell-permeable analog of cGMP, 8-pCPT-cGMP were first tested, as it is widely believed that NO signalling acts through the production of cGMP by activating sGC. We found that aqueous (AQ) 8-pCPT-cGMP produced a sustained hyperpolarization of the I_{sc} (Figure 4-19a and Table 4-16) and an increase of the steady-state $J_{net}Cl$ (Figure 4-21a and Table 4-17) while stromal (ST) addition of the reagent has no effect. The differential sidedness effects of cGMP analog have been noted before in other studies. It has been shown that another cGMP analog, 8-bromoguanosine 3:'5'-cyclic monophosphate (8-Br-cGMP), depolarized the I_{sc} when applied to the AQ side of isolated rabbit and cat CE but ST addition of the reagent either hyperpolarized the I_{sc} in the rabbit or had no effect in the cat (Carre and Civan, 1995). In a recent study using both porcine CBE and CE bilayer free of stroma (Wu et al., 2004), 8-pCPT-cGMP (AQ) also hyperpolarized the I_{sc} in a much larger extent than its ST addition. The differential sidedness effects of cGMP analogs are difficult to reconcile, since presumably the analog should be capable of freely diffuse across the cell membrane to reach its molecular target. Nevertheless, the present results of sustained increase of both the I_{sc} and $J_{net}Cl$ were consistent with the previous findings of sustained I_{sc} increase in the same species (Wu et al., 2004) indicating that activation of the cGMP downstream cascade could stimulate AHF.

If the regulation of NO on the Cl^- transport across the porcine CBE acts via the NO-sGC-cGMP pathway, NO donors will produce similar effects on the I_{sc} and $J_{net}Cl$ as the cGMP analog. However, we found that the two NO donors, sodium nitroprusside (SNP) and S-nitroso-N-acetyl-penicillamine (SNAP), produced similar

biphasic changes (Figure 4-19 b & c) of the I_{sc}. There was an only transient hyperpolarization, which was followed by a sustained depolarization (46% below basal) in case of SNP and a return to baseline in case of SNAP. SNP also reduced the steady-state J_{net}Cl by 44% while SNAP had no effect (Figure 4-21 b & c and Table 4-17). Although the extents of the two NO donors effects were slightly different which probably reflected differences in their kinetics of NO release (Feelisch, 1998), it was obvious that the effects of NO donors were not identical to that of the cGMP analog. Wu et al. (2004) observed an only transient hyperpolarization of the I_{sc} with NO donors and suggested it will increase the transepithelial transport of Cl^- in the stromal-to-aqueous direction via a sGC-cGMP-PKG pathway. However, in the present study, the NO donors inhibited the steady-state J_{net}Cl instead of stimulating it. The fact that the cGMP analog produced a sustained hyperpolarization response may be due to its stable nature that resists hydrolysis by endogenous phosphodiesterases (PDEs). However, the steady-state depolarization of the I_{sc} and reduction of the J_{net}Cl induced by SNP cannot be explained by the hydrolytic effects of PDEs alone. It is because if the intracellular cGMP concentration induced by NO was not sustained but transient, the I_{sc} and J_{net}Cl should have also returned to baseline in a similar fashion. But in fact, a steady-state inhibition of these two parameters were noted. Therefore, it is likely that NO may have two opposing effects on the J_{net}Cl. Firstly, NO may activate a cGMP-dependent pathway that increases the J_{net}Cl. A transient stimulation of the J_{net}Cl was not easily observable in our Ussing chamber set-up, therefore its existence cannot be ruled out. Secondly, NO may also activate a cGMP-independent pathway that reduces the J_{net}Cl in a slightly delayed but more sustained fashion. The steady-state effects of NO donors on the J_{net}Cl may be a resultant of the two opposite pathways.

To further test our hypothesis, we pre-treated the porcine CBE with a sGC inhibitor, 1H-[1,2,4]Oxadiazolo-[4,3,-a]quinoxalin-1-one (ODQ) and studied the subsequent effects by cGMP analog and NO donors. Presumably, ODQ would inhibit the stimulation of sGC by NO so that the cGMP-dependent pathway would be triggered in a lesser extent. As a result, the cGMP-independent responses, if any, would be revealed. Our results were consistent with the proposition of two opposing pathways. We found that both NO donors produced diminished transient hyperpolarization of the I_{sc} (compare Figure 4-20b and Figure 4-22b) and larger inhibition of the steady-state I_{sc} (compare Figure 4-20b and Figure 4-22b) and $J_{net}Cl$ (compare Figure 4-21 b & c and Figure 4-23 b & c) after pre-treating the preparation with ODQ.

Our results clearly showed that NO triggered a cGMP-independent pathway which resulted in an inhibition of the steady J_{net}Cl and thus implied a diminished AHF in pig eye. We then further studied the unknown cGMP-independent pathway. Our first aim was to look for other direct physiological effects of NO. The reaction of NO with metal complexes is facile enough to be biological relevant (Wink and Mitchell, 1998). Guanylate cyclase (GC), cytochrome P450 (Cyt P450), and nitric oxide synthase (NOS) all belong to this family of metal complexes. Cyt P450 is a family of enzymes that is involved in the synthesis and catabolism of numerous biomolecules such as fatty acids, steroids, prostaglandins, and leukotrienes (Benet and Sheiner, 1985). In earlier work of porcine CE, it was shown that the CE microsomes synthesized 12[R]-hydroxy-5, 8, 10, 14-eixosatetraenoic acid (12(R)-HETE) from arachidonic acid (AA) in a Cyt P450-mediated manner (Asakura and Shichi, 1992). The 12(R)-HETE produced in the process was shown to inhibit the Na^+, K^+-ATPase activity of rabbit CE (Delamere et al., 1991) and lower the intraocular pressure (IOP)

when administered topically to rabbits eye (Masferrer et al., 1990; Delamere et al., 1991). In renal epithelial cells (MMDD1), recent works found that NO inhibited NKCC via stimulation of a Cyt P450-dependent and cGMP-independent pathway (He et al., 2003). It was suggested that the stimulation of NO on the Cyt P450 led to the production of Cyt P450 epoxyeicosatrienoic acid (EET) metabolites from AA, possibly 14, 15-EET, which ultimately inhibited the NKCC.

If the Cyt P450 enzymes are present in our porcine CBE, NO can stimulate the enzyme and thus produce AA metabolites that may inhibit Na^+, K^+-ATPase and NKCC as above. Inhibition of these entities may then reduce the Cl^- transport activity across the porcine CBE. Our results supported the involvement of a NO-Cyt P450 pathway in the regulation of Cl^- transport across the porcine CBE as pre-treatment of 1-aminobenzotriazole (ABT), a Cyt P450 inhibitor alleviated the steady-state depolarization of the I_{sc} induced by subsequent NO donors (Figure 4-24).

To conclude, NO modulation of the J_{net}Cl across the porcine CBE involves both cGMP-dependent and cGMP-independent pathways. Stimulation of NO on the cGMP-dependent pathway may increase the J_{net}Cl while stimulation of NO on the cGMP-independent pathway has been shown to inhibit the I_{sc} and J_{net}Cl. The overall effects of NO were the resultant of the two opposing pathways and the cGMP-independent pathway was apparently the dominant pathway as the NO-cGMP-dependent hyperpolarization of the I_{sc} was only transient and the steady-state J_{net}Cl after treatment of NO donors remained low, or lower than baseline value. It was different from the sustained increase of the I_{sc} and steady-state J_{net}Cl induced by a cGMP analog. Activation of a Cyt P450-dependent pathway might be, at least in part, responsible for the cGMP-independent effect in reducing the Cl^- secretion. The

downstream cascades and the final molecular targets of the cGMP-independent pathway are yet to be elucidated.

5.7 Estimated fluid secretion rate of the *in vitro* porcine CBE

Assuming AHF is an isotonic secretion, the average net Cl^- secretion ($J_{net}Cl$) of 1.01 $\mu Eqh^{-1}cm^{-2}$ found across the *in vitro* porcine CBE (Table 4-5) will lead to an estimated fluid secretion rate (F_e) as suggested by the following equation:

$$F_e = J_{net}Cl / C \qquad (5.1)$$

where C is the concentration of Cl^- in the bathing solution (about 120 mOsm).

The estimated fluid secretion rate across the *in vitro* porcine CBE was therefore about 8.4 $\mu lh^{-1}cm^{-2}$. The net water influx reported in early study in rabbit was 9.6 $\mu lh^{-1}cm^{-2}$ (Cole, 1962). Recent attempt in measuring the spontaneous fluid transport in isolated CBE preparation in a modified Ussing chamber set up also obtained low value of about 2 μlh^{-1} per preparation of rabbit (exposed area 1.02 cm^2) and about 3 μlh^{-1} per preparation of ox (exposed area 1.36 cm^2)(Candia et al., 2005). Estimated and measured fluid transport rate obtained in *in vitro* studies was dramatically slow comparing with the *in vivo* AHF rate in human (about 165 μlh^{-1} per eye) (Brubaker, 1991) and rabbit (about 180 μlh^{-1} per eye) (Murray and Bartels, 1993;

Maren et al., 1997). The discrepancy may be attributed to the lack of the circulatory influence and the experimentally induced damages in the isolated *in vitro* preparation.

5.8 Summary and conclusions

The electrical properties and Cl^- transport across the isolated porcine CBE were investigated by the electrophysiological Ussing chamber technique. The major findings of the present study are summarized as below:

1. Viable porcine CBE were maintained *in vitro* in both the CP and ORC Ussing chambers. Functional and structural integrity of the CBE were ascertained according to three aspects: (1) maintenance of stable electrical parameters, (2) presence of characteristic electrical responses by ouabain, and (3) a small diffusional L-glucose leak.
2. A spontaneous *TEP* of approximately 1 mV was found across the porcine CBE (aqueous-side negative). The magnitude of the *TEP* and I_{sc} was dependent on both the bathing Cl^- and HCO_3^- concentrations. The findings signified the importance of anionic transport in AHF.
3. Under short-circuited condition, a significant net Cl^- transport (1.01 $\mu Eqhr^{-1}cm^{-2}$, n = 109, $p < 0.001$) in the stromal-to-aqueous direction ($J_{net}Cl$) was detected across the isolated porcine CBE in the ORC chamber. This result demonstrated an active Cl^- secretion into AH which may be a driving force for AHF in pig eye. This active Cl^- secretion is similar to that in the ox and rabbit CBE. The equivalent current (I_{Cl}) according to the $J_{net}Cl$ was about 2.2 times of the measured I_{sc}, suggesting the presence of accompanying cationic (e.g.

Na^+) transport or anionic transport (e.g. HCO_3^-) in the opposite direction or both.

4. The machineries that drive the Cl^- transport across the porcine CBE were investigated with various transport inhibitors. For the uptake of Cl^- into the PE, our results indicated that the bumetanide-sensitive $Na^+/K^+/2Cl^-$ cotransporter (NKCC) played a significant role (bilateral bumetanide reduced the $J_{net}Cl$ by 57%) while the DIDS-sensitive Cl^-/HCO_3^- anion exchanger (AE) did not. Unexpectedly, DIDS (AQ) hyperpolarized the I_{sc} and stimulated the $J_{net}Cl$ into AH. It may be due to the activity of a putative Cl^- channel, which is regulated by pH_i, on the basolateral membrane of the NPE. The validity of this proposition awaits further investigation. The intercellular gap junctions between the PE and NPE were also important in the transepithelial Cl^- transport. Blockage of the gap junction by its inhibitor, heptanol, abolished the I_{sc} and reduced the $J_{net}Cl$ (-82%). The exact identity of the Cl^- channel/efflux pathway on the NPE is still unknown. The present results indicated that the Cl^- channel on the NPE of the porcine CE was a niflumic acid (NFA)-sensitive but NPPB-insensitive type. This Cl^- channel is similar to the calcium-activated Cl^- channel (CaCC) in *Xenopus* oocytes (White and Aylwin, 1990), since both of them are strongly inhibited by NFA. Apparently, there may be species differences in this Cl^- efflux pathway at the NPE and further investigation is warrant.
5. Modulation of NO on the Cl^- secretion into the AH in pig eye may be via two opposing pathways: a cGMP-dependent pathway that stimulates the Cl^- secretion and a cGMP-independent pathway that reduces the Cl^- secretion. The cGMP-independent pathway was apparently the dominant pathway since the

NO-cGMP-dependent hyperpolarization of the I_{sc} was only transient and the steady-state $J_{net}Cl$ after treatment of NO donors remained low, or lower than baseline value. It was different from the sustained increase of the I_{sc} and steady-state $J_{net}Cl$ induced by a cGMP analog. Activation of a Cyt P450-dependent pathway might be, at least in part, responsible for the cGMP-independent effect in reducing the Cl^- secretion. Inhibition of the Cyt P450 enzyme by ABT alleviated the depolarization produced by the NO donors on the steady-state I_{sc}. The downstream cascades and the final molecular targets of the cGMP-independent pathway including the Cyt P450-dependent pathway are yet to be elucidated.

APPENDIX

		Stromal-to-aqueous (J_{sa})				Aqueous-to-stromal (J_{as})			
	n	***TEP*** **(mV)**	I_{sc} **(μAcm^{-2})**	R_t **(Ωcm^2)**	**LG**	***TEP*** **(mV)**	I_{sc} **(μAcm^{-2})**	R_t **(Ωcm^2)**	**LG**
BMT (ST)	5	-1.16 ±0.19	-15.38 ±2.62	78 ±9	54 ±8	-1.05 ±0.08	-12.98 ±1.58	84 ±7	53 ±7
BMT (AQ)	8	-0.94 ±0.19	-10.88 ±2.21	88 ±4	54 ±6	-0.86 ±0.08	-10.16 ±0.93	86 ±4	59 ±7
BMT (BS)	7	-1.03 ±0.15	-12.76 ±1.63	80 ±4	61 ±7	-0.90 ±0.11	-10.80 ±0.76	82 ±7	61 ±11
DIDS (ST)	5	-1.29 ±0.21	-14.54 ±1.38	87 ±9	48 ±6	-1.38 ±0.15	-14.91 ±1.58	94 ±9	43 ±3
DIDS (AQ)	5	-1.36 ±0.12	-14.83 ±1.00	92 ±8	55 ±6	-1.20 ±0.11	-12.66 ±0.92	94 ±3	55 ±3
Heptanol (BS)	6	-1.27 ±0.21	-16.49 ±2.83	78 ±6	59 ±6	-1.07 ±0.23	-14.11 ±2.94	76 ±3	62 ±4
NPPB (AQ)	7	-1.21 ±0.13	-14.43 ±2.01	87 ±7	43 ±3	-1.11 ±0.08	-13.21 ±1.13	86 ±5	39 ±4
NFA (AQ)	4	-1.46 ±0.37	-17.72 ±4.50	83 ±6	49 ±6	-1.10 ±0.24	-14.15 ±3.69	82 ±7	43 ±7
8-pCPT-cGMP (AQ)	10	-0.89 ±0.10	-9.55 ±1.69	96 ±6	53 ±3	-0.90 ±0.10	-9.45 ±1.60	96 ±3	48 ±3
ODQ (BS) + 8-pCPT-cGMP (AQ)	5	-1.05 ±0.22	-12.44 ±2.50	82 ±4	62 ±6	-1.06 ±0.15	-12.57 ±1.74	85 ±4	62 ±7
SNP (BS)	6	-0.98 ±0.12	-13.51 ±1.16	72 ±6	60 ±2	-0.85 ±0.07	-11.97 ±1.16	72 ±4	58 ±5
ODQ (BS) + SNP (BS)	4	-0.81 ±0.15	-10.02 ±1.84	82 ±5	53 ±3	-0.69 ±0.05	-8.44 ±0.80	82 ±5	56 ±6
SNAP (AQ)	7	-0.99 ±0.12	-12.19 ±2.04	86 ±6	63 ±7	-1.04 ±0.11	-12.34 ±1.01	85 ±7	63 ±6
ODQ (BS)+ SNAP (AQ)	4	-0.69 ±0.12	-8.73 ±1.42	79 ±7	64 ±9	-0.59 ±0.04	-7.92 ±0.59	75 ±4	67 ±5

A summary of the detailed steady-state basal electrical parameters of the paired preparations used for each experiment. The respective parameters of the J_{sa} group were not different from those of the J_{as} group in each experiment (Student's Paired t-test, p > 0.05)

REFERENCES

Abdel-Latif, A. A. (1997). Iris-ciliary body, aqueous humor and trabecular meshwork. *In* "Biochemistry of the Eye" (Harding J. J., ed.). 1st. Chapman & Hall, London, pp. 52-93.

Alvarez-Leefmans, F. J. (2001). Intracellular Chloride Regulation. *In* "Cell physiology sourcebook: a molecular approach" (Sperelakis N., ed.). 3rd. Academic Press, San Diego, pp. 301-318.

Arreola, J., Melvin, J. E. and Begenisich, T. (1995). Inhibition of Ca^{2+}-dependent Cl^- channels from secretory epithelial cells by low internal pH. *J Membr Biol* **147**, 95-104.

Asakura, T. and Shichi, H. (1992). 12(R)-hydroxyeicosatetraenoic acid synthesis by 3-methylcholanthrene- and clofibrate-inducible cytochrome P450 in porcine ciliary epithelium. *Biochem Biophys Res Commun* **187**, 455-459.

Balfour, J. A. and Wilde, M. I. (1997). Dorzolamide. A review of its pharmacology and therapeutic potential in the management of glaucoma and ocular hypertension. *Drugs Aging* **10**, 384-403.

Balshaw, D. M., Millette, L. A. and Wallick, E. T. (2001). Sodium Pump Function. *In* "Cell physiology sourcebook : a molecular approach" (Sperelakis N., ed.). 3rd. Academic Press, San Diego, pp. 261-270.

Bar-Ilan, A., Pessah, N. I. and Maren, T. H. (1984). The effects of carbonic anhydrase inhibitors on aqueous humor chemistry and dynamics. *Invest Ophthalmol Vis Sci* **25**, 1198-1205.

Barsotti, M. F., Bartels, S. P., Freddo, T. F. and Kamm, R. D. (1992). The source of protein in the aqueous humor of the normal monkey eye. *Invest Ophthalmol Vis Sci* **33**, 581-595.

Becker, B. (1955). The effects of the carbonic anhydrase inhibitor, acetazoleamide, on the composition of the aqueous humor. *Am J Ophthalmol* **40**, 129-136.

Becker, B. (1959). Carbonic anhydrase and the formation of aqueous humor. *Am J Ophthalmol* **47**, 342-361.

Becker, B. (1963). Ouabain and aqueous humor dynamics in the rabbit eye. *Invest Ophthalmol* **2**, 325-331.

Becquet, F., Courtois, Y. and Goureau, O. (1997). Nitric oxide in the eye: multifaceted roles and diverse outcomes. *Surv Ophthalmol* **42**, 71-82.

Begenisich, T. and Melvin, J. E. (1998). Regulation of chloride channels in secretory epithelia. *J Membr Biol* **163**, 77-85.

Benet, L. and Sheiner, L. (1985). Pharmacokinetics: The dynamics of drug absorption, distribution, and elimination. *In* "Goodman and Gilman's The pharmacological basis of therapeutics" (7th, ed.). Macmillian, New York, pp. 15-20.

Beyer, E. C., Paul, D. L. and Goodenough, D. A. (1990). Connexin family of gap junction proteins. *J Membr Biol* **116**, 187-194.

Bill, A. (1973). The role of ciliary blood flow and ultrafiltration in aqueous humor formation. *Exp Eye Res* **16**, 287-298.

Bill, A. (1975). Blood circulation and fluid dynamics in the eye. *Physiol Rev* **55**, 383-417.

Boucher, R. C. and Larsen, E. H. (1988). Comparison of ion transport by cultured secretory and absorptive canine airway epithelia. *Am J Physiol* **254**, C535-547.

Bours, J. (1990). The protein distribution of bovine, human and rabbit aqueous humour and the difference in composition before and after disruption of the blood/aqueous humour barrier. *Lens Eye Toxic Res* **7**, 491-503.

Bowler, J. M., Peart, D., Purves, R. D., Carre, D. A., Macknight, A. D. and Civan, M. M. (1996). Electron probe X-ray microanalysis of rabbit ciliary epithelium. *Exp Eye Res* **62**, 131-139.

Brubaker, R. F. (1991). Flow of aqueous humor in humans [The Friedenwald Lecture]. *Invest Ophthalmol Vis Sci* **32**, 3145-3166.

Burstein, N. L., Fischbaro, J., Liebovitch, L. and Cole, D. F. (1984). Electrical potential, resistance, and fluid secretion across rabbit isolated ciliary body. *Exp Eye Res* **39**, 771-779.

Butler, G. A., Chen, M., Stegman, Z. and Wolosin, J. M. (1994). Na^+- Cl^-- and HCO_3^--dependent base uptake in the ciliary body pigment epithelium. *Exp Eye Res* **59**, 343-349.

Candia, O. A. (1996). A novel system to measure labelled CO_2 and HCO_3^- fluxes across epithelia: corneal epithelium as model tissue. *Exp Eye Res* **63**, 137-149.

Candia, O. A., Shi, X. P. and Chu, T. C. (1991). Ascorbate-stimulated active Na^+ transport in rabbit ciliary epithelium. *Curr Eye Res* **10**, 197-203.

Candia, O. A., To, C. H., Gerometta, R. M. and Zamudio, A. C. (2005). Spontaneous Fluid Transport across Isolated Rabbit and Bovine Ciliary Body Preparations. *Invest Ophthalmol Vis Sci* **46**, 939-947.

Carre, D. A. and Civan, M. M. (1995). cGMP modulates transport across the ciliary epithelium. *J Membr Biol* **146**, 293-305.

Carre, D. A., Tang, C. S. R., Krupin, T. and Civan, M. M. (1992). Effect of bicarbonate on intracellular potential of rabbit ciliary epithelium. *Curr Eye Res* **11**, 609-624.

Chen, L., Wang, L. and Jacob, T. J. (1999). Association of intrinsic pI_{Cln} with volume-activated Cl^- current and volume regulation in a native epithelial cell. *Am J Physiol* **276**, C182-192.

Chu, T. C. and Candia, O. A. (1987). Electrically silent Na^+ and Cl^- fluxes across the rabbit ciliary epithelium. *Invest Ophthalmol Vis Sci* **28**, 445-450.

Chu, T. C. and Candia, O. A. (1988). Active transport of ascorbate across the isolated rabbit ciliary epithelium. *Invest Ophthalmol Vis Sci* **29**, 594-599.

Chu, T. C., Candia, O. A. and Podos, S. M. (1987). Electrical parameters of the isolated monkey ciliary epithelium and effects of pharmacological agents. *Invest Ophthalmol Vis Sci* **28**, 1644-1648.

Chuman, H., Chuman, T., Nao-i, N. and Sawada, A. (2000). The effect of L-arginine on intraocular pressure in the human eye. *Curr Eye Res* **20**, 511-516.

Civan, M. M., Coca-Prados, M. and Peterson-Yantorno, K. (1996). Regulatory volume increase of human non-pigmented ciliary epithelial cells. *Exp Eye Res* **62**, 627-640.

Civan, M. M., Peterson-Yantorno, K., Coca-Prados, M. and Yantorno, R. E. (1992). Regulatory volume decrease by cultured non-pigmented ciliary epithelial cells. *Exp Eye Res* **54**, 181-91.

Civan, M. M., Peterson-Yantorno, K., George, K. and O'Brien, T. G. (1989). Interactions of TPA and insulin on Na^+ transport across frog skin. *Am J Physiol* **256**, C569-578.

Civan, M. M., Peterson-Yantorno, K., Sanchez-Torres, J. and Coca-Prados, M. (1997). Potential contribution of epithelial Na^+ channel to net secretion of aqueous humor. *J Exp Zool* **279**, 498-503.

Coca-Prados, M., Anguita, J., Chalfant, M. L. and Civan, M. M. (1995). PKC-sensitive Cl^- channels associated with ciliary epithelial homologue of pI_{Cln}. *Am J Physiol* **268**, C572-529.

Coca-Prados, M., Ghosh, S., Gilula, N. B. and Kumar, N. M. (1992). Expression and cellular distribution of the alpha 1 gap junction gene product in the ocular pigmented ciliary epithelium. *Curr Eye Res* **11**, 113-122.

Coca-Prados, M., Sanchez-Torres, J., Peterson-Yantorno, K. and Civan, M. M. (1996). Association of ClC-3 channel with Cl^- transport by human nonpigmented ciliary epithelial cells. *J Membr Biol* **150**, 197-208.

Coffey, K. L., Krushinsky, A., Green, C. R. and Donaldson, P. J. (2002). Molecular profiling and cellular localization of connexin isoforms in the rat ciliary epithelium. *Exp Eye Res* **75**, 9-21.

Cole, D. F. (1960). Effects of some metabolic inhibitors upon the formation of the aqueous humour in rabbits. *Br J Ophthalmol* **44**, 739-750.

Cole, D. F. (1961a). Electrical potential across the isolated ciliary body observed *in vitro*. *Br J Ophthalmol* **45**, 641-653.

Cole, D. F. (1961b). Electrochemical changes associated with the formation of the aqueous humor. *Br J Ophthalmol* **45**, 202-217.

Cole, D. F. (1962). Transport across the isolated ciliary body of ox and rabbit. *Br J Ophthalmol* **46**, 577-591.

Cole, D. F. (1966). Aqueous humour formation. *Doc Ophthalmol* **21**, 116-238.

Cole, D. F. (1977). Secretion of the aqueous humour. *Exp Eye Res* **25**, 161-176.

Cole, D. F. (1984). Ocular Fluids. *In* "The Eye" (Davson H., ed.). 3rd. Academic Press, New York and London, pp. 269-390.

Cooper, D. K. C. (1992). Is Xenotransplantation a realistic clinical option? *Transplant Proc* **24**, 2393-2396.

Crook, R. B., Takahashi, K., Mead, A., Dunn, J. J. and Sears, M. L. (2000). The role of NaKCl cotransport in blood-to-aqueous chloride fluxes across rabbit ciliary epithelium. *Invest Ophthalmol Vis Sci* **41**, 2574-2583.

Crook, R. B., von Brauchitsch, D. K. and Polansky, J. R. (1992). Potassium transport in nonpigmented epithelial cells of ocular ciliary body: inhibition of a Na^+, K^+, Cl^- cotransporter by protein kinase C. *J Cell Physiol* **153**, 214-220.

Culotta, E. and Koshland, D. E., Jr (1992). NO news is good news. *Science* **258**, 1862-1865.

Cunha-Vaz, J. (1979). The blood-ocular barriers. *Surv Ophthalmol* **23**, 279-296.

Dailey, R. A., Brubaker, R. F. and Bourne, W. M. (1982). The effects of timolol maleate and acetazolamide on the rate of aqueous formation in normal human subjects. *Am J Ophthalmol* **93**, 232-237.

Davson, H. (1956). *Physiology of the Ocular and Cerebrospinal Fluids*. London, J&A Churchill Ltd.

Davson, H. (1990). The aqueous humor and the intraocular pressure. *In* "Physiology of the eye" (Davson H., ed.). 5th. Macmillan Press, London, pp. 3-95.

Dawson, D. C. (1977). Na and Cl transport across the isolated turtle colon: parallel pathways for transmural ion movement. *J Membr Biol* **37**, 213-233.

Delamere, N. A., Socci, R. R., King, K. L. and Bhattacherjee, P. (1991). The influence of 12(R)-hydroxyeicosatetraenoic acid on ciliary epithelial sodium, potassium-adenosine triphosphatase activity and intraocular pressure in the rabbit. *Invest Ophthalmol Vis Sci* **32**, 2511-2514.

Dharmsathaphorn, K., Mandel, K. G., Masui, H. and McRoberts, J. A. (1985). Vasoactive intestinal polypeptide-induced chloride secretion by a colonic epithelial cell line. Direct participation of a basolaterally localized Na^+,K^+,Cl^- cotransport system. *J Clin Invest* **75**, 462-471.

Diamond, J. and Bossert, W. H. (1967). Standing gradient osmotic flow: a mechanism for coupling of water and solute transport in epithelia. *J Gen Physiol* **50**, 2061-2083.

DiMattio, J. and Streitman, J. (1986). Facilitated glucose transport across the retinal pigment epithelium of the bullfrog (Rana catesbeiana). *Exp Eye Res* **43**, 15-28.

Do, C. W., Peterson-Yantorno, K., Mitchell, C. H. and Civan, M. M. (2004). cAMP-activated maxi-Cl^- channels in native bovine pigmented ciliary epithelial cells. *Am J Physiol Cell Physiol* **287**, C1003-C1011.

Do, C. W. and To, C. H. (2000). Chloride secretion by bovine ciliary epithelium: a model of aqueous humor formation. *Invest Ophthalmol Vis Sci* **41**, 1853-1860.

Dong, J., Delamere, N. A. and Coca-Prados, M. (1994). Inhibition of Na^+-K^+-ATPase activates Na^+-K^+-2Cl^- cotransporter activity in cultured ciliary epithelium. *Am J Physiol* **266**, C198-205.

Douglas, W. R. (1972). Of pigs and men and research: a review of applications and analogies of the pig, sus scrofa, in human medical research. *Space Life Sci* **3**, 226-234.

Dunn, J. J., Lytle, C. and Crook, R. B. (2001). Immunolocalization of the Na-K-Cl Cotransporter in Bovine Ciliary Epithelium. *Invest Ophthalmol Vis Sci* **42**, 343-353.

Edelman, J. L., Sachs, G. and Adorante, J. S. (1994). Ion transport asymmetry and functional coupling in bovine pigmented and nonpigmented ciliary epithelial cells. *Am J Physiol* **266**, C1210-1221.

Eichhorn, M., Inada, K. and Lutjen-Drecoll, E. (1991). Human ciliary body in organ culture. *Curr Eye Res* **10**, 277-286.

Elena, P. P., Fredj-Reygrobellet, D., Moulin, G. and Lapalus, P. (1984). Pharmacological characteristics of beta-adrenergic-sensitive adenylate cyclase in non pigmented and in pigmented cells of bovine ciliary process. *Curr Eye Res* **3**, 1383-1389.

Farahbakhsh, N. A. and Fain, G. L. (1987). Volume regulation of non-pigmented cells from ciliary epithelium. *Invest Ophthalmol Vis Sci* **28**, 934-944.

Feelisch, M. (1998). The use of nitric oxide donors in pharmacological studies. *Naunyn Schmiedebergs Arch Pharmacol* **358**, 113-122.

Fleischhauer, J. C., Beny, J. L., Flammer, J. and Haefliger, I. O. (2000). NO/cGMP pathway activation and membrane potential depolarization in pig ciliary epithelium. *Invest Ophthalmol Vis Sci* **41**, 1759-1763.

Flugel, C. and Lutjen-Drecoll, E. (1988). Presence and distribution of Na^+/K^+-ATPase in the ciliary epithelium of the rabbit. *Histochemistry* **88**, 613-621.

Freddo, T. F. (1999). Anatomy and pathphysiology of aqueous production and outflow. *In* "Ophthalmic Fundamentals: Glaucoma" (Sassani J. W., ed.). Thorofare, NJ, SLACK, pp. 33-51.

Freddo, T. F., Bartels, S. P., Barsotti, M. F. and Kamm, R. D. (1990). The source of proteins in the aqueous humor of the normal rabbit. *Invest Ophthalmol Vis Sci* **31**, 125-137.

Friedenwald, J. S. (1949). The formation of the intracellular fluid. *Am J Ophthalmol* **32**, 9-27.

Fromter, E. (1979). The Feldberg Lecture 1976. Solute transport across epithelia: what can we learn from micropuncture studies in kidney tubules? *J Physiol* **288**, 1-31.

Fromter, E. and Diamond, J. (1972). Route of passive ion permeation in epithelia. *Nat New Biol* **235**, 9-13.

Garg, L. C. and Oppelt, W. W. (1970). The effect of ouabain and acetazolamide on transport of sodium and chloride from plasma to aqueous humor. *J Pharmacol Exp Ther* **175**, 237-247.

Gerometta, R. M., Malgor, L. A., Vilalta, E., Leiva, J. and Candia, O. A. (2005). Cl^- concentrations of bovine, porcine and ovine aqueous humor are higher than in plasma. *Exp Eye Res* **80**, 307-312.

Geyer, O., Podos, S. M. and Mittag, T. (1997). Nitric oxide synthase activity in tissues of the bovine eye. *Graefe's Arch Clin Exp Ophthalmol* **235**, 786-793.

Ghosh, S., Freitag, A. C., Martin-Vasallo, P. and Coca-Prados, M. (1990). Cellular distribution and differential gene expression of the three alpha subunit isoforms of the Na,K-ATPase in the ocular ciliary epithelium. *J Biol Chem* **265**, 2935-2940.

Ghosh, S., Hernando, N., Martin-Alonso, J. M., Martin-Vasallo, P. and Coca-Prados, M. (1991). Expression of multiple Na^+,K^+-ATPase genes reveals a gradient of isoforms along the nonpigmented ciliary epithelium: functional implications in aqueous humor secretion. *J Cell Physiol* **149**, 184-194.

Glynn, I. M. (1993). Annual review prize lecture. 'All hands to the sodium pump'. *J Physiol* **462**, 1-30.

Goodenough, D. A., Goliger, J. A. and Paul, D. L. (1996). Connexins, connexons, and intercellular communication. *Annu Rev Biochem* **65**, 475-502.

Green, K., Bountra, C., Georgiou, P. and House, C. R. (1985). An electrophysiologic study of rabbit ciliary epithelium. *Invest Ophthalmol Vis Sci* **26**, 371-381.

Green, K. and Pederson, J. E. (1972). Contribution of secretion and filtration to aqueous humor formation. *Am J Physiol* **222**, 1218-1226.

Haas, M. and Forbush, B., III (2000). The Na-K-Cl cotransporter of secretory epithelia. *Annu Rev Physiol* **62**, 515-534.

Haefliger, I. O., Meyer, P., Flammer, J. and Luscher, T. F. (1994). The vascular endothelium as a regulator of the ocular circulation: a new concept in ophthalmology? *Surv Ophthalmol* **39**, 123-132.

Hartzell, C., Putzier, I. and Arreola, J. (2005). Calcium-Activated Chloride Channels. *Annu Rev Physiol* **67**, 719-758.

Haufschild, T., Nava, E., Meyer, P., Flammer, J., Luscher, T. F. and Haefliger, I. O. (1996). Spontaneous calcium-independent nitric oxide synthase activity in porcine ciliary processes. *Biochem Biophys Res Commun* **222**, 786-789.

He, H., Podymow, T., Zimpelmann, J. and Burns, K. D. (2003). NO inhibits Na^+-K^+-$2Cl^-$ cotransport via a cytochrome P-450-dependent pathway in renal epithelial cells (MMDD1). *Am J Physiol* **284**, F1235-1244.

Helbig, H., Korbmacher, C., Berweck, S., Kuhner, D. and Wiederholt, M. (1988a). Kinetic properties of Na^+/H^+ exchange in cultured bovine pigmented ciliary epithelial cells. *Pflugers Arch* **412**, 80-85.

Helbig, H., Korbmacher, C., Erb, C., Nawrath, M., Knuuttila, K. G., Wistrand, P. and Wiederholt, M. (1989a). Coupling of ^{22}Na and ^{36}Cl uptake in cultured pigmented ciliary epithelial cells: a proposed role for the isoenzymes of carbonic anhydrase. *Curr Eye Res* **8**, 1111-1119.

Helbig, H., Korbmacher, C., Kuhner, D., Berweck, S. and Wiederholt, M. (1988b). Characterization of Cl^-/HCO_3^- exchange in cultured bovine pigmented ciliary epithelium. *Exp Eye Res* **47**, 515-523.

Helbig, H., Korbmacher, C., Nawrath, M., Erb, C. and Wiederholt, M. (1989b). Sodium bicarbonate cotransport in cultured pigmented ciliary epithelial cells. *Curr Eye Res* **8**, 595-598.

Helbig, H., Korbmacher, C., Stumpff, F., Coca-Prados, M. and Wiederholt, M. (1988c). Na^+/H^+ exchange regulates intracellular pH in a cell clone derived from bovine pigmented ciliary epithelium. *J Cell Physiol* **137**, 384-389.

Helbig, H., Korbmacher, C., Stumpff, F., Coca-Prados, M. and Wiederholt, M. (1989c). Role of HCO_3^- in regulation of cytoplasmic pH in ciliary epithelial cells. *Am J Physiol* **257**, C696-705.

Helbig, H., Korbmacher, C. and Wiederholt, M. (1987). K^+-conductance and electrogenic Na^+/K^+ transport of cultured bovine pigmented ciliary epithelium. *J Membr Biol* **99**, 173-186.

Helbig, H., Korbmacher, C., Wohlfarth, J., Coca-Prados, M. and Wiederholt, M. (1989d). Electrical membrane properties of a cell clone derived from human nonpigmented ciliary epithelium. *Invest Ophthalmol Vis Sci* **30**, 882-889.

Holland, M. G. and Gipson, C. C. (1970). Chloride ion transport in the isolated ciliary body. *Invest Ophthalmol* **9**, 20-29.

Ignarro, L. J. (1989). Endothelium-derived nitric oxide: pharmacology and relationship to the actions of organic nitrate esters. *Pharm Res* **6**, 651-659.

Ignarro, L. J. (2000). Introduction and Overview. *In* "Nitric Oxide: Biology and pathobiology" (Ignarro L. J., ed.). Academic Press, San Diego, pp. 3-19.

Ignarro, L. J., Degnan, J. N., Baricos, W. H., Kadowitz, P. J. and Wolin, M. S. (1982). Activation of purified guanylate cyclase by nitric oxide requires heme. Comparison of heme-deficient, heme-reconstituted and heme-containing forms of soluble enzyme from bovine lung. *Biochim Biophys Acta* **718**, 49-59.

Iizuka, S., Kishida, K., Tsuboi, S., Emi, K. and Manabe, R. (1984). Electrical characteristics of the isolated dog ciliary body. *Curr Eye Res* **3**, 417-421.

Jacob, T. J. and Civan, M. M. (1996). Role of ion channels in aqueous humor formation. *Am J Physiol* **271**, C703-720.

Jahn, C. E., Leiss, O. and von Bergmann, K. (1983). Lipid composition of human aqueous humor. *Ophthalmic Res* **15**, 220-224.

Jentsch, T. J., Stein, V., Weinreich, F. and Zdebik, A. A. (2002). Molecular structure and physiological function of chloride channels. *Physiol Rev* **82**, 503-568.

Kawahara, J., Nakamura, R., Wakabayashi, Y., Nakano, E., Agawa, T. and Usui, M. (1990). Effect of transpupillary argon laser cyclophotocoagulation on anterior chamber oxygen tension in rabbit eyes. *Jpn J Ophthalmol* **34**, 450-462.

Kinsey, V. E. (1953). Comparative chemistry of aqueous humor in posterior and anterior chambers of rabbit eye, its physiologic significance. *Ama Arch Ophthalmol* **50**, 401-417.

Kinsey, V. E. and Reddy, D. V. (1959). Turnover of total carbon dioxide in the aqueous humors and the effect thereon of acetazolamide. *Ama Arch Ophthalmol* **62**, 78-83.

Kishida, K., Miwa, Y. and Iwata, C. (1986). 2-Substituted 1, 3, 4-thiadiazole-5-sulfonamides as carbonic anhydrase inhibitors: their effects on the transepithelial potential difference of the isolated rabbit ciliary body and on the intraocular pressure of the living rabbit eye. *Exp Eye Res* **43**, 981-995.

Kishida, K., Sasabe, T., Iizuka, S., Manabe, R. and Otori, T. (1982). Sodium and chloride transport across the isolated rabbit ciliary body. *Curr Eye Res* **2**, 149-152.

Kishida, K., Sasabe, T., Manabe, R. and Otori, T. (1981). Electrical characteristics of the isolated rabbit ciliary body. *Jpn J Ophthalmol* **25**, 407-416.

Kiss, B., Dallinger, S., Findl, O., Rainer, G., Eichler, H. G. and Schmetterer, L. (1999). Acetazolamide-induced cerebral and ocular vasodilation in humans is independent of nitric oxide. *Am J Physiol* **276**, R1661-1667.

Kleinstein, R. N., Kwan, M., Fatt, I. and Weissman, B. A. (1981). *In vivo* aqueous humor oxygen tension-as estimated from measurements on bare stroma. *Invest Ophthalmol Vis Sci* **21**, 415-421.

Kodama, T., Reddy, V. N. and Macri, F. J. (1985). Pharmacological study on the effects of some ocular hypotensive drugs on aqueous humor formation in the arterially perfused enucleated rabbit eye. *Ophthalmic Res* **17**, 120-124.

Koefoed-Johnsen, V. and Ussing, H. H. (1958). The nature of the frog skin potential. *Acta Physiol Scand* **42**, 298-308.

Krause, U. and Raunio, V. (1969). Proteins of the normal human aqueous humour. *Ophthalmologica* **159**, 178-185.

Krupin, T. (2000). Aqueous Humor Dynamics. *In* "The Glaucomas: Concepts and Fundamentals" (Eid T. M. and Spaeth G. L., ed.). Lippincott William & Wilkins, Philadelphia, pp. 9-18.

Krupin, T. and Civan, M. M. (1995). Physiologic basis of aqueous humor formation. *In* "The glaucomas: basic sciences" (Ritch R., Shields M. B. and Krupin T., ed.). 2nd. Mosby, St Louis, pp. 251-280.

Krupin, T., Reinach, P. S., Candia, O. A. and Podos, S. M. (1984). Transepithelial electrical measurements on the isolated rabbit iris-ciliary body. *Exp Eye Res* **38**, 115-123.

Kumar, N. M. and Gilula, N. B. (1996). The gap junction communication channel. *Cell* **84**, 381-388.

Lane, P. and Gross, S. S. (1999). Cell signaling by nitric oxide. *Semin Nephrol* **19**, 215-229.

Larsen, W. J. and Veenstra, R. D. (2001). Biology of gap junctions. *In* "Cell physiology sourcebook: a molecular approach" (Sperelakis N., ed.). 3rd ed. Academic press, San Diego, pp. 523-538.

Lindskog, S. (1997). Structure and mechanism of carbonic anhydrase. *Pharmacol Ther* **74**, 1-20.

Lowe, A. G. and Lambert, A. (1982). Chloride-bicarbonate exchange and related transport processes. *Biochim Biophys Acta* **694**, 353-374.

Lutjen-Drecoll, E. (1982). Functional morphology of the ciliary epithelium. *In* "Basic Aspects of Glaucoma Research" (Lutjen-Drecoll E., ed.). Schattauer Verlag, Stuttgart, pp. 69-87.

Macknight, A. D. C., McLaughlin, C. W., Peart, D., Purves, R. D., Carre, D. A. and Civan, M. M. (2000). Formation of the aqueous humor. *Clin Exp Pharmacol Physiol* **27**, 100-106.

Maren, T. H. (1976). The rates of movement of Na^+, Cl^-, and HCO_3^- from plasma to posterior chamber: effect of acetazolamide and relation to the treatment of glaucoma. *Invest Ophthalmol* **15**, 356-364.

Maren, T. H. (1977). Ion secretion into the posterior aqueous humor of dogs and monkeys. *Exp Eye Res* **25**, S245-247.

Maren, T. H., Godman, D. R., Pancorbo, B. M. and Vogh, B. P. (1997). Timolol decreases aqueous humor flow but not Na^+ movement from plasma to aqueous. *Invest Ophthalmol Vis Sci* **38**, 1274-1277.

Masferrer, J. L., Dunn, M. W. and Schwartzman, M. L. (1990). 12(R)-hydroxyeicosatetraenoic acid, an endogenous corneal arachidonate metabolite, lowers intraocular pressure in rabbits. *Invest Ophthalmol Vis Sci* **31**, 535-539.

Masters, B. S. (2000). Structural Variations to Accommodate Functional Themes of the Isoforms of NO synthases. *In* "Nitric Oxide: Biology and pathobiology" (Ignarro L. J., ed.). Academic Press, San Diego, pp. 91-104.

Matsui, H., Murakami, M., Wynns, G. C., Conroy, C. W., Mead, A., Maren, T. H. and Sears, M. L. (1996). Membrane carbonic anhydrase (IV) and ciliary epithelium. Carbonic anhydrase activity is present in the basolateral membranes of the non-pigmented ciliary epithelium of rabbit eyes. *Exp Eye Res* **62**, 409-417.

McCannel, C. A., Scanlon, P. D., Thibodeau, S. and Brubaker, R. F. (1992). A study of aqueous humor formation in patients with cystic fibrosis. *Invest Ophthalmol Vis Sci* **33**, 160-164.

McLaren, J. W., Dinslage, S., Dillon, J. P., Roberts, J. E. and Brubaker, R. F. (1998). Measuring oxygen tension in the anterior chamber of rabbits. *Invest Ophthalmol Vis Sci* **39**, 1899-1909.

McLaughlin, C. W., Peart, D., Purves, R. D., Carre, D. A., Macknight, A. D. C. and Civan, M. M. (1998). Effects of HCO_3^- on cell composition of rabbit ciliary epithelium: a new model for aqueous humor secretion. *Invest Ophthalmol Vis Sci* **39**, 1631-1641.

Mead, A., Sears, J. and Sears, M. (1996). Transepithelial transport of ascorbic acid by the isolated intact ciliary epithelial bilayer of the rabbit eye. *J Ocul Pharmacol Ther* **12**, 253-258.

Meyer, P., Champion, C., Schlotzer-Schrehardt, U., Flammer, J. and Haefliger, I. O. (1999). Localization of nitric oxide synthase isoforms in porcine ocular tissues. *Curr Eye Res* **18**, 375-380.

Millar, J. C., Shahidullah, M. and Wilson, W. S. (2001). Intraocular pressure and vascular effects of sodium azide in bovine perfused eye. *J Ocul Pharmacol Ther* **17**, 225-234.

Miranda, K. M., Espey, M. G., Jourd'heuil, D., Grisham, M. B., Fukuto, J. M., Feelisch, M. and Wink, D. A. (2000). The Chemical Biology of Nitric Oxide. *In* "Nitric Oxide: Biology and pathobiology" (Ignarro L. J., ed.). Academic Press, San Diego, pp. 41-56.

Moncada, S., Palmer, R. M. and Higgs, E. A. (1991). Nitric oxide: physiology, pathophysiology, and pharmacology. *Pharmacol Rev* **43**, 109-142.

Mori, N., Yamada, E. and Sears, M. L. (1991). Immunocytochemical localization of Na/K-ATPase in the isolated ciliary epithelial bilayer of the rabbit. *Arch Histol Cytol* **54**, 259-265.

Morrison, J. C. and Van Buskirk, E. M. (1984). Ciliary process microvasculature of the primate eye. *Am J Ophthalmol* **97**, 372-383.

Murad, F. (1994). The nitric oxide-cyclic GMP signal transduction system for intracellular and intercellular communication. *Recent Prog Horm Res* **49**, 239-248.

Murray, D. L. and Bartels, S. P. (1993). The relationship between aqueous humor flow and anterior chamber protein concentration in rabbits. *Invest Ophthalmol Vis Sci* **34**, 370-376.

Muther, T. F. and Friedland, B. R. (1980). Autoradiographic localization of carbonic anhydrase in the rabbit ciliary body. *J Histochem Cytochem* **28**, 1119-1124.

Nagasubramanian, S. and Poinoosawmy, D. (1986). The effects of timolol on the active transport across the ciliary epithelium. *Trans Ophthalmol Soc UK* **105**, 665-666.

Nathanson, J. A. (1992). Nitrovasodilators as a new class of ocular hypotensive agents. *J Pharmacol Exp Ther* **260**, 956-965.

Nathanson, J. A. and McKee, M. (1995). Identification of an extensive system of nitric oxide-producing cells in the ciliary muscle and outflow pathway of the human eye. *Invest Ophthalmol Vis Sci* **36**, 1765-1773.

Nauntofte, B. (1992). Regulation of electrolyte and fluid secretion in salivary acinar cells. *Am J Physiol* **263**, G823-837.

Niekrasz, M., Ye, Y., Rolf, L. L., Zuhdi, N. and Cooper, D. K. (1992). The pig as organ donor for man. *Transplant Proc* **24**, 625-626.

Noske, W., Stamm, C. C. and Hirsch, M. (1994). Tight junctions of the human ciliary epithelium: regional morphology and implications on transepithelial resistance. *Exp Eye Res* **59**, 141-149.

O'Grady, S. M., Palfrey, H. C. and Field, M. (1987). Characteristics and functions of Na-K-Cl cotransport in epithelial tissues. *Am J Physiol* **253**, C177-192.

Oh, J., Krupin, T., Tang, L. Q., Sveen, J. and Lahlum, R. A. (1994). Dye coupling of rabbit ciliary epithelial cells in vitro. *Invest Ophthalmol Vis Sci* **35**, 2509-2514.

Okisaka, S. and Kuwabara, T. (1974). Selective destruction of the pigmented epithelium in the ciliary body of the eye. *Science* **184**, 1298-1299.

Park, K. and Brown, P. D. (1995). Intracellular pH modulates the activity of chloride channels in isolated lacrimal gland acinar cells. *Am J Physiol* **268**, C647-650.

Perez, M. T., Larsson, B., Alm, P., Andersson, K. E. and Ehinger, B. (1995). Localisation of neuronal nitric oxide synthase-immunoreactivity in rat and rabbit retinas. *Exp Brain Res* **104**, 207-217.

Pesin, S. R. and Candia, O. A. (1982). Na^+ and Cl^- fluxes, and effects of pharmacological agents on the short-circuit current of the isolated rabbit iris-ciliary body. *Curr Eye Res* **2**, 815-827.

Raviola, G. and Raviola, E. (1978). Intercellular junctions in the ciliary epithelium. *Invest Ophthalmol Vis Sci* **17**, 958-981.

Rehm, W. S. (1975). Ion transport and short-circuit technique. *In* "Current Topics in Membranes and Transport" (Bronner F. and Kleinzeller A., ed.). Academic Press, New York, pp. 217-270.

Reiss, G. R., Werness, P. G., Zollman, P. E. and Brubaker, R. F. (1986). Ascorbic acid levels in the aqueous humor of nocturnal and diurnal mammals. *Arch Ophthalmol* **104**, 753-755.

Revel, J. P. and Karnovsky, M. J. (1967). Hexagonal array of subunits in intercellular junctions of the mouse heart and liver. *J Cell Biol* **33**, C7-12.

Riley, M. V. (1983). The chemistry of the aqueous humor. *In* "Biochemistry of the Eye" (Anderson R. E., ed.). American Academy of Ophthalmology, San Francisco, pp. 79-95.

Riley, M. V. and Kishida, K. (1986). ATPases of ciliary epithelium: cellular and subcellular distribution and probable role in secretion of aqueous humor. *Exp Eye Res* **42**, 559-568.

Rose, R. C. and Bode, A. M. (1991). Ocular ascorbate transport and metabolism. *Comp Biochem Physiol A* **100**, 273-285.

Rosenberg, L. F., Krupin, T., Tang, L. Q., Hong, P. H. and Ruderman, J. M. (1998). Combination of systemic acetazolamide and topical dorzolamide in reducing intraocular pressure and aqueous humor formation. *Ophthalmology* **105**, 88-92; discussion 92-93.

Russell, J. M. (2000). Sodium-potassium-chloride cotransport. *Physiol Rev* **80**, 211-276.

Saito, Y. and Watanabe, T. (1979). Relationship between short-circuit current and unidirectional fluxes of Na and Cl across the ciliary epithelium of the toad: demonstration of active Cl transport. *Exp Eye Res* **28**, 71-79.

Sanchez-Torres, J., Huang, W., Civan, M. M. and Coca-Prados, M. (1999). Effects of hypotonic swelling on the cellular distribution and expression of pI(Cln) in human nonpigmented ciliary epithelial cells. *Curr Eye Res* **18**, 408-416.

Schmetterer, L. and Polak, K. (2001). Role of nitric oxide in the control of ocular blood flow. *Prog Retin Eye Res* **20**, 823-847.

Schneeberger, E. E. and Lynch, R. D. (2004). The tight junction: a multifunctional complex. *Am J Physiol* **286**, C1213-1228.

Schuman, J. S., Erickson, K. and Nathanson, J. A. (1994). Nitrovasodilator effects on intraocular pressure and outflow facility in monkeys. *Exp Eye Res* **58**, 99-105.

Sears, M. L., Yamada, E., Cummins, D., Mori, N., Mead, A. and Murakami, M. (1991). The isolated ciliary bilayer is useful for studies of aqueous humor formation. *Trans Am Ophthalmol Soc* **89**, 131-152.

Shahidullah, M., Wilson, W. S., Yap, M. and To, C. H. (2003). Effects of ion transport and channel-blocking drugs on aqueous humor formation in isolated bovine eye. *Invest Ophthalmol Vis Sci* **44**, 1185-1191.

Shimizu, H., Riley, M. V. and Cole, D. F. (1967). The isolation of whole cells from the ciliary epithelium together with some observations on the metabolism of the two cell types. *Exp Eye Res* **6**, 141-151.

Sly, W. S. and Hu, P. Y. (1995). Human carbonic anhydrases and carbonic anhydrase deficiencies. *Annu Rev Biochem* **64**, 375-401.

Stefansson, E., Foulks, G. N. and Hamilton, R. C. (1987). The effect of corneal contact lenses on the oxygen tension in the anterior chamber of the rabbit eye. *Invest Ophthalmol Vis Sci* **28**, 1716-1719.

Stein, A., Pinke, R., Krupin, T., Glabb, E., Podos, S. M., Serle, J. and Maren, T. H. (1983). The effect of topically administered carbonic anhydrase inhibitors on aqueous humor dynamics in rabbits. *Am J Ophthalmol* **95**, 222-228.

Steinberg, R. H., Miller, S. S. and Stern, W. H. (1978). Initial observations on the isolated retinal pigment epithelium-choroid of the cat. *Invest Ophthalmol Vis Sci* **17**, 675-678.

Sugrue, M. F. (2000). Pharmacological and ocular hypotensive properties of topical carbonic anhydrase inhibitors. *Prog Retin Eye Res* **19**, 87-112.

To, C. H., Do, C. W., Zamudio, A. C. and Candia, O. A. (2001). Model of ionic transport for bovine ciliary epithelium: effects of acetazolamide and HCO. *Am J Physiol* **280**, C1521-1530.

To, C. H. and Hodson, S. A. (1998). The glucose transport in retinal pigment epithelium is via passive facilitated diffusion. *Comp Biochem Physiol A Mol Integr Physiol* **121**, 441-444.

To, C. H., Kong, C. W., Chan, C. Y., Shahidullah, M. and Do, C. W. (2002). The mechanism of aqueous humour formation. *Clin Exp Optom* **85**, 335-349.

To, C. H., Mok, K. H., Do, C. W., Lee, K. L. and Millodot, M. (1998a). Chloride and sodium transport across bovine ciliary body/epithelium (CBE). *Curr Eye Res* **17**, 896-902.

To, C. H., Mok, K. H., Tse, S. K., Siu, W. T., Millodot, M., Lee, K. L. and Hodson, S. (1998b). *In vitro* bovine ciliary body/epithelium in a small continuously perfused Ussing type chamber. *Cell Struct Funct* **23**, 247-254.

Tsukahara, S. and Maezawa, N. (1978). Cytochemical localization of adenyl cyclase in the rabbit ciliary body. *Exp Eye Res* **26**, 99-106.

Ussing, H. H. and Zerahn, K. (1951). Active transport of sodium as the source of electric current in the short-circuited isolated frog skin. *Acta Physiol Scand* **23**, 110-127.

Usukura, J., Fain, G. L. and Bok, D. (1988). [^{3}H]ouabain localization of Na-K ATPase in the epithelium of rabbit ciliary body pars plicata. *Invest Ophthalmol Vis Sci* **29**, 606-614.

Wakabayashi, S., Shigekawa, M. and Pouyssegur, J. (1997). Molecular physiology of vertebrate Na^{+}/H^{+} exchangers. *Physiol Rev* **77**, 51-74.

Wang, L., Chen, L. and Jacob, T. J. (2000). The role of ClC-3 in volume-activated chloride currents and volume regulation in bovine epithelial cells demonstrated by antisense inhibition. *J Physiol* **524**, 63-75.

Wang, R. F. and Podos, S. M. (1995). Effect of the topical application of nitroglycerin on intraocular pressure in normal and glaucomatous monkeys. *Exp Eye Res* **60**, 337-339.

Wang, R. F., Serle, J. B., Podos, S. M. and Sugrue, M. F. (1991). MK-507 (L-671,152), a topically active carbonic anhydrase inhibitor, reduces aqueous humor production in monkeys. *Arch Ophthalmol* **109**, 1297-1299.

Watanabe, T. and Saito, Y. (1978). Characteristics of ion transport across the isolated ciliary epithelium of the toad as studied by electrical measurements. *Exp Eye Res* **27**, 215-226.

White, M. M. and Aylwin, M. (1990). Niflumic and flufenamic acids are potent reversible blockers of Ca^{2+}-activated Cl^- channels in Xenopus oocytes. *Mol Pharmacol* **37**, 720-724.

Wiederholt, M., Helbig, H. and Korbmacher, C. (1991). Ion transport across the ciliary epithelium: lessons from cultured cells and proposed role of the carbonic anhydrase. *In* "Carbonic Anhydrase" (Botre F., Gross G. and Storey B. T., ed.). VCH Weinheim, New York, pp. 232-244.

Wiederholt, M., Sturm, A. and Lepple-Wienhues, A. (1994). Relaxation of trabecular meshwork and ciliary muscle by release of nitric oxide. *Invest Ophthalmol Vis Sci* **35**, 2515-2520.

Wiederholt, M. and Zadunaisky, J. A. (1986). Membrane potentials and intracellular chloride activity in the ciliary body of the shark. *Pflugers Arch* **407**, S112-115.

Wiederholt, M. and Zadunaisky, J. A. (1987). Effects of ouabain and furosemide on transepithelial electrical parameters of the isolated shark ciliary epithelium. *Invest Ophthalmol Vis Sci* **28**, 1353-1356.

Willecke, K., Eiberger, J., Degen, J., Eckardt, D., Romualdi, A., Guldenagel, M., Deutsch, U. and Sohl, G. (2002). Structural and functional diversity of connexin genes in the mouse and human genome. *Biol Chem* **383**, 725-737.

Wilson, S. M., Shahidullah, M. and Millar, C. (1993). The bovine arterially-perfused eye: an *in vitro* method for the study of drug mechanisms on IOP, aqueous humour formation and uveal vasculature. *Curr Eye Res* **12**, 609-620.

Wink, D. A. and Mitchell, J. B. (1998). Chemical biology of nitric oxide: Insights into regulatory, cytotoxic, and cytoprotective mechanisms of nitric oxide. *Free Radic Biol Med* **25**, 434-456.

Wolosin, J. M., Bonanno, J. A., Hanzel, D. and Machen, T. E. (1991). Bicarbonate transport mechanisms in rabbit ciliary body epithelium. *Exp Eye Res* **52**, 397-407.

Wolosin, J. M., Candia, O. A., Peterson-Yantorno, K., Civan, M. M. and Shi, X. P. (1997). Effect of heptanol on the short circuit currents of cornea and ciliary body demonstrates rate limiting role of heterocellular gap junctions in active ciliary body transport. *Exp Eye Res* **64**, 945-952.

Wolosin, J. M., Chen, M., Gordon, R. E., Stegman, Z. and Butler, G. A. (1993). Separation of the rabbit ciliary body epithelial layers in viable form: identification of differences in bicarbonate transport. *Exp Eye Res* **56**, 401-409.

Wu, J., Zhang, J. J., Koppel, H. and Jacob, T. J. C. (1996). P-glycoprotein regulates a volume-activated chloride current in bovine non-pigmented ciliary epithelial cells. *J Physiol* **491**, 743-755.

Wu, P., Gong, H., Richman, R. and Freddo, T. F. (2000). Localization of occludin, ZO-1, and pan-cadherin in rabbit ciliary epithelium and iris vascular endothelium. *Histochem Cell Biol* **114**, 303-310.

Wu, Q., Pierce, W. M., Jr and Delamere, N. A. (1998). Cytoplasmic pH responses to carbonic anhydrase inhibitors in cultured rabbit nonpigmented ciliary epithelium. *J Membr Biol* **162**, 31-38.

Wu, R., Flammer, J. and Haefliger, I. O. (2003). Transepithelial short circuit currents in human and porcine isolated ciliary bodies: effect of acetazolamide and epinephrine. *Klin Monatsbl Augenheilkd* **220**, 156-160.

Wu, R., Yao, K., Flammer, J. and Haefliger, I. O. (2004). Role of anions in nitric oxide-induced short-circuit current increase in isolated porcine ciliary processes. *Invest Ophthalmol Vis Sci* **45**, 3213-3222.

Yantorno, R. E., Carre, D. A., Coca-Prados, M., Krupin, T. and Civan, M. M. (1992). Whole cell patch clamping of ciliary epithelial cells during anisosmotic swelling. *Am J Physiol* **262**, C501-509.

Zhang, J. J. and Jacob, T. J. (1997). Three different Cl^- channels in the bovine ciliary epithelium activated by hypotonic stress. *J Physiol* **499**, 379-389.